Closure Approximations for Passive Scalar Turbulence: A Comparative Study on an Exactly Solvable Model with Complex Features

Peter R. Kramer* Andrew J. Majda†

Eric Vanden-Eijnden‡

December 7, 2001

Suggested running head: "Closure approximations: A Comparative Study"

Corresponding author:

Peter Kramer
301 Amos Eaton Hall
110 8th Street
RPI
Troy, NY 12180
email: kramep@rpi.edu,
phone: (518) 276-6896, fax: (518) 276-4824

*Department of Mathematical Sciences, Rensselaer Polytechnic Institute, Troy, NY
†Courant Institute of Mathematical Sciences, New York University, New York, NY
‡Courant Institute of Mathematical Sciences, New York University, New York, NY

Abstract

Some standard closure approximations used in turbulence theory are analyzed by examining systematically the predictions these approximations produce for a passive scalar advection model consisting of a shear flow with a fluctuating cross sweep. This model has a general geometric structure of a jet flow with transverse disturbances, which occur in a number of contexts, and it encompasses a wide variety of possible spatio-temporal statistical structures for the velocity field, including strong long-range correlations. Even though the Eulerian and Lagrangian velocity statistics are not equal and the passive scalar statistics exhibit broader-than-Gaussian intermittency, this model is nevertheless simple enough so that many passive scalar statistics can be computed exactly and compared systematically with the predictions of the closure approximations. Our comparative study illustrates the strength and weaknesses of the closure approximations and points out the physical phenomena that these approximations are able or not able to describe properly. In particular it is shown that the direct interaction approximation (DIA), one of the most sophisticated closure approximations available, fails to reproduce adequately the statistical features of the scalar and may even lead to absdurd predictions, even though the equations it produces are rather complicated and difficult to analyze. Two alternative closure approximations, the Modified DIA (MDIA) and the Renormalized Lagrangian Approximation (RLA), with different levels of sophistication, both are simpler to use than the DIA and perform better. In particular, it is shown that both closure approximations always reproduce exactly the second order statistics for the scalar and that the MDIA is even able to capture intermittency effects.

Keywords: Passive scalar turbulence, closure approximations, direct interaction approximation, intermittency

Contents

1 Introduction

The difficulties inherent in turbulence modeling are often summarized by the *moment closure problem* [41, 48]. We will consider this issue in the context of the evolution of a *passive scalar field* $T(\boldsymbol{r}, t)$ advected by a velocity field $\boldsymbol{v}(\boldsymbol{r}, t)$. The scalar field T describes the concentration of some physical substance immersed in the fluid which is carried with the local fluid velocity but which does not itself significantly influence the dynamics of the fluid. The immersed physical substance may be dye, contaminants, heat, etc.., and the passive scalar model has numerous applications in geophysical science and engineering [14, 15, 41, 48, 50, 51]. The passive scalar field will typically also have some intrinsic self-diffusivity κ due to microscopic Brownian motion. The dynamics of the passive scalar field are then defined by the following linear advection-diffusion equation:

$$\frac{\partial T}{\partial t} + \boldsymbol{v} \cdot \boldsymbol{\nabla} T = \kappa \Delta T. \tag{1}$$

Solving Eq. (1) is a challenge when the molecular diffusivity κ is small and the fluid is in a turbulent state, meaning that the velocity field $\boldsymbol{v}$ is excited on a very wide range of spatio-temporal scales. For instance, $\boldsymbol{v}$ might solve Navier-Stokes equation at very high Reynolds number. Then indeed the scalar field T inherits the very complicated structure of $\boldsymbol{v}$ and it is usually not possible to describe its behavior in detail. On the other hand, while such a detailed description is impossible, it is also not very useful since one is typically interested only in the behavior of T on spatio-temporal scales much larger than the finest ones that T inherits from $\boldsymbol{v}$. In other words, we would like to derive a closed expression for the mean scalar field

$$\langle T(\boldsymbol{r}, t) \rangle$$

where $\langle \cdot \rangle$ denotes some projection, or averaging, operation which removes the finest scales. This, however, is where the moment closure problem arises. Indeed, taking a direct average of Eq. (1) in an attempt to find an equation for $\langle T \rangle$ results in:

$$\frac{\partial \langle T \rangle}{\partial t} + \langle \boldsymbol{v} \cdot \boldsymbol{\nabla} T \rangle = \kappa \Delta \langle T \rangle. \tag{2}$$

This equation involves the unknown correlation function $\langle \boldsymbol{v} T \rangle$ in addition to the mean passive scalar density $\langle T \rangle$ which is being sought. Writing down the equation for $\langle \boldsymbol{v} T \rangle$ does not help since this equation involves the unknown correlation function $\langle \boldsymbol{v}\boldsymbol{v} T \rangle$, and so on. Thus, direct averaging of the transport equation in (1) leads to an infinite hierarchy of equations for the correlation functions, and there is no known way to write down a

finite closed system of equations for correlation functions of T, except in very special situations such as when the velocity field fluctuates on much smaller spatio-temporal scales than the passive scalar field [3, 8, 12, 19, 18, 27, 28, 34, 37, 43, 45, 47, 49, 53, 56, 71]. For a recent review, see Chapter 2 of [46]. Turbulent flows in most applications do not enjoy such scale separation properties.

To grapple with the moment closure problem in turbulence, a number of *closure approximations* have been proposed. These procedures implement some particular ansatz about the unknown correlation functions at some level so as to yield a set of closed equations for the correlation functions up to a given order. The most common closure approximations bear the names of Quasi-Normal Approximation (QNA) [10, 11, 57, 62, 66], Quasi-Linear Approximation (QLA) [64, 65, 66], Direct Interaction Approximation (DIA) [29, 30, 31, 60]. In addition to these ones, we will also consider in this paper the Modified Direct Interaction Approximation (MDIA) [68], and the Renormalized Lagrangian Approximation (RLA) [13, 44, 61] (see [38, 42, 48, 54] for general presentations). Despite the possibility of their systematic derivation from a perturbation series (they all fit within the so-called Zwanzig-Mori formalism, see Appendix A), none of these closure approximations are rigorous. Moreover, the equations they produce can be quite complicated and their consequences obscure. The quality of the closure approximations therefore must be assessed in some *a posteriori* manner. One possibility is to compare their theoretical predictions with data from experiments [54] or direct numerical simulations [24, 25]. Another possibility is to test the closure approximations on exactly solvable models with nontrivial behaviors. This route was already taken by Avellaneda and one of the present authors in [4], where the QNA, DIA, and a renormalization group-based closure scheme were studied asymptotically at large times on a simple shear model where the Eulerian and Lagrangian correlations in the velocity field are identical. This paper will proceed with much the same philosophy, using a model with more flexibility in the flow structure to assess systematically the performance of all the aforementioned closure approximations. In particular, a key feature of the models introduced here is that the Eulerian and Lagrangian correlations for the velocity field do not coincide, in contrast to the models from [4]. Also, we develop results both at finite times and at asymptotically large times as in [4]. To the best of our knowledge such a systematic comparative study has not yet been undertaken, though it clearly illustrates the strengths and weaknesses of the closure approximations by pointing out the physical phenomena that these approximations are able or not able to describe properly. The outcomes of our analysis of the closure approximations are summarized in the conclusion (Section 6) and in more detail at the beginning of each relevant section.

The model flow which we will consider is the Shear Flow with Cross Sweep (SFCS) model introduced by two of the authors in [46, Sec. 3]. In this model, to be described in more detail in Sec 2, it is assumed that the turbulent flow is a two-dimensional Gaussian random field which is a superposition of a spatially uniform but possibly temporally fluctuating cross sweep in the x direction, and a random shear flow (with fluctuations possible in both time and spatial x direction) in the y direction:

$$\boldsymbol{v}(x,y,t) = \begin{pmatrix} w(t) \\ v(x,t) \end{pmatrix} \tag{3}$$

The SFCS model has a number of properties which make it an excellent test model for closure approximations. First of all, the geometry is sufficiently simple to permit a great deal of exact analysis for the scalar field advected by it ([2, 5, 6],[46, Sec. 3],[26]). A second virtue of the SFCS model is that it is flexible enough to admit several physically realistic and important features. For instance, the general geometric structure of the model (3) may be viewed as a particular approximation to a jet flow with transverse disturbances, which occur in a number of contexts. For example, deterministic versions of these models have been utilized recently [9] to demonstrate explicitly the wide variety of intermittent PDF's which can describe passive scalars with a mean gradient including PDF's which occur in vastly more complicated experiments and numerical simulations (see the references in [9]). The SFCS model is also one of the simplest models for which the *Lagrangian* velocity, that is, the velocity measured by a tracer particle moving in the flow, has a different statistical structure than the *Eulerian* velocity observed at a fixed position (as defined in Eq. (3)). The combination of flexibility and analytical tractability of the model permits a precise elucidation of a number of subtle ways in which a turbulent velocity field influences the scalar field ([2, 26],[46, Sec. 3]).

The remainder of this paper is organized as follows. In Section 2 we introduce the SFCS model and derive some exact, explicit formulas for the mean scalar field $\langle T \rangle$ and related quantities in this model. In Section 3, we derive the equations for the mean scalar field $\langle T \rangle$ predicted by various closure approximations for the same model, and make general observations regarding the agreement between the closure approximations and the exact formulas when the correlation functions of the velocity in (4) are considered to be arbitrary. Thereafter, we will explore the ways in which the specific form of the velocity correlation functions influences passive scalar transport. To this end, in Section 4 we introduce a specialized version of the SFCS model, which we call the Infrared Scaling Shear Flow with Cross Sweep (IS-SFCS) model. The IS-SFCS model is broad enough that it allows for finite or infinite correlation length or time in the velocity field. We use the IS-SFCS model to focus particularly on the coarse-grained behavior at

large space and long time scales, which is often of fundamental relevance in applications. We apply a systematic renormalization procedure, previously described in [2, 5, 45], to the closure approximations to derive effective equations on large scales and long times. These can be compared with the equations arising from a rigorous, exact renormalization [2, 5, 6], which fall into several qualitative categories described in detail. Next, in Section 5, we study the detailed long-time asymptotic behavior of the fourth order cumulant $\mu_{0,4}(t)$ of the shear-parallel displacement of a passive tracer advected by the IS-SFCS flow. Indeed, this quantity offers the simplest quantitative description of the *shape* of the probability density function (PDF) for the displacement of a tracer. We can thereby assess quantitatively how well the closure approximations model this PDF shape at long times. We offer some concluding remarks and overall assessments of the closure approximations in Section 6. Appendix A provides a general, formal description of the closure approximations studied in this paper, and some technical calculations are collected in Appendices B, C and D.

2 A Class of Model Shear Flows

We will examine the performance of the various passive scalar closure approximations within the Shear Flow with Cross Sweep (SFCS) model. The SFCS model is introduced in Subsection 2.1. In Subsection 2.2, we relate the mean scalar field density $\langle T \rangle$ to the probability density function (PDF) of a tracer particle advected by the random flow and subject to molecular diffusion, and we give an exact representation formula for this PDF in the context of the SFCS model. From this representation, we show in Subsection 2.3 how to deduce explicit analytical representations for all moments of the tracer displacements, and explicitly display some which we will compare with the predictions of the closure approximations in subsequent sections. We will compare and contrast how these effects are manifested in the closure approximations in Section 3.

2.1 The Shear Flow with Cross Sweep (SFCS) Model

As mentioned in the Introduction, the turbulent flow in the SFCS model is taken to be a two-dimensional Gaussian random field which is a superposition of a spatially uniform but possibly temporally fluctuating cross sweep in the x direction and a random shear flow (with fluctuations possible in both time and space x direction) in the y direction [46, Sec. 3],

$$\boldsymbol{v}(x, y, t) = \begin{pmatrix} w(t) \\ v(x, t) \end{pmatrix}. \tag{4}$$

The sweeping component $w(t)$ is modeled as a zero-mean, statistically stationary, Gaussian random process with correlation function denoted by

$$R_w(t) = \langle w(t' + t)w(t') \rangle, \tag{5}$$

where here and below $\langle \cdot \rangle$ denotes ensemble averaging with respect to the statistics of the velocity field. The shearing component $v(x, t)$ will be modeled as a zero-mean, statistically homogenous and stationary Gaussian random process, statistically independent of $w(t)$, and with spatio-temporal correlation function denoted by

$$R_v(x, t) = \langle v(x' + x, t' + t)v(x', t') \rangle$$

It will be convenient to represent $R_v(x, t)$ in terms of the *spectral-temporal correlation function* $E(k, t)$ defined through

$$R_v(x, t) = \int_{\mathbf{R}} e^{ikx} E(k, t)\, dk. \tag{6}$$

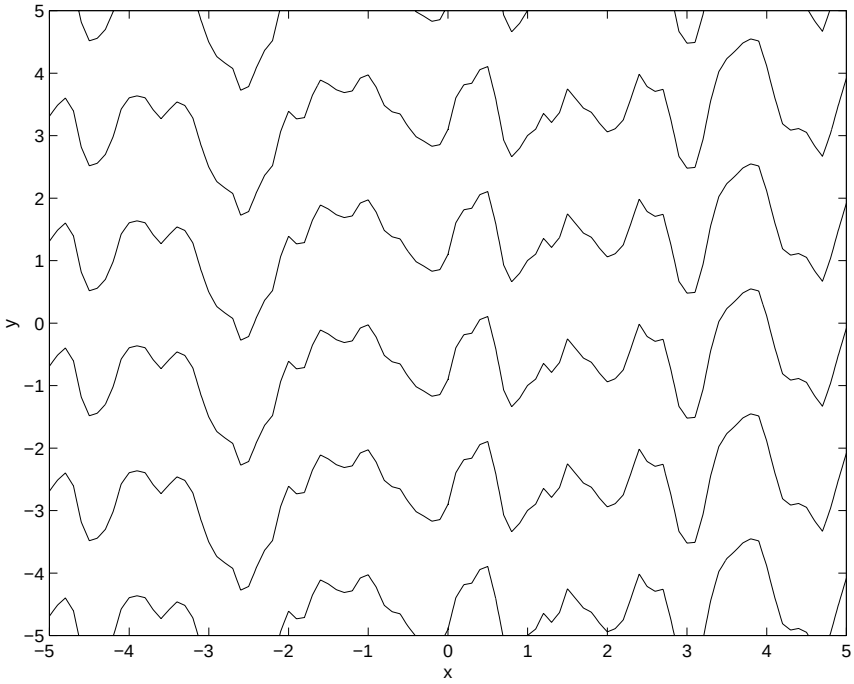

Figure 1: Instantaneous streamlines of a shear flow with cross sweep: $\boldsymbol{v}(x, y, t) = (w(t), v(x, t))$ at a moment when $w(t) = 1$. The shear flow $v(x, t)$ has energy spectrum $\bar{E}(k) = k^2 e^{-k}$ and is simulated by a Fourier method ([16],[46, Sec. 6]) with 1000 wavenumber modes with spacing $\Delta k = 0.01$.

$E(k,t)$ describes precisely the temporal correlations of the shear velocity mode with wavenumber k. At zero time delay, this function is equal to the traditional energy spectrum $E(k,t=0) = \bar{E}(|k|)$ which is a nonnegative function describing the spectral density of energy with respect to spatial wavenumber [41],[46, Sec. 3],[63].

No special assumptions on the correlation functions $R_w(t)$ and $R_v(x,t)$ (or $E(k,t)$) are necessary for the analysis, but for simplicity we shall assume that $v(x,t)$ has statistical symmetry under $x \to -x$ and $t \to -t$ independently. Then the correlation functions satisfy

$$R_w(t) = R_w(-t), \qquad R_v(x,t) = R_v(-x,t) = R_v(x,-t). \tag{7}$$

In terms of spectral-temporal correlation function this reads $E(k,t) = E(-k,t) = E(k,-t)$.

The cross sweep $w(t)$ can have strong effects on the motion of a tracer along a shear ([5, 9, 26],[46, Sec. 3]). When there is no cross sweep and molecular diffusion is small, the tracer is transported very rapidly along the streamlines of the velocity field $\boldsymbol{v}(x,y,t)$ which extend unboundedly in the y direction. On the other hand, when $w(t)$ is nonvanishing, then the streamlines of the flow are disrupted and transport of the passive scalar is impeded along the shearing direction y (see Figure 1 and [26]. When the sweeping component $w(t)$ is fluctuating and passing through zero at various moments of time, the tracer motion is then governed by an interesting combination of rapid transport periods (when $w(t)$ is very small) and blocking periods (when $w(t)$ is large) [46, Sec. 2.2].

We note that the inclusion of a nonzero constant mean velocity field could be incorporated in our analysis, but we will refrain from doing so to keep formulas simple. All closure approximations we consider can be shown to transform in the correct manner under the addition of such a constant mean sweep, so we do not gain any further information for our purposes by including it.

2.2 Functional Average Representation for Green's function

For the moment, we study the general case described by the advection-diffusion equation in (1). It will be convenient to consider the solution of this equation for the special initial condition of a Dirac distribution function centered at point $\boldsymbol{r} = \boldsymbol{r}'$ at time $t = t'$. Assuming spatio-temporal homogeneity of the velocity field $\boldsymbol{v}(\boldsymbol{r},t)$, the solution of Eq. (1) for this initial condition depends only on the differences $\boldsymbol{r} - \boldsymbol{r}'$ and $t - t'$, and we shall denote it by $G(\boldsymbol{r} - \boldsymbol{r}', t - t')$. The mean scalar field $\langle T(\boldsymbol{r},t)\rangle$ for an arbitray initial condition $T(\boldsymbol{r}, t = t') = T_0(\boldsymbol{r})$, possibly random but

statistically independent of the velocity $\boldsymbol{v}$, can be expressed in terms of G via the superposition formula

$$\langle T(\boldsymbol{r},t)\rangle = \int_{\mathbb{R}^d} G(\boldsymbol{r}-\boldsymbol{r}',t-t')\langle T_0(\boldsymbol{r}')\rangle_0 \, d\boldsymbol{r}'. \tag{8}$$

where $\langle\cdot\rangle_0$ denotes ensemble-averaging with respect to the statistics of the initial condition. The function G will be refered to as the (ensemble-averaged) Green's function and it has a very simple probabilistic interpretation as the probability density function (PDF) of a tracer advected by the flow and subject to molecular diffusion. The trajectory of a tracer, $\boldsymbol{R}(t)$, is governed by the stochastic differential equation (SDE)

$$d\boldsymbol{R}(t) = \boldsymbol{v}(\boldsymbol{R}(t),t)dt + \sqrt{2\kappa}\, d\boldsymbol{W}(t), \qquad \boldsymbol{R}(0) = 0. \tag{9}$$

Molecular diffusion is represented here through a d-dimensional ($d = 2, 3$) Wiener process $\boldsymbol{W}(t)$, a Gaussian random process with independent increments satisfying $\boldsymbol{W}(0) = \boldsymbol{0}$, $\langle d\boldsymbol{W}(t)\rangle = \boldsymbol{0}$, $\langle d\boldsymbol{W}(t) \otimes d\boldsymbol{W}(t')\rangle = \mathcal{I}\delta(t-t')\, dt\, dt'$ where $\mathcal{I}$ is the identity matrix [39]. In terms of $\boldsymbol{R}(t)$, we have the representation formula

$$G(\boldsymbol{r},t) = \frac{1}{(2\pi)^d} \int_{\mathbb{R}^d} e^{-i\boldsymbol{k}\cdot\boldsymbol{r}} \hat{G}(\boldsymbol{k},t) d\boldsymbol{k}, \tag{10}$$

where

$$\hat{G}(\boldsymbol{k},t) = \left\langle e^{i\boldsymbol{k}\cdot\boldsymbol{R}(t)} \right\rangle_{\boldsymbol{v},W}. \tag{11}$$

Here $\langle\cdot\rangle_{\boldsymbol{v},W}$ denotes expectation over both the statistics of $\boldsymbol{v}$ and $\boldsymbol{W}$. The function $\hat{G}$ is the characteristic function for the process $\boldsymbol{R}(t)$. In what follows we shall focus on studying G (or $\hat{G}$) owing to its primary importance and easy probabilistic interpretation.

Coming back to the SFCS model, $\hat{G}$ is given by

$$\hat{G}(k,p,t) = \left\langle e^{-ikX(t)-ipY(t)} \right\rangle. \tag{12}$$

Here $\boldsymbol{R}(t) \equiv (X(t), Y(t))$ satisfies

$$\begin{cases} dX(t) = w(t)\, dt + \sqrt{2\kappa}\, dW_x(t), & X(0) = 0, \\ dY(t) = v(X(t),t)\, dt + \sqrt{2\kappa}\, dW_y(t), & Y(0) = 0, \end{cases} \tag{13}$$

where $W_x(t)$ and $W_y(t)$ are two independent Wiener processes. For every realization of the random velocity field and the random molecular motion, the equation of motion for $X(t)$ in (13) is trivially integrated, and then

substituted into the equation for $Y(t)$ in (13), which is solved by quadrature:

$$\begin{cases} X(t) = \displaystyle\int_0^t w(s)\,ds + \sqrt{2\kappa}\,W_x(t), \\ Y(t) = \displaystyle\int_0^t v(X(s),s)\,ds + \sqrt{2\kappa}\,W_y(t). \end{cases} \tag{14}$$

Consequently, the tracer position $(X(t), Y(t))$ can be expressed as an explicit functional of the random fields [46, Sec. 3]. Alternatively, the Green's function for the advection-diffusion equation (before averaging over the velocity statistics) can be written precisely in terms of a functional average over an ensemble of Wiener processes [2].

Writing out the explicit expression for $Y(t)$ from (14), breaking up the full average into successive averages over the statistics of $W_y(t)$, $W_x(t)$, and $v(x,t)$, and pulling out factors which are independent of the inner partial averages, we have:

$$\begin{aligned} \hat{G}(k,p,t) &= \left\langle \exp\left[-ikX(t) - ip\left(\int_0^t v(X(s),s)\,ds + \sqrt{2\kappa}W_y(t)\right)\right]\right\rangle \\ &= \left\langle e^{-ikX(t)} \left\langle \exp\left[-ip\int_0^t v(X(s),s)\,ds\right]\right\rangle_v \right\rangle_{w,W_x} \left\langle e^{-ip\sqrt{2\kappa}W_y(t)}\right\rangle_{W_y}. \end{aligned}$$

Subscripts on the averaging symbol $\langle\cdot\rangle$ denote a partial average over the stochastic process(es) listed. The averages over v and W_y (with $X(t)$ held fixed in a given realization) are each characteristic functions of Gaussian random variables which can be computed explicitly [23, Sec. 2.13]:

$$\begin{aligned} &\hat{G}(k,p,t) = e^{-\kappa p^2 t} \\ &\times \left\langle e^{-ikX(t)} \exp\left[-\frac{1}{2}p^2\int_0^t\int_0^t R_v(X(s)-X(s'),s-s')\,ds\,ds'\right]\right\rangle_{w,W_x}. \end{aligned} \tag{15}$$

We are not aware of how to perform the average in (15) explicitly in the general case, but this expression will be used to compute the cumulants in Subsection 2.3. Note also that for somewhat trivial case where the shearing component of the flow has white-noise temporal dynamics ($R_v(x,t) = \bar{R_v}(x)\delta(t)$), the average in (15) can be computed to give

$$\hat{G}(k,p,t) = \mathrm{e}^{-k^2(\kappa t + \int_0^t ds\ (t-s)R_w(s)\,ds - p^2(\kappa + \frac{1}{2}\bar{R}_v(0))t}, \tag{16}$$

implying that the process $(X(t), Y(t))$ is Gaussian, with no statistical influence of $X(t)$ on $Y(t)$ (i.e. no statistical coupling between the sweeping and the shearing components of the flow). Another straightforward consequence of Eq. (15) is that the characteristic function corresponding to the

random process $X(t)$ alone is given by

$$\hat{G}_x(k,t) \equiv \hat{G}(k,p=0,t) = \mathrm{e}^{-k^2(\kappa t + \int_0^t (t-s)R_w(s)ds)}. \tag{17}$$

In particular, $X(t)$ is a Gaussian random process.

2.3 Cumulants for the general case

A great deal of information about the PDF for the tracer displacement can be obtained by considering the cumulants defined in terms of the characteristic function $\hat{G}(k,p,t)$ as

$$\mu_{a,b}(t) = (-i)^{a+b} \left[\frac{\partial^{a+b}}{\partial k^a \partial p^b} \ln \hat{G}(k,p,t) \right]_{k=p=0}, \tag{18}$$

where a and b are nonnegative integers. The cumulants $\mu_{a,b}(t)$ are sometimes equivalently defined as the "connected" parts of the moments $\langle X^a(t) Y^b(t) \rangle$ [59]. The cumulants contain the same information as the moments themselves, but are easier to interpret because a cumulant of a given order (a,b) is constructed in such a way as to give information not redundant with that provided by the cumulants of lower order. For instance, in the SFCS model, we have (see Proposition 1 below)

$$\begin{cases} \mu_{0,2}(t) = \langle Y^2(t) \rangle, \\ \mu_{0,4}(t) = \langle Y^4(t) \rangle - 3\langle Y^2(t) \rangle^2. \end{cases}$$

Thus, $\mu_{0,2}(t)$ is the mean square displacement of the tracer in the shear-parallel (y) direction, while $\mu_{0,4}(t)$ is a measure of the departure from Gaussianity of the PDF of $Y(t)$ since a Gaussian PDF for $Y(t)$ would have $\mu_{0,4}(t) = 0$. We shall compare the performance of the closure approximations on a set of cumulants broader than $\mu_{0,2}(t)$ and $\mu_{0,4}(t)$ (see Proposition 1 below) but we will focus mainly on these since they provide a severe test for the closure approximations (see Section 5).

The cumulants of the tracer displacement in the SFCS model can be computed exactly using Eq. (18) and the expression in (15) for $\hat{G}$. For simplicity we shall only give explicit expressions for a selected subset of them:

Proposition 1

$$
\begin{cases}
\mu_{a,b}(t) = 0 \text{ when } a \text{ or } b \text{ is odd,} \\
\mu_{2,0}(t) = 2\kappa t + 2\displaystyle\int_0^t (t-s) R_w(s) ds, \\
\mu_{a,0}(t) = 0 \text{ for } a \geq 3, \\
\mu_{0,2}(t) = 2\kappa t + 4\displaystyle\int_0^t ds\ (t-s) \int_0^\infty dq\ E(q,s) e^{-\frac{1}{2}q^2 \mu_{2,0}(s)}, \\
\mu_{2m,2}(t) = 2(-)^m \displaystyle\int_0^t ds \int_0^s ds'\ M_x^{2m}(t,0;s,s') \\
\qquad\qquad \times \displaystyle\int_{\mathbf{R}} dq\ q^{2m} E(q, s-s')\, \mathrm{e}^{-\frac{1}{2}q^2 \mu_{2,0}(s-s')} \quad \text{for } m \geq 1, \\
\mu_{0,4}(t) = 3\displaystyle\int_0^t ds_1 \int_0^t ds_2 \int_0^t ds_3 \int_0^t ds_4 \int_{\mathbf{R}^2} dq\, dq' \\
\qquad\qquad \times E(q, s_1 - s_2) E(q', s_3 - s_4) \left(e^{-qq' M_x(s_1,s_2;s_3,s_4)} - 1 \right) \\
\qquad\qquad \times e^{-\frac{1}{2}q^2 \mu_{2,0}(s_1 - s_2) - \frac{1}{2}q'^2 \mu_{2,0}(s_3 - s_4)},
\end{cases}
\tag{19}
$$

where

$$
M_x(t_1, t_2; t_3, t_4) = \int_{t_2}^{t_1} ds \int_{t_4}^{t_3} ds'\ \left(R_w(s-s') + 2\kappa\delta(s-s') \right), \tag{20}
$$

This proposition is derived in Appendix B. We observe the following:

1. The mean-square displacement of a tracer in the shear-parallel (y) direction, $\mu_{0,2}(t)$, is extensively analyzed for the present model in [46, Secs. 3.2,3.3]. Here we mention only that the random fluctuations in the cross-shear transport, reflected in $\mu_{2,0}(t)$, clearly serve to reduce the efficacy of transport in the shear-parallel direction.

2. It is evident from the formulas for $\mu_{0,2}(t)$ and $\mu_{0,4}(t)$ in (19) that $\mu_{0,2}(t) > 0$ and $\mu_{0,4}(t) > 0$ when $E(q,t) \geq 0$, and there is some random cross-shear transport ($\kappa > 0$ or $w(t) \neq 0$). Of course, we know from first principles that $\mu_{0,2}(t)$ is non-negative in general because it is the variance of the shear-parallel tracer displacement, and only vanishes if there are no random fluctuations. More interestingly, one can prove by abstract probabilistic reasoning that $\mu_{0,4}(t)$ is non-negative in general for the SFCS model, and is positive whenever $\kappa > 0$ or $w(t) \neq 0$. A positive value for $\mu_{0,4}(t)$ indicates a PDF which is broader-than-Gaussian, meaning that the shear-parallel tracer displacement has a larger probability for large excursions relative to its standard deviation than a Gaussian distribution would. The reason why $\mu_{0,4}(t) \geq 0$ in the SFCS model is that the shear-parallel

tracer displacement $Y(t)$ in (14), conditioned on a particular realization of $X(t)$, is a mean zero Gaussian random variable. Averaging then over $X(t)$, we find that $Y(t)$ can be represented as a random mixture of mean-zero Gaussian random variables. All fourth and higher even order cumulants for such a random mixture are zero if all the variances of the Gaussian random variables coincide, and strictly positive otherwise [46, p. 466].

3. Suppose we start with a system with no molecular diffusion. Then the addition of molecular diffusivity $\kappa > 0$ is equivalent to making everywhere the following replacements in the formulas for the statistics of a single tracer:

$$\begin{cases} R_w(t) \to R_w(t) + 2\kappa\delta(t), \\ E(k,t) \to E(k,t) + 2\kappa\delta(k)\delta(t). \end{cases} \tag{21}$$

The transformation for $E(k,t)$ is associated with the following transformation to the physical-space correlation function of the shear flow:

$$R_v(x,t) \to R_v(x,t) + 2\kappa\delta(t).$$

The reader will note from Proposition 1 that κ only enters the cumulants $\mu_{2,0}(t)$ and $\mu_{0,2}(t)$, and can verify that indeed the formulas for the other cumulants are invariant under the transformation (21). The above transformation properties of the tracer statistics under molecular diffusion may be summarized by saying that molecular diffusion acts equivalently as an independent Gaussian random sweeping motion (in both x and y directions) which is delta-correlated in time, i.e. *white noise*. Indeed this is evident from the stochastic differential equations for the trajectory (14).

3 Some Closure Approximations for the Model

In this section we apply five closure approximations to the advection-diffusion equation (1) associated with the SFCS flow. The general formalism of the closure approximations are derived in Appendix A. We examine here the basic properties of the equations and solutions which these closure approximations generate, and compare them with the exact results developed in Section 2. Our main conclusions are:

- the QLA and QNA suffer from a qualitative failure to represent the important physical influence of the random cross sweep on the tracer transport along the shear.
- the DIA performs better than the QLA and QNA in this respect, though it does not produce exact results even for the low order cumulants. The DIA also gives rather complicated equations which are difficult to analyze even for the second order cumulants.
- the MDIA matches the exact results for the passive scalar statistics in a larger class of flows within the Shear Flow with Cross Sweep model and to a greater extent than any other closure approximations considered.
- the RLA is a relatively simple closure approximation which produces exact predictions for the cumulants of the tracer displacement through third order, but oversimplifies the higher order statistics by always predicting a Gaussian PDF.

More detailed analytical assessments of these closure approximations will follow in subsequent sections.

The basic structure of the equations produced by the closure approximations are most readily grasped when there is no molecular diffusion ($\kappa = 0$), so in the discussion of each closure approximation we begin first with the equations for this case. The full equations, including the possibility $\kappa > 0$, will be presented at the end of each subsection on a closure approximation, and will be utilized in subsequent sections.

The following quantities defined in terms of the correlation functions of the sweeping and the shearing components of the velocity field enter the formulas below repeatedly:

$$\begin{cases} D_x^{(0)}(t) = \displaystyle\int_0^t R_w(s)ds, \\ D_y^{(0)}(t) = \displaystyle\int_0^t R_v(0,s)ds = \int_0^t \int_{\mathbf{R}} E(q,s)dqds, \\ D_y^{(\kappa)}(t) = \displaystyle\int_0^t \int_{\mathbf{R}} E(q,s)e^{-\kappa q^2 s}dqds. \end{cases} \tag{22}$$

They are just the exact time-dependent diffusivities in the x and y directions; the (0) subscript indicates a specialization to the case $\kappa = 0$.

3.1 The quasinormal approximation (QNA)

Historically the QNA was the first closure approximation introduced [10, 11, 57, 62, 66]. The QNA bears its name from the fact that it utilizes an (uncontrolled) assumption of Gaussianity for the evaluation of the triple moment, $\langle \boldsymbol{v}\boldsymbol{v}T\rangle \approx \langle \boldsymbol{v}\boldsymbol{v}\rangle\langle T\rangle$, in the equation for the second order moment $\langle \boldsymbol{v}T\rangle$. In terms of the Green's function, the QNA equation leads at $\kappa = 0$ to a convolutive linear differential equation for $\hat{G}_{\mathrm{QNA}} = \hat{G}_{\mathrm{QNA}}(k,p,t)$:

$$\begin{aligned}\frac{\partial \hat{G}_{\mathrm{QNA}}}{\partial t} = &-k^2 \int_0^t R_w(s)\hat{G}_{\mathrm{QNA}}(k,p,t-s)ds \\ &- p^2 \int_0^t R_v(0,s)\hat{G}_{\mathrm{QNA}}(k,p,t-s)ds,\end{aligned} \tag{23}$$

with $\hat{G}_{\mathrm{QNA}}|_{t=0} = 1$ and where we have used Eq. (6) to set $\int_{\mathbf{R}} E(q,t)\,dq = R_v(0,t)$. See Appendix A.1 below for a general derivation of Eq. (23). The QNA equation is naturally solved via a Laplace transform, generally defined by

$$\tilde{f}(\zeta) = \int_0^\infty \mathrm{e}^{-\zeta t} f(t)dt,$$

to give:

$$\tilde{G}_{\mathrm{QNA}}(k,p,\zeta) = \left[\zeta + k^2\tilde{R}_w(\zeta) + p^2\tilde{R}_v(0,\zeta)\right]^{-1}. \tag{24}$$

The Laplace transform of the cumulants of the passive scalar displacement can be computed from derivatives of $\ln \tilde{G}_{\mathrm{QNA}}(k,p,\zeta)$. In the time representation, the expressions for the $\mu^{\mathrm{QNA}}_{2m,2n}(t)$ are rather cumbersome and we only give the expressions for the first few:

$$\begin{cases} \mu^{\mathrm{QNA}}_{2,0}(t) = 2\displaystyle\int_0^t D_x^{(0)}(s)ds, \\ \mu^{\mathrm{QNA}}_{0,2}(t) = 2\displaystyle\int_0^t D_y^{(0)}(s)ds, \\ \mu^{\mathrm{QNA}}_{4,0}(t) = 24\displaystyle\int_0^t\int_0^s D_x^{(0)}(s-s')D_x^{(0)}(s')ds'ds - 12\left(\int_0^t D_x^{(0)}(s)ds\right)^2, \\ \mu^{\mathrm{QNA}}_{0,4}(t) = 24\displaystyle\int_0^t\int_0^s D_y^{(0)}(s-s')D_y^{(0)}(s')ds'ds - 12\left(\int_0^t D_y^{(0)}(s)ds\right)^2. \end{cases} \tag{25}$$

The equation in (25) for the mean-square displacement $\mu^{\mathrm{QNA}}_{2,0}(t)$ of the tracer across the shear is exact. However, looking back at the exact formulas in (19) and (20), we see that the other predictions would only generally

be correct for the trivial model in which both the sweeping and shearing components of the flow are white noise processes.

The most serious drawback of the QNA exhibited here is its complete failure to represent any effects of the randomly fluctuating cross sweep $w(t)$ on the transport along the shear; the components $X(t)$ and $Y(t)$ of the trajectory are predicted to be independent of each other. In particular, the mean-square displacement $\mu_{0,2}^{\mathrm{QNA}}(t)$ of the tracer along the shear completely misses the important factor $\mathrm{e}^{-\frac{1}{2}k^2\mu_{2,0}(s)}$ (see Eq. (19)) which represents the inhibition of the transport along the shear due to the tracer being randomly swept across streamlines. Furthermore, the QNA wrongly predicts the higher order statistics of the displacement $X(t)$ along the sweeping direction to be non-Gaussian.

Special Exact Solution. We note further that an explicit formula for the QNA prediction of the physical-space Green's function, $G_{x,\mathrm{QNA}}(x,t) = \int_{\mathbf{R}} G_{\mathrm{QNA}}(x,y,t)\,dy$, describing the PDF for $X(t)$ can be obtained by inversion of this Laplace transform for the special case in which the random sweeping field $w(t)$ is *steady*, i.e. a random time-independent constant w_*. The power spectrum and correlation function of $w(t)$ may then be written as

$$R_w(t) \equiv \sigma_{w_*}^2, \tag{26}$$

where σ_{w_*} is the standard deviation of the mean-zero Gaussian random distribution for the constant value of w_*. Noting that $\tilde{R}_w(\zeta) = \sigma_{w_*}^2\zeta^{-1}$ and that $G_{x,\mathrm{QNA}}(x,t)$ is the inverse Fourier-Laplace transform of $\tilde{G}_{\mathrm{QNA}}(k,p=0,\zeta)$, we find the following explicit QNA prediction [21] for the steady random sweep model:

$$G_{\mathrm{QNA}}(x,t) = \frac{1}{2}\left(\delta(x-\sigma_{w_*}t) + \delta(x+\sigma_{w_*}t)\right), \tag{27}$$

which is just the Green's function for a random steady sweep model with a probability density for the steady random sweep w_* given by

$$p(w) = \frac{1}{2}\left(\delta(w-\sigma_{w_*}) + \delta(w+\sigma_{w_*})\right).$$

This shows that the QNA predictions for the statistics of $X(t)$ are *realizable* for the case of a steady random sweep, in the sense that the predictions are consistent with a well-defined probabilistic model for the velocity field (though it differs from the Gaussian statistics assumed in the Shear Flow with Cross Sweep model). We are not aware of any statistical models underlying the QNA predictions for the general case of a random sweep $w(t)$ which fluctuates in time.

QNA with Molecular Diffusion. The QNA equation, generalized to include the possibility of molecular diffusion, reads:

$$\begin{aligned}\frac{\partial \hat{G}_{\mathrm{QNA}}}{\partial t} &= -\kappa(k^2+p^2)\hat{G}_{\mathrm{QNA}}(k,p,t) \\ &\quad - k^2\int_0^t e^{-\kappa(k^2+p^2)s}R_w(s)\hat{G}_{\mathrm{QNA}}(k,p,t-s)ds \\ &\quad - p^2\int_0^t\Big(\int_{\mathbf{R}} E(q,s)e^{-\kappa((k-q)^2+p^2)s}dq\Big)\hat{G}_{\mathrm{QNA}}(k,p,t-s)ds,\end{aligned} \tag{28}$$

The solution may be represented via a Laplace transform as

$$\tilde{G}_{\mathrm{QNA}}(k,p,\zeta) = \Big[\zeta + k^2\tilde{A}_{\mathrm{QNA}}(k,p,\zeta) + p^2\tilde{B}_{\mathrm{QNA}}(k,p,\zeta)\Big]^{-1},$$

where

$$\begin{cases} \tilde{A}_{\mathrm{QNA}}(k,p,\zeta) = \kappa + \tilde{R}_w(\zeta+\kappa(k^2+p^2)), \\ \tilde{B}_{\mathrm{QNA}}(k,p,\zeta) = \kappa + \displaystyle\int_{\mathbf{R}} \tilde{E}(q,\zeta+\kappa[(k-q)^2+p^2])dq. \end{cases}$$

Some important cumulants are:

$$\begin{cases} \mu_{2,0}^{\mathrm{QNA}}(t) = 2\kappa t + 2\displaystyle\int_0^t D_x^{(0)}(s)ds, \\ \mu_{0,2}^{\mathrm{QNA}}(t) = 2\kappa t + 2\displaystyle\int_0^t D_y^{(\kappa)}(s)ds, \\ \mu_{4,0}^{\mathrm{QNA}}(t) = 24\displaystyle\int_0^t\int_0^s D_x^{(0)}(s-s')D_x^{(0)}(s')ds'ds - 12\left(\int_0^t D_x^{(0)}(s)ds\right)^2, \\ \mu_{0,4}^{\mathrm{QNA}}(t) = 24\displaystyle\int_0^t\int_0^s D_y^{(\kappa)}(s-s')D_y^{(\kappa)}(s')ds'ds - 12\left(\int_0^t D_y^{(\kappa)}(s)ds\right)^2. \end{cases} \tag{29}$$

We note that the QNA formulas undergo an additional nontrivial transformation beyond that prescribed by the exact transformation laws (21) under the addition of molecular diffusivity. The further change causes the tracer motion along the shearing direction to feel the inhibiting effects due to molecular diffusion acting across the streamlines (through the factor $e^{-\kappa(k-q)^2 s}$ multiplying $E(q,s)$ in (28)), whereas the the tracer motion along the shearing direction feels no effects of the random sweep $w(t)$ across the streamlines. In particular, the QNA formulas are more accurate when molecular diffusion is treated in the advection-diffusion equation through a deterministic operator $\kappa\Delta$ instead of through a random advection term $\sqrt{2\kappa}u_x(t)\partial/\partial x + \sqrt{2\kappa}u_y(t)\partial/\partial y$ with $u_x(t)$ and $u_y(t)$ each independent

white noise, whereas either of these approaches should produce equivalent results for the Green's function under an exact treatment. For example, the formula in (29) for the mean-square tracer displacement $\mu_{0,2}^{\mathrm{QNA}}(t)$ differs from the exact result in (19) only by missing the factor $e^{-k^2\int_0^t (t-s)R_w(s)ds}$ representing the influence of the random cross sweep. The reason for the different treatment of a rapidly decorrelating cross sweep $w(t)$ and molecular diffusion can be traced to the fact that molecular diffusion will enter the "bare" operator $H_0(t|t')$ appearing in the QNA formula (158) in Appendix A, whereas a randomly fluctuating cross sweep does not.

We therefore conclude that the QNA will automatically be a poor approximation whenever the random cross sweep $w(t)$ plays an important role in influencing the shear-parallel transport. But when $w(t)$ is either absent or negligible relative to other cross-shear transport processes (see Section 4), the QNA may be viable. While the formulas for the higher order cumulants along the shear, $\mu_{0,2n}^{\mathrm{QNA}}(t)$, are not exact for $n \geq 2$ even when $w(t) = 0$, it is not clear by simple inspection how far they deviate from the exact results. We will therefore focus our asymptotic studies in Sections 4 and 5 on how well the QNA performs for the case where $w(t)$ is negligible.

3.2 The quasilinear approximation (QLA)

The QLA was introduced about at the same time as the QNA, and may be viewed as its convolution-free analogue [64, 65, 66]. Both equations are obtained at the same order of truncation of two exact (but formal) series representations for the kernel appearing in the equation for the Green's function (see Appendix A). The QLA leads to the following equation when $\kappa = 0$:

$$\frac{\partial \hat{G}_{\mathrm{QLA}}}{\partial t} = -\big(k^2 D_x^{(0)}(t) + p^2 D_y^{(0)}(t)\big)\hat{G}_{\mathrm{QLA}}, \tag{30}$$

with $\hat{G}_{\mathrm{QLA}}|_{t=0} = 1$ and again $\int_{\mathbf{R}} E(q,t)dq = R_v(0,t)$ has been used. The QLA equation takes the form of a linear diffusion equation with time-dependent diffusivities $D_x^{(0)}(t)$ and $D_y^{(0)}(t)$ in the x and y directions, and involves no convolutions. The solution of Eq. (30) is

$$\hat{G}_{\mathrm{QLA}}(k,p,t) = \mathrm{e}^{-k^2\int_0^t D_x^{(0)}(s)ds - p^2\int_0^t D_y^{(0)}(s)ds}. \tag{31}$$

Hence, according to the QLA, there are only two non-zero cumulants

$$\begin{cases} \mu_{2,0}^{\mathrm{QLA}}(t) = 2\displaystyle\int_0^t D_x^{(0)}(s)ds, \\ \mu_{0,2}^{\mathrm{QLA}}(t) = 2\displaystyle\int_0^t D_y^{(0)}(s)ds \end{cases} \tag{32}$$

The QLA therefore is exact insofar as the sweeping motion $X(t)$ of the tracer is concerned (which is an improvement over the QNA), but completely misses the effects of the sweeping on the tracer displacement $Y(t)$ along the shear in the same way that the QNA does. Therefore the QLA is exact precisely when there is no sweeping or the shear flow is either spatially uniform or a white noise process in time so that the sweeping would have no influence on the transport along the shear. Put differently, for any SFCS model flow, the QLA predicts statistics of the tracer as if the flow were spatially uniform with the same Gaussian temporal statistics as the actual flow, i.e.

$$\boldsymbol{v}^{\mathrm{QLA}}(x,y,t) = \begin{pmatrix} w(t) \\ v(0,t) \end{pmatrix}. \tag{33}$$

Thus, the QLA is a relevant approximation if the time-decorrelation associated with the shearing component of the flow is so strong that the sweeping effects can be neglected. Moreover, the QLA will always produce *realizable* predictions, in the sense that they are consistent with some well-defined underlying probabilistic model for the velocity field (33) (though it differs from the exact statistics of the SFCS model).

QLA with Molecular Diffusion. Generalized to include the effect of molecular diffusion, the QLA equation becomes:

$$\frac{\partial \hat{G}_{\mathrm{QLA}}}{\partial t} = -\big(k^2(\kappa + D_x^{(0)}(t)) + p^2(\kappa + D_y^{(\kappa)}(k,t))\big)\hat{G}_{\mathrm{QLA}}, \tag{34}$$

where

$$D_y^{(\kappa)}(t) = \int_0^t \int_{\mathbf{R}} E(q,s) e^{-\kappa(q^2 - 2kq)s} dq ds. \tag{35}$$

Its solution is:

$$\hat{G}_{\mathrm{QLA}}(k,p,t) = e^{-k^2\left(\kappa t + \int_0^t D_x^{(0)}(s)ds\right) - p^2\left(\kappa t + \int_0^t D_y^{(\kappa)}(s)ds\right)}, \tag{36}$$

and the only nontrivial cumulants involving the statistics of $X(t)$ and $Y(t)$ separately are:

$$\begin{cases} \mu_{2,0}^{\mathrm{QLA}}(t) = 2\kappa t + 2\displaystyle\int_0^t D_x^{(0)}(s)ds, \\ \mu_{0,2}^{\mathrm{QLA}}(t) = 2\kappa t + 2\displaystyle\int_0^t D_y^{(\kappa)}(s)ds. \end{cases} \tag{37}$$

Therefore, $X(t)$ and $Y(t)$ are each Gaussian random processes, but their *joint statistics* are predicted to be non-Gaussian because mixed cumulants such as

$$\mu_{2m,2}^{\mathrm{QLA}}(t) = 2(-)^m \int_0^t (t-s)(2\kappa s)^{2m} \int_{\mathbf{R}} q^{2m} E(q,s) \mathrm{e}^{-\kappa q^2 s} dq ds$$

are nonzero when $\kappa \neq 0$.

Like the QNA, the QLA undergoes a further nontrivial transformation beyond that prescribed for the exact statistics (21) under the addition of molecular diffusion. Molecular diffusion is also handled much more accurately in the QLA when represented by the deterministic operator $\kappa\Delta$ than with a white noise advection operator $\sqrt{2\kappa}u_x(t)\partial/\partial x + \sqrt{2\kappa}u_y(t)\partial/\partial y$. Indeed, the full statistics of $X(t)$ as well as all the cumulants $\mu_{a,2}(t)$ are correctly predicted by the QLA whenever $w(t) = 0$. Cumulants $\mu_{a,b}(t)$ with $b \geq 4$ however are not exactly predicted by the QLA except for the trivial case that the shear flow has no spatial variation or is white noise in time. The extent to which the QLA prediction that $\mu_{0,4}^{\mathrm{QLA}}(t) = 0$ departs from the exact result when $w(t) = 0$ will be examined through large-scale, long-time asymptotics in Sections 4 and 5.

3.3 The direct interaction approximation (DIA)

The DIA was introduced by Kraichnan [29, 30, 31] to remedy some defects of the QNA in the context of hydrodynamic turbulence, and was applied to passive scalar advection by Roberts [60]. Roughly speaking, the DIA belongs to the same class of approximations as the QNA but it involves a further resummation before truncation of the series expansion for the kernel appearing in the equation for the Green's function (see Appendix A). The DIA leads to the following equation when $\kappa = 0$:

$$\begin{aligned}\frac{\partial \hat{G}_{\mathrm{DIA}}}{\partial t} &= -k^2 \int_0^t R_w(t-s)\hat{G}_{\mathrm{DIA}}(k,p,t-s)\hat{G}_{\mathrm{DIA}}(k,p,s)ds \\ &\quad -p^2 \int_0^t \Big(\int_{\mathbf{R}} E(q,t-s)\hat{G}_{\mathrm{DIA}}(k-q,p,t-s)dq \Big) \hat{G}_{\mathrm{DIA}}(k,p,s)ds,\end{aligned} \tag{38}$$

with $\hat{G}_{\mathrm{DIA}}|_{t=0} = 1$. This equation involves a convolution of the approximate Green's function with itself and the energy spectrum. Even for our simple model, the analytical solution of Eq. (38) for general $E(k,t)$ is not available. We simply note that the formal solution of Eq. (38) may be written in the Laplace representation as

$$\tilde{G}_{\mathrm{DIA}}(k,p,\zeta) = \Big[\zeta + k^2 \tilde{A}_{\mathrm{DIA}}(k,p,\zeta) + p^2 \tilde{B}_{\mathrm{DIA}}(k,p,\zeta) \Big]^{-1}, \tag{39}$$

where the new functions $\tilde{A}_{\mathrm{DIA}}(k,p,\zeta)$ and $\tilde{B}_{\mathrm{DIA}}(k,p,\zeta)$ satisfy the following equations equivalent to Eq. (38):

$$\begin{cases} \tilde{A}_{\mathrm{DIA}}(k,p,\zeta) = \dfrac{1}{2\pi i} \displaystyle\int_{\mathcal{C}} \tilde{R}_w(\zeta')\hat{\tilde{G}}(k,p,\zeta-\zeta')d\zeta', \\ \tilde{B}_{\mathrm{DIA}}(k,p,\zeta) = \dfrac{1}{2\pi i} \displaystyle\int_{\mathbf{R}} \int_{\mathcal{C}} \tilde{E}(q,\zeta')\hat{\tilde{G}}(k-q,p,\zeta-\zeta')d\zeta' dq. \end{cases} \tag{40}$$

The integrals over the variable ζ' are to be taken along a Bromwich contour $\mathcal{C}$ in the complex plane which lies parallel to the imaginary axis and intersects the real axis at any point between 0 and Re ζ.

The evaluation of the DIA predictions for even the simplest cumulants appears to be rather complicated due to the nonlinear implicit relationship in (39) and (40) for the DIA Green's function. The Laplace transform of the cumulants of the sweeping component $X(t)$ of the tracer motion can be obtained recursively, and lead to the following DIA predictions in the time representation:

$$\left\{\begin{array}{l} \mu_{2,0}^{\mathrm{DIA}}(t) = 2\displaystyle\int_0^t D_x^{(0)}(s)ds, \\ \mu_{4,0}^{\mathrm{DIA}}(t) = 24\displaystyle\int_0^t\int_0^s \Big[D_x^{(0)}(s-s')D_x^{(0)}(s') - D_x^{(0)}(s)D_x^{(0)}(s') \\ \qquad\qquad +(t-s)R_w(s)D_x^{(0)}(s')\Big]\, ds'ds. \end{array}\right. \tag{41}$$

We are unaware of how to formulate a closed expression for the DIA predictions of cumulants $\mu_{a,b}^{\mathrm{DIA}}(t)$ with $b \geq 2$. For example, the formal expression obtained for the Laplace transform of the mean-square displacement along the shear flow from differentiation of Eq. (39) is:

$$\tilde{\mu}_{0,2}^{\mathrm{DIA}}(\zeta) = \frac{1}{i\pi\zeta^2}\int_{\mathbf{R}}\int_{\mathcal{C}} \frac{\tilde{E}(q,\zeta')}{\zeta - \zeta' + q^2\tilde{A}_{\mathrm{DIA}}(-q,0,\zeta-\zeta')}d\zeta' dq. \tag{42}$$

This expression is not closed since it involves $\tilde{A}_{\mathrm{DIA}}(-q,0,\zeta-\zeta')$ which, from (40), is the solution to the nonlinear integral relation:

$$\tilde{A}_{\mathrm{DIA}}(k,0,\zeta) = \frac{1}{2\pi i}\int_{\mathcal{C}} \frac{\tilde{R}_w(\zeta')}{\zeta - \zeta' + k^2\tilde{A}_{\mathrm{DIA}}(k,0,\zeta-\zeta')}d\zeta'. \tag{43}$$

The only case for which we know how to solve this equation are the extreme cases in which the random cross sweep $w(t)$ is either white noise or a steady random constant. The case of white noise sweeping is, as we shall see and discuss below, equivalent under the the DIA to the action of molecular diffusion. In the case of a steady random constant $w(t) = w_*$, with energy spectrum and correlation function given by Eq. (26), we have $\tilde{R}_w(\zeta) = \sigma_{w_*}^2\zeta^{-1}$ so that $\tilde{A}_{\mathrm{DIA}}(k,p,\zeta) = \sigma_{w_*}^2\tilde{G}_{\mathrm{DIA}}(k,p,\zeta)$ and Eq. (39) becomes a pointwise quadratic equation for $\tilde{G}_{x,\mathrm{DIA}}(k,\zeta) = \tilde{G}_{\mathrm{DIA}}(k,p=0,\zeta)$. Upon taking an inverse Fourier-Laplace transform on the resulting solution, we find [21, 31]

$$G_{x,\mathrm{DIA}}(x,t) = (\pi\sigma_{w_*}t)^{-1}\sqrt{(1-(x/2\sigma_{w_*}t)^2)_+},$$

where $(f)_+ \equiv \max(f, 0)$. This solution is the Green's function for a steady random sweep model with probability distribution for w_* given by a semi-circle distribution

$$p^{\mathrm{DIA}}_{w_*}(w) = (\pi\sigma_{w_*})^{-1}\sqrt{(1-(w/2\sigma_{w_*})^2)_+}.$$

Therefore, the DIA prediction for the statistics for $X(t)$ is realizable for a steady random sweep model. However, we will provide in Subsection 5.1 a class of fluctuating random sweep models for which the DIA may be shown explicitly to be unrealizable. We do not dwell further on the steady random constant case in this paper because its lack of ergodicity produces statistical artifacts (though it is of some interest as an extreme limiting case of a slowly decorrelating random sweep).

One main disadvantage of the DIA which has already become evident is that even when applied to simple models such as those considered in this paper, the equations can be difficult to solve. Indeed, it is not difficult to compute $\mu_{0,2}(t)$ exactly in the present model, whereas the DIA prediction for this quantity requires the solution of the nonlinear integral equation (43). On the other hand, the DIA does improve upon the simpler QNA in that the random cross sweep $w(t)$ does influence the shear-parallel transport under the DIA. The precise relationship predicted by the DIA is difficult to resolve, though we will see in Section 4 that correct scaling relationships between space and time variables are predicted at large scales and long times. Moreover, if the random sweep is white noise, the exact formula for $\mu_{0,2}(t)$ (but not higher order cumulants) is recovered. Provided the characteristic time-scale $\tau_\star$ associated with $w(t)$ is small enough, then, the DIA gives an approximation for the second moment of $y(t)$ which is qualitatively valid for times large compared with $\tau_\star$. In particular, assuming that

$$\lim_{\substack{\zeta\to 0^+\\ k\to 0}} \tilde{A}_{\mathrm{DIA}}(k,0,\zeta) = \int_0^\infty R_w(s)ds \quad \text{exists and is nonzero,} \tag{44}$$

the expression for the physical time representation of Eq. (42) may be estimated asymptotically as

$$\mu^{\mathrm{DIA}}_{0,2}(t) \sim 2\int_0^t (t-s)\int_{\mathbf{R}} E(q,s)\mathrm{e}^{-q^2 t\int_0^\infty R_w(s')ds'}dqds, \qquad \text{as } t\to\infty, \tag{45}$$

which can be compared with the exact result in (19). In other respects it is not clear how significantly the DIA improves upon the QNA. For example, both of these closure approximations correctly reproduce $\mu_{2,0}(t)$, whereas both wrongly predict (different) nonzero values for $\mu_{4,0}(t)$ corresponding to spurious non-Gaussian corrections to the statistics of $X(t)$. Like the QNA

equation (23), the full DIA equation (38) is exact only in the trivial case that both the sweeping components and shearing components of the flow are white-noise processes in time.

DIA with Molecular Diffusion. The DIA equation, generalized to include the possibility of molecular diffusion, reads:

$$\begin{aligned}\frac{\partial \hat{G}_{\mathrm{DIA}}}{\partial t} &= -\kappa(k^2+p^2)\hat{G}_{\mathrm{DIA}} \\ &\quad - k^2\int_0^t R_w(s)\hat{G}_{\mathrm{DIA}}(k,p,s)\hat{G}_{\mathrm{DIA}}(k,p,t-s)ds \\ &\quad - p^2\int_0^t \Big(\int_{\mathbf{R}} E(q,s)\hat{G}_{\mathrm{DIA}}(k-q,p,t-s)dq\Big)\hat{G}_{\mathrm{DIA}}(k,p,t-s)ds.\end{aligned} \tag{46}$$

In Laplace representation, this equation reads

$$\tilde{G}_{\mathrm{DIA}}(k,p,\zeta) = \Big[\zeta + k^2\tilde{A}_{\mathrm{DIA}}(k,p,\zeta) + p^2\tilde{B}_{\mathrm{DIA}}(k,p,\zeta)\Big]^{-1}, \tag{47}$$

where

$$\begin{cases} \tilde{A}_{\mathrm{DIA}}(k,p,\zeta) = \kappa + \dfrac{1}{2\pi i}\displaystyle\int_{\mathcal{C}} \tilde{R}_w(\zeta')\tilde{G}_{\mathrm{DIA}}(k,p,\zeta-\zeta')d\zeta', \\ \tilde{B}_{\mathrm{DIA}}(k,p,\zeta) = \kappa + \dfrac{1}{2\pi i}\displaystyle\int_{\mathbf{R}}\int_{\mathcal{C}} \tilde{E}(q,\zeta')\tilde{G}_{\mathrm{DIA}}(k-q,p,\zeta-\zeta')d\zeta' dq. \end{cases} \tag{48}$$

Since $\tilde{G}_{\mathrm{DIA}}(k,p=0,\zeta-\kappa k^2)$ is independent of κ, it follows that the cumulants $\mu_{a,0}(t)$ for $X(t)$ are identical to their $\kappa=0$ values in (41) except that:

$$\mu_{2,0}^{\mathrm{DIA}}(t) = 2\kappa t + 2\int_0^t D_x^{(0)}(s)ds. \tag{49}$$

We do not know how to evaluate the cumulants $\mu_{a,b}^{\mathrm{DIA}}(t)$ for $b=2$ in a general closed form, but it will suffice for our investigations to present the following formulas valid when $w(t)=0$:

$$\begin{cases} \mu_{0,2}^{\mathrm{DIA}}(t) &= 2\kappa t + 2\displaystyle\int_0^t D_y^{(\kappa)}(s)ds, \\ \mu_{0,4}^{\mathrm{DIA}}(t) &= 24\displaystyle\int_0^t\int_0^s D_y^{(\kappa)}(s-s')D_y^{(\kappa)}(s')ds'ds - 12\left(\int_0^t D_y^{(\kappa)}(s)ds\right)^2 \\ &\quad +24\displaystyle\int_0^t\int_0^s (t-s)(s-s') \\ &\quad\quad \times\displaystyle\int_{\mathbf{R}^2} E(q,s)E(q',s')e^{-\kappa q^2 s-\kappa(q'^2+2qq')s'}dq'dqds'ds. \end{cases} \tag{50}$$

The DIA formulas obey the exact transformation law (21) under the addition of molecular diffusion. While the DIA improves upon the QNA in taking the effects of $w(t)$ into account on the shear-parallel transport, the comparison of these approximations for the case $w(t) \equiv 0$ (but $\kappa > 0$) is less obvious. Their predictions for $\mu_{0,2}(t)$ agree and are correct, but their predictions for $\mu_{0,4}(t)$ differ. In Section 5, we will examine the accuracy of these approximations for $\mu_{0,4}(t)$ at long times in a steady shear with $\kappa > 0$, and find that there are situations in which the DIA prediction is worse even though the method is more sophisticated.

3.4 The modified direct interaction approximation (MDIA)

The MDIA was introduced in [68]. It belongs to the same class of approximation as the QLA, but involves a further resummation before truncation of the formal series expansion for the kernel in the equation for the Green's function. In this respect, the MDIA is to the QLA what the DIA is to the QNA. See Appendix A.4 below for a derivation. The MDIA leads to the following equation for $\kappa = 0$:

$$\frac{\partial \hat{G}_{\mathrm{MDIA}}}{\partial t} = -\big(k^2 D_x^{(0)}(t) + p^2 D_{y,\mathrm{MDIA}}^{(0)}(k,p,t)\big)\hat{G}_{\mathrm{MDIA}}, \tag{51}$$

where $\hat{G}_{\mathrm{MDIA}}|_{t=0} = 1$ and

$$D_{y,\mathrm{MDIA}}^{(0)}(k,p,t) = \int_0^t \int_{\mathbf{R}} E(q,s) \frac{\hat{G}_{\mathrm{MDIA}}(k-q,p,s)}{\hat{G}_{\mathrm{MDIA}}(k,p,s)} dq ds. \tag{52}$$

The MDIA equation for our SFCS model does not involve any time convolutions, but is not a simple diffusion equation because $D_{y,\mathrm{MDIA}}^{(0)}$ depends on the wavenumbers $(k,\ p)$, and is nonlinear because this coefficient depends on the solution $\hat{G}_{\mathrm{MDIA}}$. Equation (51) is equivalent to the following equation for the cumulant generating function $\rho = \ln \hat{G}_{\mathrm{MDIA}}$:

$$\frac{\partial^2 \rho_{\mathrm{MDIA}}}{\partial t^2} = -k^2 R_w(t) - p^2 \int_{\mathbf{R}} E(q,t) e^{\rho_{\mathrm{MDIA}}(k-q,p,t) - \rho_{\mathrm{MDIA}}(k,p,t)}\, dq, \tag{53}$$

with the initial condition $\rho_{\mathrm{MDIA}}|_{t=0} = \partial \rho_{\mathrm{MDIA}}/\partial t|_{t=0} = 0$. This equation is easily solved when $p = 0$:

$$\rho_{\mathrm{MDIA}}(k, p=0, t) = -\frac{1}{2} k^2 \mu_{2,0}(t), \tag{54}$$

which implies that $X(t)$ is predicted to be a Gaussian random process with mean zero and the exact variance:

$$\mu_{2,0}^{\mathrm{MDIA}}(t) = 2 \int_0^t D_x^{(0)}(s) ds.$$

The full analytical solution of Eq. (51) [or Eq. (53)] is not available, but equations for the cumulants of $\{X(t), Y(t)\}$ can be derived from Eq. (53). The procedure used hereafter could in principle be applied for obtaining equations for $\mu_{a,b}^{\mathrm{MDIA}}(t)$ for all $\{a, b\} \in \mathbb{N}^2$. However, the procedure becomes rapidly very cumbersome for the higher moments in the y-direction, and we shall only give the equations for $\mu_{2m,2}^{\mathrm{MDIA}}(t)$ for all $m \in \mathbb{N}$ and for $\mu_{0,4}^{\mathrm{MDIA}}(t)$.

Consider first $\mu_{0,2}^{\mathrm{MDIA}}(t)$. Using Eq. (53) and Eq. (54), it follows that this quantity satisfies the following second order ordinary differential equation

$$\frac{d^2}{dt^2}\mu_{0,2}^{\mathrm{MDIA}}(t) = 2\int_{\mathbf{R}} E(q,t)\mathrm{e}^{-\frac{1}{2}q^2\mu_{2,0}(t)}dq, \tag{55}$$

with the initial condition $\mu_{0,2}^{\mathrm{MDIA}}|_{t=0} = d\mu_{0,2}^{\mathrm{MDIA}}/dt|_{t=0} = 0$. Note that the exact formula $\mu_{0,2}(t)$ from Eq. (19) exactly satisfies Eq. (55) with the same initial conditions, so that $\mu_{0,2}^{\mathrm{MDIA}}(t) = \mu_{0,2}(t)$.

Consider next $\mu_{2m,2}(t)$. Using Eq. (53) and Eq. (54), we obtain:

$$\frac{d^2}{dt^2}\mu_{2m,2}^{\mathrm{MDIA}}(t) = 2(-)^m\mu_{2,0}^{2m}(t)\int_{\mathbf{R}} q^{2m}E(q,t)\mathrm{e}^{-\frac{1}{2}q^2\mu_{2,0}(t)}dq, \tag{56}$$

for the initial condition $\mu_{2m,2}^{\mathrm{MDIA}}|_{t=0} = d\mu_{2m,2}^{\mathrm{MDIA}}/dt|_{t=0} = 0$. The solution of this equation is

$$\mu_{2m,2}^{\mathrm{MDIA}}(t) = 2(-)^m\int_0^t (t-s)\mu_{2,0}^{2m}(s)\int_{\mathbf{R}} q^{2m}E(q,s)\mathrm{e}^{-\frac{1}{2}q^2\mu_{2,0}(s)}dqds. \tag{57}$$

Finally, consider $\mu_{0,4}^{\mathrm{MDIA}}(t)$. Using Eq. (53), we obtain

$$\frac{d^2}{dt^2}\mu_{0,4}^{\mathrm{MDIA}}(t) = -12\int_{\mathbf{R}} E(q,t)\mathrm{e}^{-\frac{1}{2}q^2\mu_{2,0}(t)}\left[\mu_{0,2}(t) + r(-q,t)\right]dq, \tag{58}$$

where $\mu_{0,4}^{\mathrm{MDIA}}|_{t=0} = d\mu_{0,4}^{\mathrm{MDIA}}/dt|_{t=0} = 0$ and we have defined

$$r(k,t) = \left[\frac{\partial^2}{\partial p^2}\rho(k,p,t)\right]_{p=0}. \tag{59}$$

Since it follows from Eq. (53) that $r(k,t)$ satisfies

$$\frac{\partial^2 r(k,t)}{\partial t^2} = -2\int_{\mathbf{R}} E(q,t)\mathrm{e}^{-\frac{1}{2}(q^2-2kq)\mu_{2,0}(t)}dq, \tag{60}$$

for the initial condition $r|_{t=0} = \partial r/\partial t|_{t=0} = 0$, we may combine Eqs. (55), (58), (60) to obtain

$$\begin{aligned}\frac{d^2}{dt^2}\mu_{0,4}^{\mathrm{MDIA}}(t) &= 24\int_0^t (t-s)\int_{\mathbf{R}^2} E(q,t)E(q',s) \\ &\quad \times\mathrm{e}^{-\frac{1}{2}q^2\mu_{2,0}(t)-\frac{1}{2}q'^2\mu_{2,0}(s)}\left(\mathrm{e}^{-qq'\mu_{2,0}(s)}-1\right)dq'dqds.\end{aligned} \tag{61}$$

Integrating by quadrature, we obtain

$$\mu_{0,4}^{\mathrm{MDIA}}(t) = 24 \int_0^t (t-s) \int_0^s (s-s') \int_{\mathbf{R}^2} E(q,s)E(q',s') \\ \times e^{-\frac{1}{2}q^2\mu_{2,0}(s)-\frac{1}{2}q'^2\mu_{2,0}(s')} \left(e^{-qq'\mu_{2,0}(s')} - 1\right) dq'dqds'ds. \tag{62}$$

This expression is exact if the shearing component of the flow is a white-noise. The validity of Eq. (62) will be further discussed below.

As mentioned above, the MDIA prediction for the statistics of $X(t)$ is exact, but the full statistics for $Y(t)$ are correctly predicted only for the trivial cases in which the shear flow is spatially uniform or a white noise noise process in time or when there is no sweeping at all. However, the mean-square displacement along the shear $\mu_{0,2}(t)$ is correctly predicted in general, and the cumulants $\mu_{a,2}(t)$ are correctly predicted whenever the random cross sweep $w(t)$ is a white noise process, whatever the statistics of the shear flow $v(x,t)$. In one sense, then, the MDIA performs the best of any closure approximation on the SFCS model because it recovers the exact results under more general conditions than any of the other closure approximations. The MDIA improves upon the QLA in the same way the DIA improves upon the QNA in taking into account the effect of the random cross sweep $w(t)$ on the motion of the tracer along the shear $Y(t)$ in a way which is exact to second order. We examine the MDIA predictions involving the higher order statistics of $Y(t)$ through large-scale, long-time asymptotic studies in Sections 4 and 5.

MDIA with Molecular Diffusion. Generalized to include the possibility of molecular diffusion, the MDIA equation becomes:

$$\frac{\partial \hat{G}_{\mathrm{MDIA}}}{\partial t} = -\big(k^2(\kappa + D_x^{(0)}(t) + p^2(\kappa + D_y^{(0)}(k,p,t))\big)\hat{G}_{\mathrm{MDIA}}, \tag{63}$$

It is readily verified from this equation that $\hat{G}_{\mathrm{MDIA}}(k,p,t)$ transforms under the addition of molecular diffusion through the exact transformation formula (21) so the formulas for the cumulants can be deduced from those

developed for the case $\kappa = 0$:

$$\left\{\begin{array}{l}
\mu_{2,0}^{\mathrm{MDIA}}(t) = \mu_{2,0}(t) = 2\kappa t + 2\displaystyle\int_0^t D_x^{(0)}(s)ds, \\
\mu_{a,0}^{\mathrm{MDIA}}(t) = 0 \text{ for } a \geq 3, \\
\mu_{0,2}^{\mathrm{MDIA}}(t) = 2\kappa t + 2\displaystyle\int_0^t \int_{\mathbf{R}} (t-s)E(q,s)\mathrm{e}^{-\frac{1}{2}q^2\mu_{2,0}(s)}dqds, \\
\mu_{2m,2}^{\mathrm{MDIA}}(t) = 2(-)^m \displaystyle\int_0^t (t-s)\mu_{2,0}^{2m}(s) \int_{\mathbf{R}} q^{2m}E(q,s)\mathrm{e}^{-\frac{1}{2}q^2\mu_{2,0}(s)}dqds, \\
\mu_{0,4}^{\mathrm{MDIA}}(t) = 24\displaystyle\int_0^t (t-s)\int_0^s (s-s')\int_{\mathbf{R}^2} E(q,s)E(q',s') \\
\qquad\qquad \times e^{-\frac{1}{2}q^2\mu_{2,0}(s)-\frac{1}{2}q'^2\mu_{2,0}(s')}\Big(e^{-qq'\mu_{2,0}(s')}-1\Big)\,dqdq'ds'ds.
\end{array}\right. \tag{64}$$

Because the MDIA statistics obey the exact transformation law (21), these formulas are exact under the same conditions as those discussed above for $\kappa = 0$. We will examine the accuracy of the MDIA prediction for $\mu_{0,4}^{\mathrm{MDIA}}(t)$ for some special submodels in Section 5.

3.5 The Renormalized Lagrangian Approximation (RLA)

The final closure approximation which we consider is derived within the same framework as the other closure approximations previously discussed (see Appendix A for a derivation). This Renormalized Lagrangian Approximation (RLA) bears its name from the fact that its governing equations can also be derived by expressing the effective diffusivity of the passive scalar field in terms of the Lagrangian velocity correlation function, and then computing this function by invoking the Corrsin assumption [13] that the cumulative tracer displacement and the velocity field are statistically independent [44, 61]). The RLA can also be viewed as a simplified variation of the abridged version of the Lagrangian History DIA (ALHDIA) which was introduced by Kraichnan [33] to remedy the inability of the DIA to predict the Kolmogorov $-5/3$ exponent for the energy spectrum in high Reynolds number Navier-Stokes turbulence [32]. A version of the ALHDIA especially designed for the passive scalar problem was later proposed in [36]. The RLA has much the same structure as the ALHDIA equation in [36] but is less complicated and easier to derive, especially for time-dependent velocity fields.

The RLA leads to the following equation when $\kappa = 0$:

$$\frac{\partial \hat{G}_{\mathrm{RLA}}}{\partial t} = -\big(k^2 D_x^{(0)}(t) + p^2 D_{y,\mathrm{RLA}}^{(0)}(t)\big)\hat{G}_{\mathrm{RLA}}, \tag{65}$$

where $\hat{G}_{\mathrm{RLA}}|_{t=0} = 1$ and

$$D^{(0)}_{y,\mathrm{RLA}}(t) = \int_0^t \int_{\mathbf{R}} E(q,s)\hat{G}_{\mathrm{RLA}}(-q,0,s)dqds. \tag{66}$$

The form of the RLA equation for the SFCS model is, in a way, of intermediate complexity between that of the QLA and the MDIA. Like the QLA, the RLA takes the form of a diffusion equation with time-dependent diffusivities $D^{(0)}_x(t)$ and $D^{(0)}_{y,\mathrm{RLA}}(t)$. However, the RLA equation is nonlinear, since the coefficient $D^{(0)}_{y,\mathrm{RLA}}(t)$ depends on the solution $\hat{G}_{\mathrm{RLA}}$, though in a simpler way than in the MDIA (see Eq. (52)).

The solution of Eq. (65) is

$$\hat{G}_{\mathrm{RLA}}(k,p,t) = \mathrm{e}^{-\frac{1}{2}k^2\mu_{2,0}(t)-\frac{1}{2}p^2\mu_{0,2}(t)}, \tag{67}$$

where $\mu_{2,0}(t)$ and $\mu_{0,2}(t)$ take their *exact* values

$$\begin{cases} \mu^{\mathrm{RLA}}_{2,0}(t) = 2\displaystyle\int_0^t D^{(0)}_x(s)ds, \mu_{2,0}(t) = 2\int_0^t (t-s)R_w(s)ds, \\ \mu^{\mathrm{RLA}}_{0,2}(t) = 2\displaystyle\int_0^t (t-s)\int_{\mathbf{R}} E(q,s)\mathrm{e}^{-\frac{1}{2}q^2\mu_{2,0}(s)}dqds. \end{cases} \tag{68}$$

All other cumulants are predicted to vanish by the RLA because the Green's function (67) is Gaussian. But this Gaussianity only holds for trivial cases in which the shear flow is spatially uniform or white noise in time or when there is no cross sweep $w(t) = 0$. The $X(t)$ statistics are always correctly predicted by the RLA.

RLA with Molecular Diffusion. The RLA can be generalized to include molecular diffusion as explained in Appendix A, and it is readily checked that the statistics transform according to the exact relationship (21):

$$\frac{\partial \hat{G}_{\mathrm{RLA}}}{\partial t} = -\big(k^2(\kappa + D^{(0)}_x(t)) + p^2(\kappa + D^{(0)}_{y,\mathrm{RLA}}(t))\big)\hat{G}_{\mathrm{RLA}}, \tag{69}$$

The exact solution is

$$\hat{G}_{\mathrm{RLA}}(k,p,t) = \mathrm{e}^{-\frac{1}{2}k^2\mu_{2,0}(t)-\frac{1}{2}p^2\mu_{0,2}(t)},$$

where the following cumulants predicted by the RLA agree with their exact values:

$$\begin{cases} \mu^{\mathrm{RLA}}_{2,0}(t) = \mu_{2,0}(t) = 2\kappa t + 2\displaystyle\int_0^t D^{(0)}_x(s)ds, \\ \mu^{\mathrm{RLA}}_{0,2}(t) = \mu_{0,2}(t) = 2\kappa t + 2\displaystyle\int_0^t (t-s)\int_{\mathbf{R}} E(q,s)\mathrm{e}^{-\frac{1}{2}q^2\mu_{2,0}(s)}dqds. \end{cases}$$

All other cumulants are predicted by the RLA to vanish. The RLA is exact whenever $w(t) = 0$ or if the shear flow is spatially uniform or white noise in time.

4 Renormalized Closure Equations for Large-Scale, Long-Time Behavior of Green's Functions

In applications, one is often most interested in the effective transport of a passive scalar field over large scales and long times. The small-scale, finite time evolution of the passive scalar field will depend of course on a variety of particulars of the geometry and statistics of the flow field. One can hope, however, that from a coarse-grained point of view, the passive scalar dynamics can be described by effective equations which depend on the flow field only through a small set of parameters. The simplest instance of this is when the velocity field has sufficiently short-range correlations in space and/or time so that *homogenization theory* applies [3, 19, 47, 49, 53, 56], and the Green's function for the tracer displacement can be shown rigorously to be well described by an ordinary diffusion equation at large scales and long times. The effects of the turbulent flow on large scales and long times is in this case completely described by its mean component and by some effective diffusivity tensor. Homogenization theory fails in the presence of strong long-range correlations in space and time, and in particular is inapplicable to fully developed turbulence. Nonetheless, one can hope that large scales and long times, some sort of practical effective equation might be derived which depends on only a few bulk or integrated properties of the velocity field.

We therefore will consider how the equations for the Green's function furnished by the various closure approximations behave when rescaled to large scales and long times [4]. We shall introduce rescaling factors α, λ, ρ, and A, which will be linked together in some way to be specified, so that we can generically consider α, λ, and A each as a function of ρ. Then working with a Fourier representation in space, we consider the evolution equation obeyed by the rescaled approximate Green's function:

$$\hat{G}^{(\rho)}_{\text{app}}(k,p,t) \equiv A(\rho)\hat{G}_{\text{app}}\left(k\alpha(\rho), p\lambda(\rho), t/\rho^2\right),$$

which corresponds to the physical-space rescaling:

$$G^{(\rho)}_{\text{app}}(x,y,t) = A(\rho)(\alpha(\rho))^{-1}(\lambda(\rho))^{-1}G_{\text{app}}\left(x/\alpha(\rho), y/\lambda(\rho), t/\rho^2\right).$$

We choose the relationships between the scaling factors so that $\hat{G}^{(\rho)}_{\text{app}}(k,p,t)$ converges to a finite limit as $\rho \to 0$, corresponding to a large-scale, long-time limit:

$$\hat{\bar{G}}_{\text{app}}(k,p,t) \equiv \lim_{\rho\to 0} \hat{G}^{(\rho)}_{\text{app}}(k,p,t).$$

We call this limiting Green's function the *renormalized* Green's function ([2, 5]); it plays the role of a "fixed point" in renormalization group termi-

nology. The rescaling factors indicate how we must link the coarse-graining in space and time to follow the nontrivial development of the dynamics. We can immediately see, by noting that $\hat{G}_{\rm app}(0,0,1) \equiv 1$, that the amplitude rescaling must always be trivial:

$$A = 1,$$

so the general rescaling procedure can be simplified to:

$$\hat{G}^{(\rho)}_{\rm app}(k,p,t) \equiv \hat{G}_{\rm app}\left(k\alpha(\rho), p\lambda(\rho), t/\rho^2\right). \tag{70}$$

If homogenization theory prevails and the passive scalar Green's function spreads diffusively in both x and y directions, then the corresponding "standard" scalings are:

$$\rho = \alpha = \lambda.$$

The passive scalar spreads superdiffusively across the shear when ρ vanishes more slowly than α, and superdiffusively along the shear when ρ vanishes more slowly than λ. Large scales should quite generally be associated with long times, and therefore we will generally assume that α and λ both vanish with ρ. An exceptional situation arises, however, when the motion is trapped along a certain direction, as we will discuss in Paragraph 4.2.1 below.

Another reason to consider the renormalized equations for the Green's functions produced by the closure approximations is that they may be compared against explicit and rigorous results ([2],[5]). Indeed, Avellaneda and Majda [4] already carried out this program for the DIA and QNA equations for a shear flow model with molecular diffusion ($\kappa > 0$) but no cross sweep ($w(t) \equiv 0$) where the Eulerian and Lagrnagian velocity correlations coincide. Here we will extend their approach to embrace all closure approximations considered in the present paper, as well as the possibility of a cross sweep which creates differences between the Eulerian and Lagrangian velocity correlations.

For the purpose of more detailed quantitative assessments of the closure approximations, particularly at large scales and long times, we introduce in Subsection 4.1 the Infrared Scaling Shear Flow with Cross Sweep (IS-SFCS) model in which we provide a concrete specification for the spatio-temporal statistical structure of the fluctuating cross sweep $w(t)$ and the shear flow $v(x,t)$. This model involves parameters describing the large-scale, long-time statistical properties of the velocity field, which play a primary role in determining the evolution of passive scalar field at large scales and long times. Different choices of these parameters allow us to consider the approximations in regimes with qualitatively different kinds of physical features. The main conclusions that we draw from this analysis are as follows:

1. The MDIA is again superior to the other closure approximations in predicting the large-scale, long-time properties for the Green's function in the IS-SFCS model in that it correctly predicts the renormalized Green's function under a broader set of parameters than any other closure approximation. Moreover, the MDIA correctly predicts whether the full statistics of the tracer displacement in the IS-SFCS model should become asymptotically Gaussian or not. No other closure approximation enjoys this property.

2. The inability of the QNA and QLA to resolve the influence of the cross sweep $w(t)$ on the statistics of the shear-parallel motion $Y(t)$ will cause serious errors in their prediction of the large-scale, long-time properties of the Green's function whenever the random cross sweep is the dominant cross-shear transport mechanism. With this exception, all closure approximations otherwise correctly predict when the large-scale, long-time statistics of the passive scalar field can be described by a simple (homogenized) effective diffusion equation. The effective diffusion coefficient for the shear-parallel motion $Y(t)$ is however incorrectly predicted by the QNA and DIA when a cross sweep $w(t)$ is present.

3. The DIA predicts the correct space-time scaling exponents in most, but not all cases. However, the DIA makes unrealizable predictions violating moment inequalities for the simple sweeping motion (along x) of the tracer for certain kinds of correlation functions.

4. The RLA always predicts the correct space-time scaling exponents. Since it always predicts a Gaussian form for the Green's functions, it misses the persistent non-Gaussianity that emerges in certain regimes.

5. The large-scale, long-time predictions of the closure approximations differ most strongly from each other when the tracer motion is either subdiffusive or superdiffusive. In these situations, the MDIA emerges as the clearly superior closure approximation. It is interesting to note that the renormalized equations predicted by the QNA and DIA can in fact be considerably more complicated than the true renormalized equation.

4.1 Definition of Infrared Scaling Shear Flow with Cross Sweep Model

We now specify the large-scale spatio-temporal structure of the velocity fields in terms of spatial wavenumbers k and temporal frequencies ω. We therefore introduce the Fourier transforms of the velocity correlation func-

tions:

$$\begin{cases} R_w(t) = \int_{\mathbf{R}} e^{i\omega t} E_w(\omega) d\omega, \\ R_v(x,t) = \int_{\mathbf{R}^2} e^{i(kx+\omega t)} \hat{E}(k,\omega) dk d\omega. \end{cases} \tag{71}$$

The function $E_w(\omega)$, which we shall call the *power spectrum* of the fluctuating cross sweep, is a nonnegative even function which resolves the energy of $w(t)$ with respect to frequency [70, Sec. 9]. The function $\hat{E}(k,\omega)$, which we call the *spatio-temporal energy spectrum* of the shear flow, is similarly a nonnegative even function (in both k and ω separately) representing the density of the distribution of energy in the shear flow amongst its wavenumber and frequency modes. The spatio-temporal energy spectrum is related to the spectral temporal correlation function defined in (6) by a Fourier transform:

$$E(k,t) = \int_{\mathbf{R}} e^{i\omega t} \hat{E}(k,\omega) d\omega,$$

and this relation can be used to represent the formulas for the tracer statistics in terms of $\hat{E}(k,\omega)$, as was done in [46, Sec. 3.3]. We note that $E_w(\omega)$ and $\hat{E}(k,\omega)$ can be an arbitrary non-negative function whereas the constraints on the possible forms of $R_w(t)$ and $E(k,t)$ (or $R_v(x,)$) are not so simply expressed [70, Sec. 4,9]. This is the main reason we use the former to define our IS-SFCS model.

Sweeping component. The power spectrum of the cross sweep is taken to be a function with power-law scaling at low frequency:

$$E_w(\omega) = A_{E,w} |\omega|^{-\beta} \psi_w(|\omega|). \tag{72}$$

The function ψ_w is a smooth, dimensionless, rapidly decaying function on the positive real axis with $\psi_w(\omega) = 1 + C_h \omega^h + o(\omega^h)$ as $\omega \to 0$ for some finite constants C_h and $h > 0$. The factor $A_{E,w}$ is just a constant with appropriate dimensions setting the amplitude of the sweeping component.

The exponent β in (72) describes how strongly the energy of the fluctuating cross sweep is concentrated at low frequency; we shall therefore refer to it as an *infrared scaling exponent*, and we demand $\beta < 1$ so that the total energy is finite. Larger values of β correspond to stronger long-range temporal correlations of $w(t)$. This is reflected also in the long-time scaling property implied by Eq. (72) (see Subsubsection 4.2.1)

$$\int_0^t R_w(s) ds = O(t^{\beta+1}) \quad \text{for } -1 < \beta < 1.$$

Shearing component. The spatio-temporal properties of the shear flow in the IS-SFCS model will be completely described by the energy density residing in each wavenumber,

$$\bar{E}(k) = \int_{\mathbf{R}} \hat{E}(k,\omega)d\omega = \frac{1}{2\pi}\int_{\mathbf{R}} R_v(x,0)e^{-ikx}dx \tag{73}$$

and a single *Eulerian correlation time scale* $\tau(k)$ associated to each wavenumber through the following general form:

$$\hat{E}(k,\omega) = \bar{E}(k)\hat{\phi}(\omega\tau(k))\tau(k). \tag{74}$$

The function $\hat{\phi}$ will be assumed to be a smooth, even, rapidly decaying, dimensionless function on the real axis with $\int_{\mathbf{R}} \hat{\phi}(x)dx = 1$ which describes the common shape of the temporal structure of each spatial Fourier mode of the shear velocity field. The energy spectrum $\bar{E}(k)$, which sets the amplitude of the fluctuations at each wavenumber, will be taken to have power-law scaling at low wavenumber:

$$\bar{E}(k) = A_E|k|^{1-\varepsilon}\psi(|k|). \tag{75}$$

The strength of the long-range spatial correlations of the velocity field is determined by the amount of energy in the low wavenumber modes, which is primarily described by the infrared scaling exponent ε. Larger values of ε correspond to stronger long-range spatial correlations in the shear flow, but we restrict attention to $\varepsilon < 2$ so that the total energy of the shear flow is finite. (To examine the $\varepsilon \to 2$ limit of very strong long-range correlations, the scaling coefficient A_E should be taken to scale with $(2-\varepsilon)$ so as to keep the energy of the shear flow bounded.) The function $\psi(k)$ is a smooth dimensionless function on $k > 0$ which satisfies $\psi(0) = 1$ and decays sufficiently rapidly so that $\bar{E}(k) + k|\bar{E}'(k)|$ is bounded by a monotonically decreasing, integrable functions. A_E is a constant amplitude prefactor with appropriate dimensions. The correlation time $\tau(k)$ of the Eulerian velocity field shear mode of wavenumber k will be assumed to be a smooth, decreasing function of k (as it is in most physical situations) with power-law scaling at low wavenumbers:

$$\tau(k) \sim A_\tau|k|^{-z} \quad \text{as } k \to 0,$$

with constant amplitude prefactor $A_\tau 0$ and infrared scaling exponent $z \geq 0$.

We will often find it instructive to examine a version of the IS-SFCS Model with a steady shear velocity field $v(x)$. In this case, we simply set

$$\hat{E}(k,\omega) = \bar{E}(k) \qquad \text{(steady shear velocity)},$$

with $\bar{E}(k)$ prescribed in (75).

The IS-SFCS model just described is virtually identical to what was called the Random Spatio-Temporal Shear model in [46, Sec. 3.3], and is based on ideas extending back to [2]. The IS-SFCS model encompasses velocity fields with strong long-range spatio-temporal correlations (for β close to 1, ε close to 2, and z moderate or large), which makes it a severe test case for the closure approximation.

4.2 Large-Scale, Long-Time Renormalization of Shear-Transverse Motion

The shear-transverse motion is entirely independent of the shear-parallel motion, and we therefore first focus on the approximate Green's function $\hat{G}_{x,\mathrm{app}}(k,t)$ for the shear-transverse motion, which may be identified with $\hat{G}_{\mathrm{app}}(k,p=0,t)$ (see Eq. (17)). This analysis will reveal the long-time growth predicted for the mean-square tracer displacement across the shear, and thereby set a specific linkage between the rescaling factors α and ρ. The renormalized Green's functions $\hat{\tilde{G}}_{x,\mathrm{app}}(k,t)$ for the cross-shear transport derived in this process will then be used in Subsection 4.3 as a stepping stone for obtaining the full renormalized Green's functions $\hat{\tilde{G}}_{\mathrm{app}}(k,p,t)$ along with the appropriate connection between the rescaling factors, α, λ, and ρ, predicted by the various closure approximations.

We begin in Subsubsection 4.2.1 by describing the renormalization of the exact Green's function $G_x(x,t)$ associated purely to the shear-transverse sweeping motion $X(t)$ of the tracer. After summarizing the exact results, we compare these with the renormalization of the approximate closure equations in the subsequent subsubsections. Note that the only scaling factors which are connected to the shear-transverse dynamics are α and ρ; λ plays no role.

4.2.1 Exact results for Renormalization of Shear-Transverse Green's Function

As shown in Eq. (17), the exact shear-transverse Green's function has the Gaussian form:

$$\hat{G}_x(k,t) = e^{-\frac{1}{2}k^2\mu_{2,0}(t)}. \tag{76}$$

We could renormalize this function directly, but to maintain continuity with our treatment of the closure approximations where exact solutions are not always available, we instead (equivalently) renormalize the exact evolution equation for this Green's function:

$$\frac{\partial \hat{G}_x}{\partial t} = -D_x(t)k^2\hat{G}_x, \tag{77}$$

with $\hat{G}_x|_{t=0} = 1$ and where the time-dependent diffusion coefficient appearing in this equation may be expressed, using Eq. (19), as follows:

$$D_x(t) = \frac{1}{2}\frac{d\mu_{2,0}(t)}{dt} = \kappa + \int_0^t R_w(s)\, ds. \tag{78}$$

We now rescale to large scales and long times according to the prescription (70) (with $\hat{G}_{\rm app}$ replaced by $\hat{G}$), and find that the rescaled Green's function obeys the following equation:

$$\frac{\partial \hat{G}_x^{(\rho)}}{\partial t} = -\left(\frac{\alpha^2(\rho) D_x(t/\rho^2)}{\rho^2}\right) k^2 \hat{G}_x^{(\rho)}, \tag{79}$$

with $\hat{G}_x^{(\rho)}|_{t=0} = 1$. Now the relationship between α and ρ is chosen so as to yield the most nontrivial equation possible in the limit $\rho \to 0$.

Case of No Molecular Diffusion When $\kappa = 0$, then the rescaling parameters only appear in the combination

$$\frac{\alpha^2(\rho) D_x^{(0)}(t/\rho^2)}{\rho^2}, \tag{80}$$

where

$$D_x^{(0)}(t) = \int_0^t R_w(s) ds$$

is the shear-transverse diffusivity contributed by the velocity fluctuations. We wish to render the combination (80) finite in the $\rho \to 0$ limit so as to capture the nontrivial dynamics on the large scales and long times. Clearly the proper scaling will require the ascertainment of the long-time behavior of $D_x^{(0)}(t)$, which can be obtained rigorously through asymptotic evaluation [17] of the oscillatory integral in (71) expressing $R_w(t)$ in terms of $E_w(\omega)$:

$$D_x^{(0)}(t) \sim K_x^\sharp t^\beta \quad \text{as } t \to \infty,$$

where

$$K_x^\sharp = 2^{-\beta}\sqrt{\pi} A_{E,w} \frac{\Gamma((1-\beta)/2)}{\Gamma((2+\beta)/2)}. \tag{81}$$

Specifically, if $\beta = 0$, the fluctuating velocity field $w(t)$ produces a finite enhanced diffusivity at long times:

$$K_x^* = \frac{1}{2} A_{E,w} = \int_0^\infty R_w(s) ds. \tag{82}$$

If $\beta > 0$, the velocity fluctuations give rise to a diffusivity which forever grows with time, whereas if $\beta < 0$, the enhancement $D_x^{(0)}(t)$ of the diffusivity decays with time.

Consequently, we have:

$$\left(\frac{\alpha^2(\rho)D_x^{(0)}(t/\rho^2)}{\rho^2}\right) \sim \alpha^2\rho^{-2-2\beta}K_x^\sharp t^\beta \quad \text{as } \rho \to 0, t \to \infty.$$

A finite, nonzero limit will emerge if we link the space and time rescaling as follows:

$$\rho = \alpha^{1/(1+\beta)}. \tag{83}$$

Note that the relation (83) is only consistent with α and ρ vanishing together when $-1 < \beta < 1$. Restricting ourselves to this range of parameters for the moment, we find the following equation for the renormalized exact shear-transverse Green's function $\hat{\bar{G}}_x(k,t) = \lim_{\alpha\to 0}\hat{G}_{x,\mathrm{app}}(k,t)$:

$$\frac{\partial\hat{\bar{G}}_x}{\partial t} = -K_x^\sharp t^\beta k^2\hat{\bar{G}}_x, \tag{84}$$

with $\hat{\bar{G}}_x|_{t=0} = 1$. The renormalized equation for the shear-transverse tracer motion is therefore a diffusion equation, with constant diffusion coefficient for $\beta = 0$ and a time-dependent diffusion coefficient for $-1 < \beta < 0$ and $0 < \beta < 1$. This equation is easily solved:

$$\hat{\bar{G}}_x(k,t) = \exp\left(-\frac{1}{1+\beta}k^2K_x^\sharp t^{\beta+1}\right) \quad \text{for } -1 < \beta < 1. \tag{85}$$

This corresponds to a Gaussian real-space Green's function (or tracer PDF)

$$\bar{G}(x,t) = \frac{\exp\left(-(1+\beta)x^2/4K_x^\sharp t^{\beta+1}\right)}{\sqrt{4\pi K_x^\sharp t^{\beta+1}/(1+\beta)}} \quad \text{for } -1 < \beta < 1. \tag{86}$$

The long-time asymptotics of the variance of the shear-transverse tracer displacement may be read off from Eq. (85) or (86) as

$$\mu_{2,0}(t) \sim \frac{2}{1+\beta}K_x^\sharp t^{\beta+1} \quad \text{as } t \to \infty \text{ for } -1 < \beta < 1, \tag{87}$$

which agrees with what would have been obtained by taking a direct long-time limit of the finite-time formula in (19) for $\mu_{2,0}(t)$.

We note that specifying the initial condition for the renormalized Green's function in (84) is a somewhat subtle manner because the large-scale, long-time asymptotic limit could introduce a discontinuity at $t = 0$. Here it is easily checked by renormalization of the exact solution (76) that no such discontinuity plagues us here, but this issue will be significant for the case considered next.

Trapping Case For $\beta < -1$, the diffusivity $D_x^{(0)}(t)$ decays sufficiently rapidly that the tracer never progresses over large scales in a statistical sense; its motion is *trapped*. Therefore, the appropriate scaling for $\beta < -1$ is $\alpha = 1$ and $\rho^2 \to 0$ (at an arbitrary rate). In this limit process, the right hand side of the rescaled equation (79) vanishes:

$$\frac{\alpha^2 D_x(t/\rho^2)}{\rho^2} k^2 \sim K_x^\sharp (t/\rho^2)^\beta \rho^{-2} k^2 \to 0 \quad \text{for } \beta < -1.$$

Consequently, the renormalized equation for the shear-transverse Green's function reduces to a trivial form,

$$\frac{\partial \hat{\bar{G}}_x}{\partial t} = 0,$$

but renormalization of the exact solution (76) shows that there will be a discontinuity of $\hat{\bar{G}}_x(k,t)$ at $t = 0$. While $\hat{\bar{G}}_x(k, t = 0) = 1$,

$$\lim_{t \to 0} \hat{\bar{G}}_x(k,t) = e^{-\frac{1}{2} K_x^\circ k^2},$$

where ([7],[46, Sec. 3.1.2.4])

$$\lim_{t \to \infty} \mu_{2,0}(t) = K_x^\circ \equiv 4 \int_0^\infty E_w(\omega) \omega^{-2} d\omega \quad \text{for } \beta < -1. \tag{88}$$

Thus, for $t > 0$, the renormalized Green's function is just:

$$\hat{\bar{G}}_x(k,t) \equiv e^{-\frac{1}{2} K_x^\circ k^2} \quad \text{for } \beta < -1,$$

which corresponds to a physical-space shear-transverse Green's function (or tracer displacement PDF) $\bar{G}_x(x,t)$ which remains fixed at a Gaussian distribution with mean zero and variance K_x°.

The various behaviors for the tracer motion across the shear which we have obtained are summarized in Table I ([46, Sec. 3.1]). For $\beta = 0$, ordinary diffusive (linear) growth of the mean-square tracer displacement prevails at long times. For $0 < \beta < 1$, the mean-square tracer displacement grows faster than linearly in time, and the motion is said to be *superdiffusive*. On the other hand, for $-1 < \beta < 0$, the mean-square tracer displacement grows more slowly than linearly in time, and the motion is *subdiffusive*. For $\beta < -1$, the mean-square tracer displacement saturates at a finite value, and is said to be *trapped* in the shear-transverse direction.

Table I illustrates a phenomenon which will permeate much of the following discussion: the long-time behavior of the tracer motion falls into

Table I: Long-time asymptotics of mean-square tracer displacement $\mu_{2,0}(t)$ across the shear, with $\kappa = 0$. Scaling coefficients are given by (81), and (82) and (88) (Reproduced/adapted from [46]).

Parameter Regime	Asymptotic Mean Square Displacement $\lim_{t\to\infty} \mu_{2,0}(t)$	Qualitative Behavior
$\beta < -1$	$K_x^{\circ} t^0$	trapping
$-1 < \beta < 0$	$\frac{2}{1+\beta} K_x^{\sharp} t^{1+\beta}$	subdiffusive
$\beta = 0$	$2K_x^{*} t$	diffusive
$0 < \beta < 1$	$\frac{2}{1+\beta} K_x^{\sharp} t^{1+\beta}$	superdiffusive

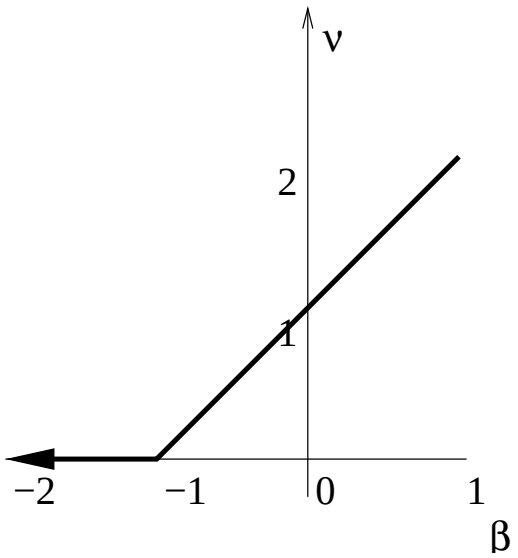

Figure 2: Phase diagram for scaling exponent (89) of long-time asymptotics of sweeping motion $X(t)$ in IS-SFCS model with $\kappa = 0$.

qualitatively different categories depending on some parameters (such as β here) describing the properties of the random flow field ([2],[5],[7] [46, Sec. 3]). The parameter space $\beta < 1$ may therefore be divided into different *phase regimes* of qualitatively different long-time tracer behavior, separated by *phase transitions* or *phase boundaries*. The scaling exponent ν of the long-time asymptotics of the mean-square displacement

$$\mu_{2,0}(t) = O(t^\nu) \quad \text{as } t \to \infty, \tag{89}$$

can serve as an order parameter to distinguish the phase regimes, and is plotted in Figure 2. In the present discussion of shear-transverse motion with $\kappa = 0$, there is a definite phase transition at $\beta = -1$ because the formulas for the long-time asymptotics are sharply different for $\beta < -1$ and $\beta > -1$, and the graph of the scaling exponent ν as a function of β changes abruptly. The renormalized behavior at the phase transition value $\beta = -1$ involves logarithms, and we choose not to dwell on these special boundary cases to avoid distraction from the main development.

Case of Nonzero Molecular Diffusion The presence of molecular diffusion $\kappa > 0$ does not affect the renormalization when $0 < \beta < 1$ because then the fluctuating velocity field creates superdiffusion across the shear, and therefore dominates the contribution to $D_x(t)$ at long times. If however, $\beta < 0$ or there is no fluctuating cross sweep ($w(t) \equiv 0$), then

$$\frac{\alpha^2(\rho) D_x(t/\rho^2)}{\rho^2} \sim \frac{\alpha^2}{\rho^2}\kappa \quad \text{as } \rho \to \infty,$$

so the appropriate choice of temporal scaling function is $\rho = \alpha$, and the renormalized equation is the ordinary diffusion equation:

$$\frac{\partial \hat{\tilde{G}}_x}{\partial t} = -\kappa k^2 \hat{\tilde{G}}_x,$$

with $\hat{\tilde{G}}_x|_{t=0} = 1$.

If $\beta = 0$, then both molecular diffusion and the fluctuating velocity field $w(t)$ give rise to a codominant diffusive contribution at long times, with rescaling $\rho = \alpha$. The renormalized equation for the Green's function is an ordinary diffusion equation with constant diffusivity $\kappa + K_x^*$, where the turbulent enhancement K_x^* is given in (82).

Summary. The appropriate relationship between the temporal rescaling parameter ρ and the spatial rescaling parameter α for shear transverse motion may be summarized for most cases as:

$$\rho = \alpha^{1/\nu}, \tag{90}$$

where

$$\nu = \begin{cases} 1+\beta & \text{if } \kappa > 0 \text{ and } 0 \le \beta < 1, \text{ or } \kappa = 0 \text{ and } -1 < \beta < 1, \\ 1 & \text{if } \kappa > 0 \text{ and } \beta < 0. \end{cases} \tag{91}$$

The only case not covered above is the trapping situation in which $\kappa = 0$ and $\beta < -1$. In this case, α should be held fixed at $\alpha = 1$ while $\rho \to 0$.

The renormalized equation for the shear-transverse Green's function takes the general form

$$\frac{\partial \bar{G}_x}{\partial t} = \bar{D}_x(t) \frac{\partial^2 \bar{G}_x}{\partial x^2}, \tag{92}$$

in physical space, or equivalently

$$\frac{\partial \hat{\bar{G}}_x}{\partial t} = -k^2 \bar{D}_x(t) \hat{\bar{G}}_x(k,t), \tag{93}$$

in Fourier space. The initial data for the renormalized shear-transverse Green's function is

$$\bar{G}_x(x, t=0) = \begin{cases} \dfrac{e^{-x^2/(2K_x^\circ)}}{\sqrt{2\pi K_x^\circ}} & \text{if } \beta < -1 \text{ and } \kappa = 0 \text{ (trapping case)}, \\ 1 & \text{otherwise} \end{cases} \tag{94}$$

in physical space, and

$$\hat{\bar{G}}_x(k, t=0) = \begin{cases} e^{-\frac{1}{2}K_x^\circ k^2} & \text{if } \beta < -1 \text{ and } \kappa = 0, \\ 1 & \text{otherwise.} \end{cases} \tag{95}$$

in Fourier space. The renormalized diffusivity $\bar{D}_x(t)$ has the following form:

$$\bar{D}_x(t) = \begin{cases} K_x^\sharp t^\beta & \text{for } \kappa = 0,\ -1 < \beta < 1, \text{ or } \kappa > 0,\ 0 < \beta < 1, \\ \kappa & \text{for } \kappa > 0,\ \beta < 0, \\ \kappa + K_x^\sharp & \text{for } \kappa > 0,\ \beta = 0, \\ 0 & \text{for } \kappa = 0,\ \beta < -1. \end{cases} \tag{96}$$

4.2.2 Renormalization of Closure Approximations of Shear-Transverse Green's Function

We next turn to the renormalization of equations for the shear-transverse Green's function produced by the closure approximations. We collect and compare the results here, and indicate the manner in which the approximate equations are renormalized in Appendix C.1:

1. The relation between the rescaling parameters α and ρ^2 are correctly predicted by all approximations, except for the DIA in the parameter range $\beta < -\frac{1}{2}$.

2. By taking $p = 0$ in the QLA (34), RLA (69), and MDIA (63) equations, we find that each of these approximations produce the exact equation (77) for the shear-transverse Green's function. Consequently, the large-scale, long-time renormalization of the shear-transverse tracer motion in each of these approximations will necessarily agree with the exact renormalization results described in (90)-(96).

3. The renormalized QNA and DIA equations, however, are correct only when $\beta = 0$, or $\kappa > 0$ and $\beta \leq 0$ (in which case $\bar{D}_x(t)$ is a positive constant). In the cases where the QNA and DIA do not renormalize correctly, they predict a persistently non-Gaussian form for the renormalized shear-transverse Green's function, although the shear-transverse mean-square displacement $\mu_{2,0}(t)$ in (19) is correctly predicted for all time.

We describe next in some detail the results of the renormalization of the DIA and QNA in the parameter regimes where they disagree with the exact results. The details behind the renormalization procedure for QNA and DIA may be found in Appendix C.1.

For the case of superdiffusive shear-transverse motion ($\beta > 0$), the QNA and DIA predict the following incorrect nonlocal renormalized equations with convolution in time, to be compared with the exact local time-dependent diffusion equation (84):

$$\frac{\partial \hat{\bar{G}}_{x,\mathrm{QNA}}}{\partial t} = -k^2 \left(\int_0^t \bar{D}'_x(s) \hat{\bar{G}}_{x,\mathrm{QNA}}(k, t-s) ds \right), \tag{97}$$

with $\hat{\bar{G}}_{x,\mathrm{QNA}}|_{t=0} = 1$, and

$$\frac{\partial \hat{\bar{G}}_{x,\mathrm{DIA}}}{\partial t} = -k^2 \left(\int_0^t \bar{D}'_x(s) \hat{\bar{G}}_{x,\mathrm{DIA}}(k, s) \hat{\bar{G}}_{x,\mathrm{DIA}}(k, t-s) ds \right), \tag{98}$$

with $\hat{\bar{G}}_{x,\mathrm{DIA}}|_{t=0} = 1$. Here $\bar{D}'_x(t) \equiv d\bar{D}_x/dt$.

For the regime of subdiffusive sweeping motion ($\kappa = 0$ and $-1 < \beta < 0$), the renormalized QNA equations takes a similar convolution-in-time form,

$$\frac{\partial \hat{\bar{G}}_{x,\mathrm{QNA}}}{\partial t} = -k^2 \left(\int_0^\infty \bar{D}'_x(s) (\hat{\bar{G}}_{x,\mathrm{QNA}}(k, t-s) - 1) ds \right), \tag{99}$$

with $\hat{\bar{G}}_{x,\mathrm{QNA}}|_{t=0} = 1$, which again disagrees with the exact local time-dependent diffusion equation (84). For a statistically trapped motion ($\kappa = 0$ and $\beta < -1$), the QNA equations renormalize to a correct trivial equation but with incorrect initial data:

$$\frac{\partial \hat{\bar{G}}_{x,\mathrm{QNA}}}{\partial t} = 0, \qquad \hat{\bar{G}}_{x,\mathrm{QNA}}(k, t=0) = \left[1 + \frac{1}{2} k^2 K_x^\circ \right]^{-1}.$$

The physical-space solution for the renormalized QNA shear-transverse Green's function is

$$\bar{G}_{x,\mathrm{QNA}}(x,t) = \frac{e^{-\sqrt{2/K_x^\circ}|x|}}{\sqrt{2K_x^\circ}},$$

which corresponds to an exponential distribution with the finite variance K_x°. The exact renormalized solution has a Gaussian profile with the same variance.

The DIA renormalizes to the natural analogue of the renormalized QNA equation (99) when $\kappa = 0$ *only over the restricted domain of parameters* $-\frac{1}{2} < \beta < 0$:

$$\frac{\partial \hat{\bar{G}}_{x,\mathrm{DIA}}}{\partial t} = -k^2 \int_0^\infty \bar{D}_x'(s) \left(\hat{\bar{G}}_{x,\mathrm{DIA}}(k,s) \hat{\bar{G}}_{x,\mathrm{DIA}}(k,t-s) - \hat{\bar{G}}_{x,\mathrm{DIA}}(k,t) \right) ds \tag{100}$$

with $\hat{\bar{G}}_{x,\mathrm{DIA}}|_{t=0} = 1$. The DIA predicts a spurious phase transition at the value $\beta = -\frac{1}{2}$ to another subdiffusive regime for $\beta < -\frac{1}{2}$, with the incorrect rescaling relationship $\alpha = \rho^{1/2}$, and the following renormalized equation:

$$\frac{\partial \hat{\bar{G}}_{x,\mathrm{DIA}}}{\partial t} = -K_{4,\mathrm{DIA}}^\circ k^4 \hat{\bar{G}}_{x,\mathrm{DIA}}, \tag{101}$$

with $\hat{\bar{G}}_{x,\mathrm{DIA}}|_{t=0} = 1$. This is readily solved to give

$$\hat{\bar{G}}_{x,\mathrm{DIA}}(k,t) = e^{-K_{4,\mathrm{DIA}}^\circ k^4 t}. \tag{102}$$

This renormalized Green's function is *unrealizable* in the sense that it cannot be the characteristic function for the random process $X(t)$ (see Eq. (12)). This follows either from Marcinkiewicz's theorem [58], which states the cumulant generating function $\ln \hat{G}(k,t)$ cannot be a finite polynomial of degree higher than two, or by directly noting that the fourth order cumulant, $\mu_{4,0}^{\mathrm{DIA}}(t)$, associated to Eq. (102) is negative. We therefore conclude that the DIA suffers serious deficiencies in representing the statistics of a tracer being swept at a subdiffusive rate. The phase diagram for the scaling functions is altered from Figure 2 to that shown in Figure 3, and the DIA prediction becomes nonsensical at large scales and long times for $\beta < -\frac{1}{2}$. This is presumably a manifestation of the inability of the DIA to track the influence of random coherent oscillations in the environment [67, Sec. 3.3].

All told, then, it appears that the DIA is the most problematic closure approximation for predicting the sweeping motion $X(t)$, though its equation for $\hat{G}_{x,\mathrm{DIA}}(k,t)$ is the most complicated of the approximations. We

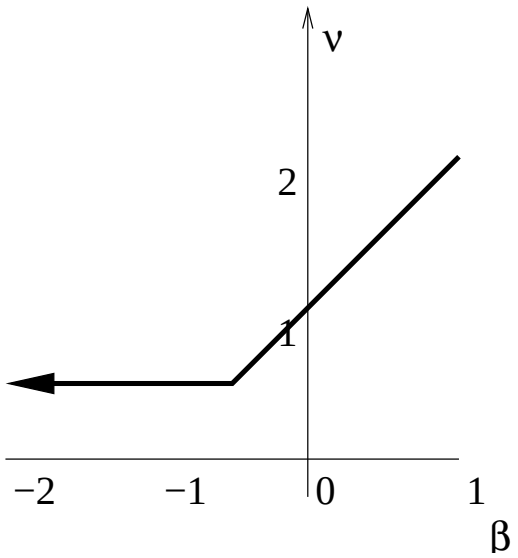

Figure 3: Phase diagram for scaling exponent (89) of long-time asymptotics of sweeping motion $X(t)$ in the IS-SFCS model with $\kappa = 0$, under DIA.

examine this issue in more detail by consideration of the long-time behavior of the cumulants $\mu_{2,0}(t)$ and $\mu_{4,0}(t)$ in Section 5.1.

For the later full renormalization of the closure approximations, it will be helpful to represent the shear-transverse terms of the renormalized QNA and DIA equations in some unified fashion. It is readily checked then that the following equation:

$$\frac{\partial \hat{\bar{G}}_{x,\mathrm{QNA}}}{\partial t} = -k^2 \frac{\partial}{\partial t}\left(\int_0^t \bar{D}_x(s) \hat{\bar{G}}_{x,\mathrm{QNA}}(k,t-s) ds \right), \tag{103}$$

with $\hat{\bar{G}}_{x,\mathrm{QNA}}|_{t=0} = 1$, is equivalent to the QNA equations stated above for all the various cases considered. We are unaware of a way to write down a corresponding single unified equation for the renormalized DIA equation. We therefore simply write

$$\frac{\partial \hat{\bar{G}}_{x,\mathrm{DIA}}}{\partial t} = \mathcal{D}^{\mathrm{DIA}}(\hat{\bar{G}}_{x,\mathrm{DIA}}(k,\cdot),k,t), \tag{104}$$

with $\hat{\bar{G}}_{x,\mathrm{DIA}}|_{t=0} = 1$, and where $\mathcal{D}^{\mathrm{DIA}}$ is a formal operator defined in one of the following ways, depending on the parameters of the model:

- For diffusive sweeping motion,

  $$\mathcal{D}^{\mathrm{DIA}}(\hat{\bar{G}}_{\mathrm{DIA}}(k,p,\cdot),k,t) = -(\kappa + K_x^*)k^2 \hat{\bar{G}}_{\mathrm{DIA}}(k,p,t),$$

  for $\beta = 0$ or $\kappa > 0$, $\beta < 0$, where K_x^* is defined in (82).

- For superdiffusive sweeping motion ($0 < \beta < 1$) refer to Eq. (98) with $\hat{\bar{G}}_{x,\mathrm{DIA}} \to \hat{\bar{G}}_{\mathrm{DIA}}$.

- For subdiffusive or trapping sweeping motion ($\kappa = 0, -\frac{1}{2} < \beta < 0$), refer to Eq. (100) with $\hat{\bar{G}}_{x,\mathrm{DIA}} \to \hat{\bar{G}}_{\mathrm{DIA}}$.

We abandon the case ($\kappa = 0$, $\beta < -\frac{1}{2}$) as hopelessly lost for the DIA, since the sweeping motion is already predicted in an unrealizable fashion, and the incorrect scaling relationship between α and ρ will contaminate the renormalization results for the shear-parallel motion.

We also define the initial data for the renormalized shear-transverse QNA Green's function in physical space:

$$\bar{G}_{x,\mathrm{QNA}}(x,t=0) \equiv \begin{cases} \frac{e^{-\sqrt{2/K_x^\circ}|x|}}{\sqrt{2K_x^\circ}} & \text{if } \beta < -1,\ \kappa = 0, \\ \delta(x) & \text{otherwise,} \end{cases} \tag{105}$$

and in Fourier space:

$$\hat{\tilde{G}}_{x,\mathrm{QNA}}(k,t=0) \equiv \begin{cases} \left[1+\frac{1}{2}k^2 K_x^\circ\right]^{-1} & \text{if } \beta<-1,\ \kappa=0, \\ 1 & \text{otherwise.} \end{cases} \tag{106}$$

Recall that the range $\beta < -1$, $\kappa = 0$ corresponds to the trapping situation.

4.3 Large-Scale, Long-Time Renormalization of Total Tracer Motion

With the large-scale, long-time behavior of the shear-transverse transport fully discussed, we are now prepared to consider the shear-parallel motion and thereby renormalize the full Green's function. The relationship between the scaling parameters α and ρ has been set by the previous analysis of Subsection 4.3, and therefore we are left with finding an appropriate relationship between ρ and λ which will lead to a nontrivial fixed point for the rescaled Green's function Eq. (70). We begin with a discussion of what is known for the large-scale, long-time behavior of the exact Green's function, then show how well the renormalizations of the various closure approximations agree with the exact picture.

4.3.1 Renormalization of Exact Green's Function

The exact Green's function for the shear-transverse motion satisfies an explicit PDE (77). No such closed evolution equation is known for the full Green's function $\hat{G}(k,p,t)$. One can, however, rigorously renormalize the functional integral expression (15) for it. Under the rescaling (70), this formula reads:

$$\hat{G}^{(\rho)}(k,p,t) = e^{-\kappa\lambda^2\rho^{-2}p^2 t}\left\langle e^{-i\alpha k X(t/\rho^2)-\frac{1}{2}\lambda^2 p^2 M(t/\rho^2)}\right\rangle_{w,W_x}. \tag{107}$$

where

$$M(t) = \int_0^t ds \int_0^t ds' \int_{\mathbf{R}} dq\, \bar{E}(q)\phi((s-s')/\tau(q))e^{iq(X(s)-X(s'))}.$$

We then wish to find the relationship between the scaling functions λ and ρ which, along with the appropriate relationship (91) between the scaling functions α and ρ found in Subsection 4.2, produces a nontrivial limit for $\hat{G}^{(\rho)}(k,p,t)$ as $\rho \to 0$. The details of the renormalization procedure are presented in [2, 5], and will not be reproduced here. We will simply state and discuss the results to set the framework for comparison with the renormalization of the closure approximations. We remark that the renormalized equations stated in [2, 5] are those resulting from an *isotropic*

renormalization (with $\alpha = \lambda$ always enforced), whereas we are employing an anisotropic renormalization in which the spatial rescaling may proceed at different rates in the shear-parallel and shear-transverse directions. Moreover, the work [2, 5] incorporated an infrared (low wavenumber) cutoff. The renormalization procedure developed in [2, 5] is, however, easily modified to treat anisotropic renormalization with no infrared cutoff, and we shall present these modified results.

To any particular choice of cross-shear transport processes, there is associated a *phase diagram* in (ε, z) parameter space, demarcating different regimes of different large-scale, long-time behavior of the tracer motion along the shear. Recall from Subsection 4.1 that these parameters characterize the large-scale, long-time statistical properties of the shear velocity field, just as β characterized the long-time properties of the fluctuating cross sweep. We summarize in Table II the phase regimes that emerge. .

The phase regimes and transitions in the large-scale, long-time behavior of a tracer in a *steady* shear flow can be deduced in most cases from the (ε, z) phase diagrams by taking a horizontal, constant z slice in the $z \to \infty$ limit ([2, 5],[46, Sec. 3]). The reason for this is that the strength of the low wavenumber modes of the shear velocity field play the greatest role in determining the nature of the tracer transport, and as $z \to \infty$, these low-wavenumber shear modes have correlation times $\tau(k) \sim A_\tau |k|^{-z} \to \infty$.

We will first present the renormalized equations for one (or zero) active particular cross-shear transport mechanism, then provide a summary for the renormalization picture for superpositions of cross-shear transport processes.

Case of No Cross-Shear Transport. When $\kappa = w(t) \equiv 0$, then the phase diagram for the shear-parallel tracer motion is presented in Figure 4 and breaks up into two regimes, one diffusive (D), and one superdiffusive (SD-t). As we are not yet including any cross-shear transport mechanisms, the long-time tracer motion in both the superdiffusive regime and diffusive regime is determined only by the temporal flucutations in the shear velocity field.

D The diffusive regime is the region $\varepsilon + z < 2$, over which space and time are diffusively linked: $\rho = \lambda$. The renormalized Green's function in the D regime obeys an ordinary diffusion equation:

$$\frac{\partial \bar{G}}{\partial t} = \tilde{K}_0^* \frac{\partial^2 \bar{G}}{\partial y^2},$$

Table II: Phase regimes for Shear-Parallel Transport.

Label	Transport Rate	Dominant Mechanism Limiting Transport
D	diffusive	all relevant
SD-t	superdiffusive	temporal fluctuations in $v(x,t)$
SD-κ	superdiffusive	molecular diffusion κ
SD-w	superdiffusive	random sweeping $w(t)$

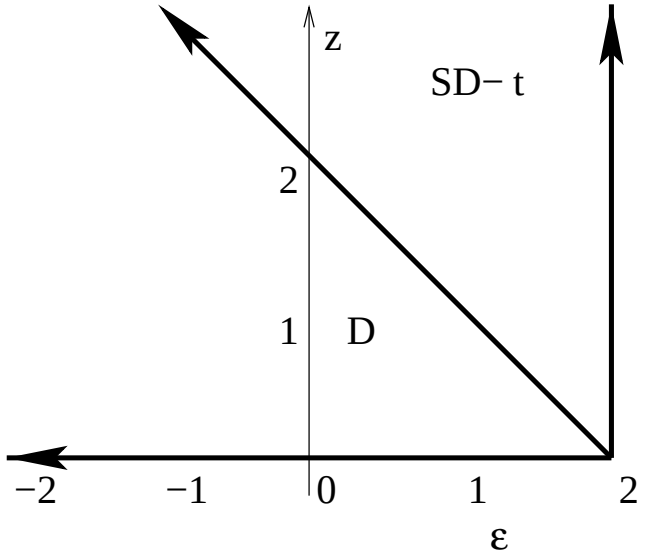

Figure 4: Phase diagram for long-time asymptotics of shear-parallel transport in Infrared Scaling Shear Flow with Cross Sweep model with $\kappa = w(t) = 0$. The phase transition occurs along the line $\varepsilon + z = 2$.

with $\bar{G}|_{t=0} = \delta(x)\delta(y)$, and a constant diffusion coefficient:

$$K_y^* = \int_0^\infty \int_{\mathbf{R}} E(q,t)dqdt = \hat{\phi}(0) \int_0^\infty \bar{E}(q)\tau(q)dq. \tag{108}$$

SD-t On the other hand, for $\varepsilon + z > 2$, the tracer motion along the shear is superdiffusive

$$\rho = \lambda^{z/(2z+\varepsilon-2)} \gg \lambda \quad \text{as } \lambda \to 0, \tag{109}$$

and the renormalized equation for the Green's function involves a growing, time-dependent diffusivity:

$$\frac{\partial \bar{G}}{\partial t} = \tilde{K}_0^\sharp t^{(z+\varepsilon-2)/z} \frac{\partial^2 \bar{G}}{\partial y^2}, \tag{110}$$

where $\bar{G}|_{t=0} = \delta(x)\delta(y)$. The scaling constant here is given by [46, Eq. (163b)]:

$$\tilde{K}_0^\sharp = \frac{2}{\varepsilon + z - 2} A_E A_\tau^{(2-\varepsilon)/z} \int_0^\infty \phi(s) s^{(2-\varepsilon-z)/z} ds. \tag{111}$$

The above results follow from the analysis of [46, 3.3.1], along with the observation that the PDF for the tracer displacement along the shear must be Gaussian because it can be expressed as a definite integral over a Gaussian random field.

Case of Molecular Diffusion. The introduction of molecular diffusion $\kappa > 0$ changes the phase diagram by broadening the D regime and creating a new regime of superdiffusive behavior along the shearing direction besides SD-t, which we label SD-κ. (Figure 5). Note that this phase diagram is concerned with the shear-parallel transport; the cross-shear transport is of course always diffusive in this case ($\rho = \alpha$). The results we present can be rigorously derived by adapting the procedure in [2] to the case in which the energy spectrum has no infrared cutoff, though the phase diagram changes somewhat. The correspondence between our regimes and those in [2] are as follows: the D regime is Region I, the SD-t regime is Region IV, and the SD-κ regime is Region V.

D In the D regime, space and time are diffusively linked ($\rho = \lambda$) and the renormalized equation is an ordinary diffusion equation:

$$\frac{\partial \bar{G}}{\partial t} = \kappa \frac{\partial^2 \bar{G}}{\partial x^2} + K_y^* \frac{\partial^2 \bar{G}}{\partial y^2}, \tag{112}$$

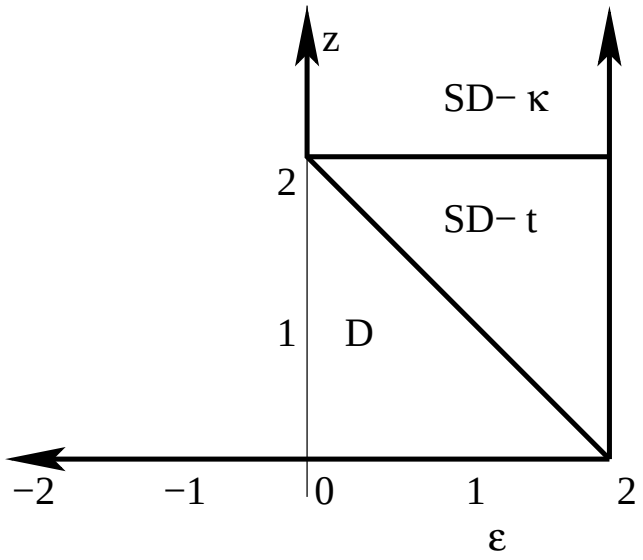

Figure 5: Phase diagram for long-time asymptotics of shear-parallel transport in Infrared Scaling Shear Flow with Cross Sweep model with $\kappa > 0$ and $w(t) = 0$. The phase transition lines lie along segments of $\varepsilon = 0$, $z = 2$, and $\varepsilon + z = 1$.

with $\bar{G}|_{t=0} = \delta(x)\delta(y)$. The constant renormalized diffusivity along the y direction is enhanced due to the shearing motion:

$$K_y^* = \kappa + \int_0^\infty \int_{\mathbf{R}} E(q,t)\hat{G}_x(-q,t)dqdt. \tag{113}$$

We have stated the formula (113) in a form involving the shear-transverse Green's function because it is generally applicable for all random cross-shear transport processes discussed in this section. For the particular case in which tracers move across the shear only due to molecular diffusion, then

$$\hat{G}_x(k,t) = e^{-\kappa k^2 t}. \tag{114}$$

The D regime describes precisely the energy spectra for which homogenization theory [3, 19, 49, 53, 56] applies to the shear-parallel tracer motion.

SD-t The SD-t regime has identical renormalized characteristics as was presented above. Molecular diffusion is irrelevant under the renormalization in this regime.

SD-κ On the other hand, the temporal fluctuations of the velocity field become negligible after renormalization in the complementary superdiffusive regime, SD-κ. Here molecular diffusion is the dominant cross-shear mechanism limiting transport along the shearing direction. The linkage between space and time rescaling in this domain is $\rho = \lambda^{2/(2+\varepsilon)} \gg \lambda$ as $\lambda \to \infty$. In contrast with the other two regimes, the renormalized Green's function in the SD-κ regime is not a Gaussian. In fact, the PDF for the shear-parallel tracer displacement is representable as a certain average of Gaussians of different widths, and is therefore known by general principles to have a broader-than-Gaussian shape. The reader is referred to the references ([2],[6],[46, Sec. 3.4.1.2]) for further details about the renormalized Green's function for the SD-κ regime; there will be some differences in the details because of our anisotropic renormalization procedure.

Case of a Temporally Fluctuating Cross Sweep. The phase diagram for the shear-parallel motion of a tracer in a flow with temporally fluctuating cross sweep $w(t) \neq 0$ but no molecular diffusion $\kappa = 0$ is presented in Figure 6. It is qualitatively similar to the cases discussed already for other cross-shear transport mechanisms, with a regime D with ordinary diffusive behavior, and two different superdiffusive regimes: one (SD-t) where temporal decorrelation of the velocity field plays the dominant role in determining the tracer motion at large scales and long times, and one (SD-w) where spatial decorrelation plays the primary role. The location

of the phase boundaries depend on the strength of the long-range correlations of the fluctuating random field $w(t)$, as described by the infrared scaling exponent β of its energy spectrum (72). This phase diagram for a fluctuating cross sweep is identical to the one in which only molecular diffusion is active (Figure 5) when $\beta = 0$, which is exactly the case in which the tracer motion across the shear proceeds at an ordinary diffusive rate ($\mu_{2,0}(t) \sim 2K_x^* t$ as $t \to \infty$). As the strength of the long-range fluctuations of $w(t)$ as measured by the infrared scaling exponent β increases, i.e. in the limit as $\beta \to 1$, the D regime is broadened to larger values of ε, and the phase transition between the two superdiffusive regimes slides to smaller values of z. But as β decreases toward -1, the vertical and horizontal boundaries of the SD-w regime slide up and left until they disappear entirely (along with the SD-w regime) when β crosses the value -1. Indeed, for $\beta < -1$, the cross-shear transport is so feeble that it is trapping (Subparagraph 4.2.1)), and the large-scale, long-time behavior of the shear-parallel motion is essentially the same as for the case of no cross shear transport discussed above. (The diffusion constant in the D regime is slightly modified by the weakly fluctuating field $w(t)$ however, see [46, Sec. 3.3.4]).

The phase diagram in Figure 6 has been worked out rigorously for the long-time behavior of the second order moments of the tracer displacement along the shear [46, Sec, 3.3.4]. The rigorous renormalization of the full Green's function, however, has not yet been accomplished for the case of a fluctuating cross sweep as it has been for the case of molecular diffusion and/or a mean cross sweep [2, 5]. We shall however, based on the rigorous results available for these cases, conjecture that the phase diagram for the renormalized tracer PDF along the shear is identical to that for the second order moment of the shear-parallel tracer displacement. We also conjecture that in the D regime, the tracer motion along the shear homogenizes and is completely described by a constant diffusion coefficient (113). It can be shown using the techniques of [2, 5] that the equation for the Green's function will renormalize in the SD-t regime to the same limit, (109)–(111) as in the other cases discussed. (The mode of cross-shear transport should formally be irrelevant at large scales and long times in this regime.) We expect, based on the rigorous results for the case of molecular diffusion alone, that in the SD-w regime, the Green's function can only be described by a complicated nonlocal PDE. The appropriate space-time rescaling in this regime can be shown to be $\rho = \lambda^{2/(2+\varepsilon-\beta(2-\varepsilon))}$ [46, Sec. 3.2.3].

We pose the rigorous verification of these natural conjectures as an open problem to the reader; the techniques of [6] may be useful in this regard.

Summary of Renormalized Green's Functions for Arbitrary Cross-Shear Transport. The renormalization of the tracer cross-shear motion

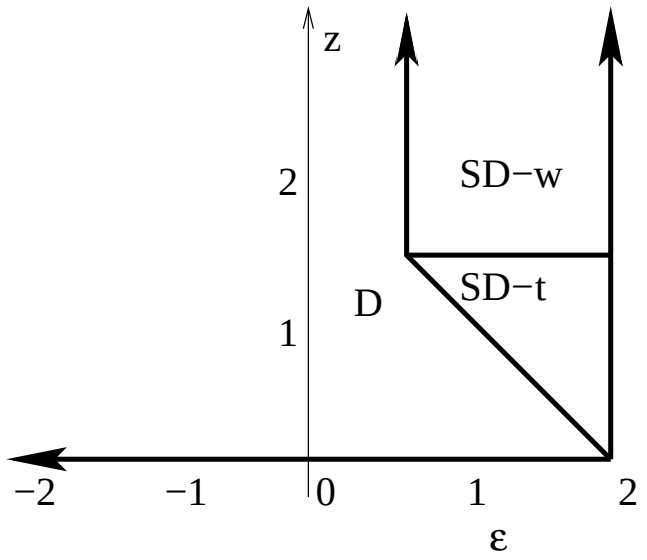

Figure 6: Phase diagram for long-time asymptotics of shear-parallel transport in Infrared Scaling Shear Flow with Cross Sweep model with $w(t) \neq 0$ and $\kappa = 0$. For $-1 < \beta < 1$, the phase boundaries lie along segments of the lines $\varepsilon + z = 2$, $\varepsilon = \frac{2\beta}{1+\beta}$, and $z = \frac{2}{1+\beta}$. This figure uses the value $\beta = \frac{1}{2}$ as an example.

was summarized in (90)-(96). We now extend that summary to include transport along the shear as well. Three possible renormalized equations result, depending on the phase regime in which the parameters ε and z fall. The appropriate phase diagram for a given combination of cross-shear transport processes is given by the one of Figures 4, 5, or 6 which corresponds to the active cross-shear transport process which is fastest [46, Ch. 3].

D In general, there is always a D regime within which the space-time rescaling along the shearing direction is diffusive ($\rho = \lambda$) and the tracer motion along the shear "homogenizes." The renormalized Green's function satisfies a local diffusion equation

$$\frac{\partial \bar{G}}{\partial t} = \bar{D}_x(t)\frac{\partial^2 \bar{G}}{\partial x^2} + K_y^* \frac{\partial^2 \bar{G}}{\partial y^2}, \tag{115}$$

with $\bar{G}|_{t=0} = \bar{G}_x^0(x)\delta(y)$ and where the diffusivity in the shear-transverse direction may be time dependent (see 96) but the diffusivity in the shear-parallel direction is a constant given by the following general formula:

$$K_y^* = \kappa + \int_0^\infty \int_{\mathbf{R}} E(q,t)\hat{G}_x(-q,t)dqdt. \tag{116}$$

Note that $\hat{G}_x(k,t)$ is just the shear-transverse Green's function, which is explicitly presented in (90)–(96).

SD-t There is also generally a SD-t phase regime, where the shear-parallel tracer motion is superdiffusive,

$$\rho = \lambda^{z/(2z+\varepsilon-2)} \gg \lambda \quad \text{as } \lambda \to \infty, \tag{117}$$

and asymptotically dependent only on the spatio-temporal properties of the shear velocity field and not on any cross-shear transport processes. The renormalized Green's function in the SD-t phase regime obeys a equation of diffusive type but with a shear-parallel diffusion coefficient which grows with time:

$$\frac{\partial \bar{G}}{\partial t} = \bar{D}_x(t)\frac{\partial^2 \bar{G}}{\partial x^2} + \bar{D}_y(t)\frac{\partial^2 \bar{G}}{\partial y^2}, \tag{118}$$

with $\bar{G}|_{t=0} = \bar{G}_x^0(x)\delta(y)$ and

$$\bar{D}_y(t) \equiv \tilde{K}_0^\sharp t^{(z+\varepsilon-2)/z} \quad \text{as } t \to \infty. \tag{119}$$

The formula for the scaling coefficient $\tilde{K}_0^\sharp$ is presented in (111) and depends only on properties of the shear velocity field. As a consequence of (118), the renormalized Green's function is Gaussian.

SD-s When an effective cross-shear transport mechanism is present, then a third phase regime, which we will generically refer to as SD-s, completes the phase diagram. The SD-s regime could be either of SD-κ, SD-w, or mixed type, depending on the relative strength of the cross-shear processes. In the SD-s phase regime, the tracer motion at large scales and long times is superdiffusive ($\rho \gg \lambda$) and dependent only on the fastest cross-shear transport process present and on the *spatial* structure of the velocity field. In other words, the temporal fluctuations of the velocity are too slow to play a leading role in affecting the coarse-grained tracer behavior, so the renormalized limit is the same as it would be if the velocity field were frozen (steady) in time. The linkage between the space-time rescaling functions in the SD-s regime is generally given by $\rho = \alpha^{1/\nu} = \lambda^{2/(4+\nu(\varepsilon-2)}$, where ν is given in (91). (Note how the exponent ν describing the rate of cross-shear transport explicitly influences the rescaling function λ in the SD-s regime, but not in the SD-t regime, see Eq. (117)). The renormalized Green's function in the SD-s regime is broader-than-Gaussian and does not solve a local PDE.

4.3.2 General Remarks About Renormalization of Closure Approximations.

We now present the renormalized equations predicted by the closure approximations, and compare them with the exact ones described above. Just as in the exact analysis, each closure approximation will predict one of three classes of renormalized equations depending on the values of the infrared scaling parameters and whether $\kappa > 0$. Moreover, the DIA, RLA, and MDIA always correctly locate the phase boundaries as well as the relationship between the rescaling variables α, λ, and ρ. Therefore, for these approximations, we can directly compare their predictions with the exact results, phase regime by phase regime.

The QNA and QLA, however, both completely miss the interaction between the fluctuating cross sweep $w(t)$ and the shear flow $v(x,t)$. Consequently, whenever $w(t)$ is the dominant cross-shear transport mechanism, the phase diagram will be incorrectly predicted by the QNA and QLA.

The mechanics of renormalizing the various approximations are mostly contained within Appendix C.

4.3.3 Renormalized QNA Green's Function

The QNA ignores the influence of $w(t)$ on shear-parallel transport, and generally predicts non-Gaussian renormalized equations except in the D regime, where a constant-coefficient, ordinary diffusion equation results. But none of the non-Gaussian renormalized equations predicted by QNA

are correct. We conclude therefore that *the renormalized QNA Green's function is exact only within the D regime, when* $w(t) \equiv 0$.

We now report the renormalized equations predicted by QNA in the various phase regimes. See Appendix C for the details. We will assume in what follows that $w(t) \equiv 0$ or that at least the fluctuating cross sweep $w(t)$ is not the dominant cross-sweep mechanism. Only in these situations will QNA produce the correct phase diagram and the correct relationship between the scaling functions ρ, α and λ.

D An ordinary diffusion equation (115) for the QNA Green's function is predicted in the D Regime, with renormalized diffusivity:

$$K_y^{*,QNA} \equiv \kappa + \int_0^\infty \int_{\mathbf{R}} E(q,t) e^{-\kappa q^2 t} dq dt.$$

This is in turn equal to the correct diffusivity K_y^* (116) whenever $w(t) \equiv 0$.

SD-t In the SD-t regime, the renormalized QNA equation is:

$$\frac{\partial \hat{\bar{G}}_{\mathrm{QNA}}}{\partial t} = -\kappa k^2 \hat{\bar{G}}_{\mathrm{QNA}} - p^2 \int_0^t \hat{\bar{G}}_0(k,0,s) \bar{D}_y'(s) \hat{\bar{G}}_{\mathrm{QNA}}(k,p,t-s) ds, \quad (120)$$

with $\hat{\bar{G}}_{\mathrm{QNA}}|_{t=0} = \hat{\bar{G}}^0_{x,\mathrm{QNA}}(k)\delta(p)$ and $\hat{\bar{G}}^0_{x,\mathrm{QNA}}(k)$ defined in (105). We have introduced here the function $\hat{\bar{G}}_0(k,p,t)$ representing the large-scale, long-time limiting behavior of the Green's function in absence of random velocity fluctuations (see Appendix A), $\hat{G}_0(k,p,t) = e^{-\kappa(k^2+p^2)t}$. Direct renormalization of this function results in the expressions:

$$\hat{\bar{G}}_0(k,p,t) = \begin{cases} e^{-\kappa(k^2+p^2)t} & \text{if } \kappa > 0, \\ 1 & \text{if } \kappa = 0. \end{cases} \quad (121)$$

Also, note that $\bar{D}_y'(t) = d\bar{D}_y/dt$ is the time derivative of the *exact* renormalized, time-dependent diffusivity in the SD-t regime.

The exact renormalized equation (118) differs from this QNA equation in the SD-t Regime in the following major respects:

1. The exact renormalized equation is a PDE which is local in space and time, whereas the QNA involves a spurious time convolution.

2. Moreover, when $\kappa > 0$, $\hat{\bar{G}}_0(k,0,t)$ is a transcendental function of k, and the renormalized QNA equation cannot therefore be expressed as a PDE in physical space variables.

3. The solution to the exact renormalized equation is Gaussian, whereas it can be readily checked that no Gaussian satisfies the QNA renormalized equation.

4. The appearance of $\hat{\bar{G}}_0(k,0,s)$ in the QNA convolution kernel has no analogue in the exact equation.

SD-κ We consider only the SD-κ regime with dominant spatial decorrelation, since QNA will clearly give the wrong equation in the SD-w regime as the effects of the fluctuating cross sweep on the shear-parallel transport are ignored. The renormalized equation for the Green's function is:

$$\frac{\partial \hat{\bar{G}}_{\mathrm{QNA}}}{\partial t} = -\kappa k^2 \hat{\bar{G}}_{\mathrm{QNA}} - p^2 \int_0^t \bar{d}^{(\kappa)}_{\mathrm{QNA}}(k,s)\hat{\bar{G}}_{\mathrm{QNA}}(k,p,t-s)ds, \qquad (122)$$

with $\hat{\bar{G}}_{\mathrm{QNA}}|_{t=0} = 1$ and where

$$\bar{d}^{(\kappa)}_{\mathrm{QNA}}(k,t) = A_E \int_{\mathbf{R}} |q|^{1-\varepsilon} e^{-\kappa(k-q)^2 t} dq. \qquad (123)$$

Both the renormalized exact and QNA equations are nonlocal, but have different structure. We shall assess the quantitative difference between the exact and QNA large-scale, long-time solutions in the SD-κ regime of a *steady* velocity field through consideration of the fourth order cumulant of the shear-parallel displacement, $\mu_{0,4}(t)$, in Subsubsection 5.2.3.

4.3.4 Renormalized QLA Green's Function

The QLA always predicts a Green's function which is Gaussian when considered separately as a function of x and y, and which satisfies a local diffusion equation with possibly time-dependent diffusivity. Moreover, the QLA correctly predicts the diffusivity whenever $w(t) \equiv 0$. The renormalized QLA Green's function is jointly Gaussian and exact under the following circumstances:

1. In the D regime, when $w(t) \equiv 0$.

2. In the SD-t regime.

3. In a steady flow $v(x,t) = v(x)$ with $\kappa = w(t) = 0$.

The only regime in which the QLA predicts a renormalized Green's function which is not fully Gaussian is in the SD-κ regime, where the renormalized QLA Green's function satisfies the equation:

$$\frac{\partial \hat{G}_{\mathrm{QLA}}}{\partial t} = -\bar{D}_x(t)k^2 \hat{G}_{\mathrm{QLA}} - \bar{D}_{y,\mathrm{QLA}}(k,t)p^2 \hat{G}_{\mathrm{QLA}}, \qquad (124)$$

with $\hat{G}_{\mathrm{QLA}}|_{t=0} = 1$ and where

$$\bar{D}_{y,\mathrm{QLA}}(k,t) = A_E \int_0^t \int_{\mathbf{R}} q^{1-\varepsilon} e^{-\kappa(q^2-2q\kappa)s} dq ds.$$

While this equation is nonlocal in physical space, like the exact result, it suffers from the particular inaccuracy of predicting that the statistics for $Y(t)$ will be always Gaussian in the SD-κ regime whereas the exact statistics are persistently broader-than-Gaussian.

The QLA also misses the influence of $w(t)$ on the diffusion coefficient in the D regime.

4.3.5 Renormalized DIA Green's Function

From Subsections 3.1 and 3.3, we see that the DIA equations are closely related to the QNA equations, with the key difference that occurrences of the "bare" Green's function $\hat{G}_0(k,p,t)$ in the QNA equations are replaced by the full Green's function $\hat{G}_{\mathrm{DIA}}(k,p,t)$ in the DIA equations. This makes the DIA equations nonlinear, and not generally amenable to explicit solution by Laplace transform. Moreover, this change makes the DIA distinctly better than the QNA whenever the fluctuating cross sweep $w(t)$ is the strongest cross-shear transport mechanism, because the DIA does recognize that this fluctuating cross sweep influences the shear-parallel transport. In fact, the DIA renormalization always predicts the correct relationships among the rescaling parameters α, λ, and ρ, and consequently the correct phase diagram. *The actual renormalized equations themselves, however, are only correct within the D regime, when* $w(t) \equiv 0$, which is the same condition under which the QNA renormalization is exact. To gain some understanding of whether the renormalized DIA or renormalized QNA equations are closer to the truth when this condition is not satisfied, we will examine quantitatively the long-time asymptotics of the fourth order cumulant of the shear-parallel displacement in some special submodels in Section 5. We will find that even though the DIA equations are more complicated, they are not always superior to the QNA equations, particularly when $w(t) \equiv 0$.

We now report the renormalized DIA equations in the various phase regimes. See Appendix C for the details. Recall the definition of the differential operator $\mathcal{D}^{\mathrm{DIA}}$ associated to the shear-transverse motion, which is presented following Eq. (104). As discussed in Subsubsection 4.2.2, we have already surrendered the case $\kappa = 0, \beta < -\frac{1}{2}$, where the predicted (subdiffusive) shear-transverse motion is already hopelessly befuddled, and exclude this range of parameters from further consideration below.

D The DIA Green's function renormalizes in the D regime to an equation which is diffusive in the shear-parallel direction:

$$\frac{\partial \hat{\bar{G}}_{\mathrm{DIA}}}{\partial t} = \mathcal{D}^{\mathrm{DIA}}(\hat{\bar{G}}_{\mathrm{DIA}}(k,p,\cdot),k,t) - p^2 K_y^{*,DIA}\hat{\bar{G}}_{\mathrm{DIA}}, \tag{125}$$

with $\hat{\bar{G}}_{\mathrm{DIA}}|_{t=0} = 1$, and renormalized shear-parallel diffusivity:

$$K_y^{*,DIA} \equiv \kappa + \int_0^\infty \int_{\mathbf{R}} E(q,t)\hat{G}_{\mathrm{DIA}}(-q,0,t)dqdt. \tag{126}$$

Note that $\hat{G}_{\mathrm{DIA}}(-q,0,t)$ is the unrenormalized solution of the shear-transverse DIA equation (104), which has nothing to do with the constant $K_y^{*,DIA}$. Therefore, Eq. (126) is really a closed formula, though we are not aware of an explicit expression for $\hat{G}_{\mathrm{DIA}}(-q,0,t)$. When $w(t) = 0$, then $\bar{D}_x(t) \equiv \kappa$ and the exact Gaussian renormalized solution to Eq. (115) is also a solution to the renormalized DIA equation (125). But when $w(t) \neq 0$, even if it is not the dominant cross-shear transport mechanism, the solutions to the renormalized DIA and renormalized exact equations differ in two aspects:

1. the shear-transverse motion $X(t)$ is incorrectly predicted to be non-Gaussian by the DIA, and

2. the effective diffusion coefficient $K_y^{*,DIA}$ for the shear-parallel motion $Y(t)$ differs from the exact result precisely because of the discrepancy between the predicted and exact statistics of $X(t)$.

SD-t The renormalized DIA equation in the SD-t regime is

$$\begin{aligned}\frac{\partial \hat{\bar{G}}_{\mathrm{DIA}}}{\partial t} = \mathcal{D}^{\mathrm{DIA}}&(\hat{\bar{G}}_{\mathrm{DIA}}(k,p,\cdot),k,t) \\ &- p^2 \int_0^t \bar{D}_y'(s)\hat{\bar{G}}_{\mathrm{DIA}}(k,p,s)\hat{\bar{G}}_{\mathrm{DIA}}(k,p,t-s)ds,\end{aligned} \tag{127}$$

with $\hat{\bar{G}}_{\mathrm{DIA}}|_{t=0} = 1$. This equation differs from the exact renormalized equation (118) in the SD-t Regime in the same ways that the QNA renormalized equation (120) does. Indeed, the only difference between the renormalized equations is in the treatment of the shear-transverse transport and the appearance of $\hat{\bar{G}}_{\mathrm{DIA}}(k,p,s)$ in place of $\hat{\bar{G}}_0(k,0,s)$. The same remarks as were made for the QNA in the SD-t regime apply for the DIA.

SD-s In the SD-s regime, the renormalized DIA equation is:

$$\begin{aligned}\frac{\partial \hat{\bar{G}}_{\mathrm{DIA}}}{\partial t} &= \mathcal{D}^{\mathrm{DIA}}(\hat{\bar{G}}_{\mathrm{DIA}}(k,p,t=0),k,t) \\ &\quad - p^2 \int_0^t \bar{d}_{\mathrm{DIA}}(k,p,s)\hat{\bar{G}}_{\mathrm{DIA}}(k,p,t-s)ds,\end{aligned} \tag{128}$$

with $\hat{\bar{G}}_{\mathrm{DIA}}|_{t=0} = 1$ and where

$$\bar{d}_{\mathrm{DIA}}(k,p,t) = A_E \int_{\mathbf{R}} |q|^{1-\varepsilon} \hat{\bar{G}}_{\mathrm{DIA}}(k-q,p,t)dq. \tag{129}$$

This equation is generally nonlocal with non-Gaussian solutions. The exact renormalized Green's function also has these properties in the SD-κ and SD-w regimes, but the details differ in a way which we will explore quantitatively in Subsubsection 5.2.4.

Furthermore, when the shear flow is steady $v(x,t) = v(x)$ and there is no cross-shear transport, $\kappa = w(t) = 0$, the DIA again predicts an incorrectly non-Gaussian Green's function. Even worse, for $\varepsilon < \frac{1}{2}$, which includes the full regime of trapping behavior and part of the regime of subdiffusive behavior, the DIA predicts the wrong rescaling function relationship $\lambda = \rho^{1/2}$ and an unrealizable Green's function. The problems here are direct analogues of those discussed for subdiffusive sweeping motion in Subsubsection 4.2.2.

4.3.6 Renormalized MDIA Green's Function

Like the DIA, the MDIA equations are nonlinear and not explicitly solvable, and renormalization must therefore proceed through assumptions whose self-consistency are subsequently checked. As shown in Appendix C, the MDIA does reproduce the correct phase diagram and the exact relationships between the scaling parameters α, λ, and ρ. Moreover, the renormalized MDIA Green's function is exact in the following situations:

1. within the D regime.

2. within the SD-t regime.

3. whenever $\kappa = 0$ and $w(t) = 0$.

In other words, only in the SD-κ and SD-w regimes does the renormalized MDIA Green's function suffer any inaccuracy.

These results can be recast as follows: The MDIA reproduces, under renormalization, a Gaussian form for the Green's function with exact evolution laws for its mean and covariance whenever the exact renormalized Green's function is Gaussian.

D The renormalized MDIA Green's function is exact in the D Regime. It is a Gaussian which obeys the homogenized diffusion equation (115) with exact diffusion coefficients.

SD-t The renormalized MDIA Green's function is exact in the SD-t Regime. It is a Gaussian which obeys the time-dependent diffusion equation (118) with exact coefficients.

SD-s

$$\frac{\partial \hat{\bar{G}}_{\rm MDIA}}{\partial t} = -k^2 \bar{D}_x(t) \hat{\bar{G}}_{\rm MDIA} - p^2 \bar{D}_{y,{\rm MDIA}}(k,p,t) \hat{\bar{G}}_{\rm MDIA}, \tag{130}$$

with $\hat{\bar{G}}_{\rm MDIA}|_{t=0} = \hat{\bar{G}}_{x,0}(k)$. Here

$$\bar{D}_{y,{\rm MDIA}}(k,p,t) = A_E \int_0^t \int_{\mathbf{R}} |q|^{1-\varepsilon} \frac{\hat{\bar{G}}_{\rm MDIA}(k-q,p,s)}{\hat{\bar{G}}_{\rm MDIA}(k,p,s)} dq ds. \tag{131}$$

and $\hat{\bar{G}}_{x,0}(k)$ is defined in (95). Unlike the other regimes, this renormalized MDIA equation is nonlinear and nonlocal. This is qualitatively in accord with the exact results known for the SD-κ regime [2].

We assess the accuracy of the MDIA renormalized equations (130) in the SD-κ regime through consideration of the fourth order shear-parallel cumulant in Subsection 5.2.5.

4.3.7 Renormalized RLA Green's Function

Since the RLA equation (65) for the Green's function is just a time-dependent diffusion equation (with Gaussian solution), it can be renormalized quite simply in a manner similar to that employed for the exact renormalization of the shear-transverse Green's function. The renormalized RLA Green's function will be perforce Gaussian and satisfies the time-dependent diffusion equation:

$$\frac{\partial \bar{G}_{\rm RLA}}{\partial t} = \bar{D}_x(t) \frac{\partial^2 \bar{G}_{\rm RLA}}{\partial x^2} + \bar{D}_y(t) \frac{\partial^2 \bar{G}_{\rm RLA}}{\partial y^2},$$

with $\bar{G}_{\rm RLA}|_{t=0} = \bar{G}^0_x(x)\delta(y)$ and where the shear-parallel diffusivity $\bar{D}_y(t)$ is half the derivative of the *exact* asymptotic shear-parallel mean-square displacement:

$$\frac{1}{2}\lambda^2 \rho^2 \frac{d\mu_{0,2}(t/\rho^2)}{dt} \sim \bar{D}_y(t) \quad \text{as } t \to \infty,$$

and the initial data $\bar{G}_x^0(x)$ is specified in (94). In particular, the long-time asymptotics predicted by the RLA for the mean-square shear-parallel tracer displacement (and the full statistics for the shear-transverse tracer displacement) are exact. The relationships between the rescaling functions α, λ, and ρ to give a nontrivial renormalized limit are all correct. But the RLA prediction that the renormalized Green's function is Gaussian makes it correct only:

1. within the D regime (where $\bar{D}_y(t) = K_y^*$ is constant), and

2. within the SD-t regime.

The persistent non-Gaussian features of the renormalized Green's function within the SD-w and SD-κ regimes are completely missed by the RLA.

5 Long-Time Behavior of Fourth Order Cumulants in Some Special Steady Models

Our renormalization in Section 4 of the equations furnished by the closure approximations provided some general insight into their predictions for the large-scale, long-time behavior of the Green's function, or equivalently, the tracer displacement PDF. In particular, we were able to ascertain whether the closure approximations correctly or incorrectly predicted an asymptotically Gaussian shape for the tracer displacement PDF at long times. In the present section, we examine the large-scale, long-time predictions of the closure approximations in more quantitative detail for some special cases of the IS-SFCS model. In particular, we examine the long-time predictions for the fourth-order cumulants in both the sweeping (x) and shearing (y) directions through rigorous asymptotic calculations. Our purpose is to quantify asymptotic departures from Gaussianity or relaxation to Gaussianity, as appropriate, so as to provide a sharper means of assessing the accuracy of the closure approximations. Indeed, a Gaussian PDF has vanishing fourth (and higher) order cumulants, so $\mu_{0,4}(t)$ can be used to represent how far the PDF is from a Gaussian shape. More precisely, we compute the *flatness factors* (or *kurtoses*), which are just the ratio of the fourth order tracer displacment moments to the square of the second order moments:

$$\begin{cases} F_{X,4}(t) \equiv \dfrac{\langle X^4(t)\rangle}{\langle X^2(t)\rangle^2} = 3 + \dfrac{\mu_{4,0}(t)}{(\mu_{2,0}(t))^2}, \\ F_{Y,4}(t) \equiv \dfrac{\langle Y^4(t)\rangle}{\langle Y^2(t)\rangle^2} = 3 + \dfrac{\mu_{0,4}(t)}{(\mu_{0,2}(t))^2}, \end{cases} \tag{132}$$

which take the value 3 for a Gaussian, and larger (smaller) values for PDF's which have a broader (thinner) than Gaussian shape. By the moment inequalities [20], a realizable probability distribution for the tracer displacement must have $F_{X,4}(t) \geq 1$ and $F_{Y,4}(t) \geq 1$. If the flatness of the tracer displacement PDF approaches an asymptotic limit (as it does in most cases considered here), we denote it by

$$F^*_{X,4} \equiv \lim_{t\to\infty} F_{X,4}(t), \qquad F^*_{Y,4} \equiv \lim_{t\to\infty} F_{Y,4}(t). \tag{133}$$

Since this section concerns the long-time asymptotics of the tracer displacement statistics, we will take the limit $t \to \infty$ as understood when reporting asymptotic behavior for $\mu_{0,4}(t)$ or $\mu_{4,0}(t)$ (through the standard $\sim$ notation).

We consider the following two relatively simple examples:

1. The behavior of the cumulant $\mu_{4,0}(t)$ the tracer coordinate $X(t)$, which responds only to the sweeping velocity field $w(t)$. The presence of molecular

diffusion leads to trivial modifications, so for clarity we set $\kappa = 0$ in this study (Subsection 5.1).

2. The behavior of the cumulant $\mu_{0,4}(t)$ of the tracer coordinate $Y(t)$ responding to a steady shear flow with molecular diffusion $\kappa > 0$ but no cross sweep $w(t) = 0$. (Subsection 5.2)

More general situations can be analyzed similarly, though the calculations already become quite difficult and tedious for the second example. From these studies, we learn the following:

1. The QLA and RLA always predict Gaussian behavior for $X(t)$ and $Y(t)$ and therefore miss departures from Gaussianity in the shear flow with molecular diffusion model.

2. The MDIA performs better than all of the other closure approximations considered, yielding a correct Gaussian behavior in the random sweeping model and a prediction satisfying $\frac{1}{2}\mu_{0,4}(t) \leq \mu_{0,4}^{\mathrm{MDIA}}(t) \leq \mu_{0,4}(t)$ for all times in the steady shear flow with molecular diffusion model.

3. The DIA and QNA both have a tendency to wrongly predict persistently thinner-than-Gaussian PDF's when the tracer motion is superdiffusive in all models considered.

4. The DIA fails miserably in tracking subdiffusive tracer motion, even yielding unrealizable predictions.

5. The DIA is in some ways worse than the QNA for the first example, but does yield some improvements for the steady shear flow with molecular diffusion model.

We only report and discuss the results in the main text. The details behind the rigorous asymptotic calculations may be found in Appendix D.

5.1 Sweeping Motion

We consider first the long-time statistics of the displacement $X(t)$ of the tracer in the x direction induced by the sweeping velocity component $w(t)$. For simplicity, we take $\kappa = 0$; molecular diffusion changes the results in trivial ways. The structure of the shear flow $v(x, t)$ is irrelevant.

All closure approximations agree with the exact formulas for all cumulants through third order (see Section 3), of which only the second order cumulant $\mu_{2,0}(t)$ is nontrivial. The long-time asymptotics for all models then of course agree with the exact result (87). The QLA, RLA, and MDIA all correctly predict that the PDF for $X(t)$ is Gaussian, and that therefore

all cumulants $\mu_{a,0}(t)$ with $a \neq 2$ vanish. The DIA and QNA, however, incorrectly predict nonzero values for $\mu_{4,0}(t)$, and we now examine the long time asymptotics of these predictions in some detail.

5.1.1 QNA Predictions for Long-Time Asymptotics

$$\mu_{4,0}^{\mathrm{QNA}}(t) \sim \begin{cases} 12K_x^{\sharp\,2}\left(\dfrac{2(\Gamma(\beta+1))^2}{\Gamma(2\beta+3)}-1\right)t^{2\beta+2} & \text{for } -1<\beta<1, \\ 3K_x^{\circ} & \text{for } \beta<-1. \end{cases}$$

These asymptotics imply that the QNA prediction for the tracer PDF has the following asymptotic flatness factor:

$$F_{X,4}^{*,\mathrm{QNA}} = \begin{cases} \dfrac{6(\Gamma(\beta+2))^2}{\Gamma(2\beta+3)} & \text{for } -1<\beta<1, \\ 6 & \text{for } \beta<-1. \end{cases}$$

The graph of this asymptotic flatness factor is presented in Figure 7, along with the horizontal line corresponding to the correct value of 3 corresponding to the Gaussian statistics in our IS-SFCS model. We see that the QNA prediction for the flatness decreases with the infrared scaling exponent β, crossing the Gaussian value 3 at $\beta = 0$. The QNA is a realizable approximation for the case $R_w(t) = w_* e^{-\gamma|t|}$ belonging to the class $\beta = 0$, in that it exactly describes the tracer motion when the sweeping field $w(t)$ is a dichotomous Markov process jumping back and forth between the values $\pm w_*$ [21]. Though this underlying sweeping process is non-Gaussian, it produces Gaussian statistics for the tracer displacement at long times because of the central limit theorem. As $\beta \to 1$ and the correlations in the random sweeping becomes long-ranged, the QNA prediction for the flatness of the tracer PDF approaches the value 1, consistent with its prediction for the case of a random steady sweep (viewed as an extreme limit of a randomly fluctuating sweep with long-range temporal correlations). (See Subsection 3.1). In the trapping regime $\beta < -1$, the QNA predicts a flatness of 6, consistent with the prediction of an exponentially distributed PDF at long times in this regime (Subsubsection 4.2.2).

5.1.2 DIA Predictions for Long-Time Asymptotics

$$\mu_{4,0}^{\mathrm{DIA}}(t) \sim \begin{cases} \frac{12K_x^{\sharp\,2}}{(1+\beta)(1+2\beta)}\left(\dfrac{(\Gamma(\beta+1))^2}{\Gamma(2\beta+1)}-1\right)t^{2\beta+2} & \text{for } -\frac{1}{2}<\beta<1, \\ -24\left(\displaystyle\int_0^\infty ds\,\left(\int_0^s ds'\,R_w(s')\right)^2\right)t & \text{for } \beta<-\frac{1}{2}. \end{cases}$$

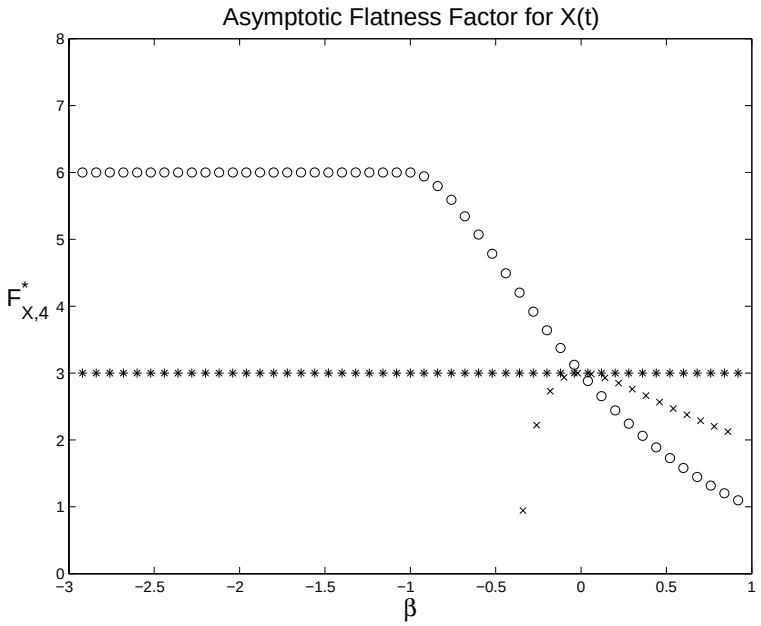

Figure 7: Asymptotic flatness factors $F^*_{X,4}$ for $X(t)$ predicted by QNA (circles: 'o') and DIA (crosses: 'x'). Correct value 3 of flatness factor is indicated by the horizontal line of stars '*'.

These asymptotics imply that the DIA prediction for the tracer PDF has the following asymptotic flatness factor:

$$F_{X,4}^{*,\mathrm{DIA}} = 3\left(\frac{\Gamma(\beta+2)\Gamma(\beta+1)}{\Gamma(2\beta+2)} + \frac{\beta}{2\beta+1}\right) \text{ for } -\frac{1}{2} < \beta < 1.$$

For $\beta < -\frac{1}{2}$, the flatness of the PDF diverges to large negative numbers at long times. This is of course a nonsensical prediction. Indeed, the flatness of any PDF must be greater than or equal to one by elementary moment inequalities [20]. The DIA violates this criterion for all $\beta < -0.3378$, which includes part of the subdiffusive regime and all of the trapping regime. Therefore the DIA is certainly not realizable for a random sweeping model with power spectrum having infrared scaling exponent $\beta < -0.3378$ in that there is no statistical model for the random sweeping which would give results in agreement with the DIA prediction. For $\beta = 0$, the DIA predicts the correct Gaussian value of 3 for the flatness. For all other values of β, the DIA predicts subdiffusive behavior, with the $\beta \to 1$ limit consistently approaching its prediction of $F_{Y,4}^{*,\mathrm{DIA}} = 2$ for a steady random sweep [21].

5.2 Steady Random Shear Flow with Molecular Diffusion

The second example we consider is a steady shear flow with no cross sweep:

$$\boldsymbol{v}(x,y,t) = \begin{pmatrix} 0 \\ v(x) \end{pmatrix},$$

but with active molecular diffusion $\kappa > 0$. Unlike the previous examples, the exact long-time asymptotics of the tracer displacement can be Gaussian or non-Gaussian, depending on the infrared scaling parameter ε of the energy spectrum $\bar{E}(k)$ (75), as we shall describe in Subsubsection 5.2.1.

All approximations correctly predict the mean-square displacement $\mu_{0,2}(t)$, which has the long-time asymptotics [2, 46]:

$$\mu_{0,2}(t) \sim \begin{cases} 2K_y^* t & \text{for } \varepsilon < 0, \\ \dfrac{4}{2+\varepsilon} K_2^\sharp t^{1+\varepsilon/2} & \text{for } 0 < \varepsilon < 2. \end{cases} \tag{134}$$

The scaling constants are given by:

$$\begin{cases} K_y^* = \kappa + 2\displaystyle\int_0^\infty \frac{\bar{E}(q)}{\kappa q^2} dq \\ K_2^\sharp = -\Gamma\left(-\frac{\varepsilon}{2}\right) A_E \kappa^{-(2-\varepsilon)/2}. \end{cases}$$

The comparison of the predictions of their closure predictions will focus on the fourth order statistics of $Y(t)$ through the quantitites $\mu_{0,4}(t)$ and $F_{Y,4}(t)$ (132). The QLA and RLA, which always predict Gaussian statistics for $Y(t)$ are discussed first in Subsection 5.2.2.

In subsequent subsections, we discuss the predictions made by the QNA (Subsection 5.2.3), the DIA (Subsection 5.2.4), and the MDIA (Subsection 5.2.5). Our findings may be summarized as follows:

1. All closure approximations correctly predict an asymptotically Gaussian PDF in the D (homogenization) regime $\varepsilon < 0$, though they disagree with the exact result in certain details concerning the approach to Gaussianity.

2. The asymptotic flatnesses predicted by the closure approximations in the superdiffusive regime $0 < \varepsilon < 2$ are presented in Figure 8. The MDIA is the only closure approximation which even qualitatively agrees with the exact results, in that the tracer displacement becomes Gaussian in the limits $\varepsilon \to 0$ and $\varepsilon \to 2$, and is super-Gaussian for $0 < \varepsilon < 2$.

3. The MDIA prediction is always within a factor of 2 of the exact result for $\mu_{0,4}(t)$, and consequently, MDIA predicts the correct scaling exponents and phase transition values, including the rates of approach to Gaussianity in the D (homogenization) regime.

4. The DIA and QNA, on the other hand, make a number of inaccurate predictions, with DIA offering some minor improvements over the QNA. Both err qualitatively for sufficiently large values of ε (sufficiently strong superdiffusive motion) by predicting the tracer displacement to be thinner than Gaussian.

The rigorous derivations of the results presented here may be found in Appendix D.

5.2.1 Exact Results for Long-Time Asymptotics

$$\mu_{0,4}(t) \sim \begin{cases} K_4^* t^{3/2} & \text{for } \varepsilon < -\frac{1}{2}, \\ K_4^\sharp t^{2+\varepsilon} & \text{for } -\frac{1}{2} < \varepsilon < 2, \end{cases}$$

The scaling constants are given by:

$$\begin{cases} K_4^* = \dfrac{128\sqrt{\pi}}{\kappa^{5/2}} \displaystyle\int_0^\infty (\bar{E}(q))^2 q^{-4} dq, \\ K_4^\sharp = \dfrac{384 A_E^2}{\kappa^{2-\varepsilon}\Gamma(3+\varepsilon)} \displaystyle\int_0^\infty \int_0^\infty I(q,q') dq' dq, \end{cases} \tag{135}$$

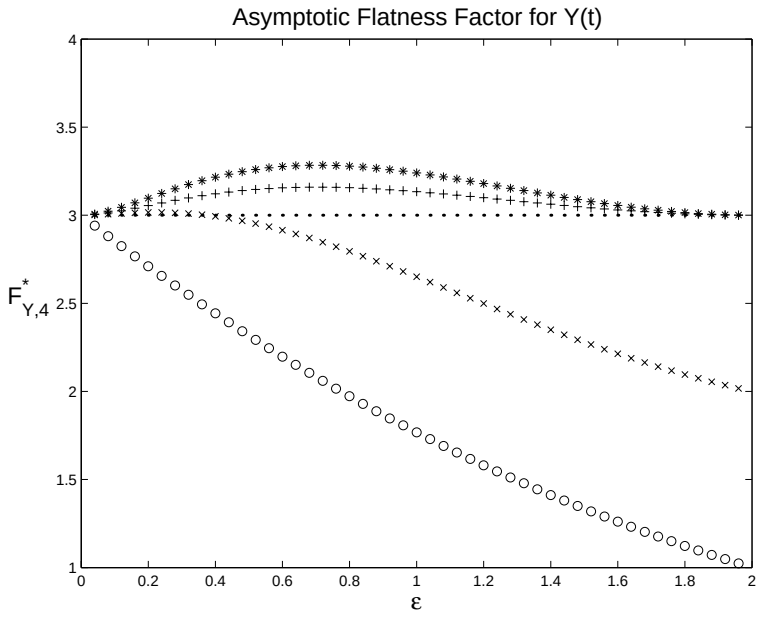

Figure 8: Asymptotic flatness $F_4^\sharp$ predicted for tracer displacement $Y(t)$ along a steady shear flow when molecular diffusion is present $\kappa > 0$ but no cross sweep $w(t) = 0$. Exact: stars '*', QNA: circles 'o', QLA and RLA: dots '.', DIA: crosses 'x', MDIA: pluses '+'.

where

$$I(q,q') = \frac{(qq')^{3-\varepsilon}}{(1+q^2)(1+(q-q')^2)(1+(q+q')^2)(1+q^2+q'^2)} \times \left(\frac{1}{1+q^2}+\frac{1}{1+q'^2}\right). \tag{136}$$

Note that the phase transition for $\mu_{0,4}(t)$ occurs at a different place ($\varepsilon = -\frac{1}{2}$) than the phase transition for $\mu_{0,2}(t)$. Nonetheless, the transition from homogenizing to persistent non-Gaussian behavior is identical with the transition ($\varepsilon = 0$) from diffusive to superdiffusive behavior:

$$F_{Y,4}(t) = \begin{cases} 3 + K_F^* t^{-1/2} + o(t^{-1/2}) & \text{for } \varepsilon < -\frac{1}{2}, \\ 3 + K_F^\bullet t^\varepsilon + o(t^\varepsilon) & \text{for } -\frac{1}{2} < \varepsilon < 0, \\ F_4^\sharp + o(1) & \text{for } 0 < \varepsilon < 2, \end{cases}$$

where:

$$\begin{cases} K_F^* = \dfrac{K_4^*}{4(K_y^*)^2}, \\ K_F^\bullet = \dfrac{K_4^\sharp}{4(K_y^*)^2}, \\ F_4^\sharp = 3 + \dfrac{(2+\varepsilon)^2 K_4^\sharp}{16(K_2^\sharp)^2}. \end{cases}$$

The result for the superdiffusive regime could alternatively be derived by computations beginning with the renormalized Green's function in [6].

An asymptotic calculation shows that

$$\begin{cases} F_4^\sharp = 3 + G_4^\sharp \varepsilon^2 + O(\varepsilon^3) & \text{as } \varepsilon \to 0, \\ F_4^\sharp = 3 + o(1) & \text{as } \varepsilon \to 2, \end{cases}$$

where

$$G_4^\sharp \approx 4.7. \tag{137}$$

That is, the limits as $\varepsilon \to 0$ and $\varepsilon \to 2$ are Gaussian. The reason is that as $\varepsilon \to 2$, the shear becomes so strong that the transverse fluctuations due to molecular diffusion become negligible, and the tracer is moving effectively according to a (steady) random sweep along its shear streamline. The $\varepsilon \to 0$ limit is a transition to the homogenization regime.

5.2.2 QLA and RLA Predictions

The fourth order cumulant is predicted to be zero by the QLA, since the QLA always predicts a Gaussian PDF for $Y(t)$. The QLA therefore completely misses the persistent non-Gaussianity of the shear-parallel tracer

displacement in the superdiffusive regime ($\varepsilon > 0$), in addition to finite time departures from Gaussianity which exist for all ε. If the molecular diffusion is represented as a Gaussian white noise random sweeping velocity field $w(t)$, then the RLA, like the QLA, always predicts a Gaussian PDF for $Y(t)$.

5.2.3 QNA Predictions for Long-Time Asymptotics

$$\mu_{0,4}^{\mathrm{QNA}}(t) \sim \begin{cases} K_4^{*,QNA} t & \text{for } \varepsilon < -2, \\ K_4^{\bullet,QNA} t^{2+\varepsilon/2} & \text{for } -2 < \varepsilon < 0, \\ K_4^{\sharp,QNA} t^{2+\varepsilon} & \text{for } 0 < \varepsilon < 2, \end{cases}$$

The scaling coefficients are given by:

$$\begin{cases} K_4^{*,QNA} = -96\kappa^{-3} \left(\displaystyle\int_0^\infty \bar{E}(q) q^{-2} dq \right) \left(\displaystyle\int_0^\infty \bar{E}(q) q^{-4} dq \right), \\ K_4^{\bullet,QNA} = 24 A_E \varepsilon \Gamma(-(4+\varepsilon)/2) \kappa^{(\varepsilon-4)/2} \displaystyle\int_0^\infty \bar{E}(q) q^{-2} dq, \\ K_4^{\sharp,QNA} = 12 A_E^2 \kappa^{\varepsilon-2} \left(\Gamma(-(2+\varepsilon)/2)\right)^2 \left(\dfrac{2(\Gamma((4+\varepsilon)/2))^2}{\Gamma(\varepsilon+3)} - 1 \right). \end{cases}$$

All these scaling coefficients are negative, because $\bar{E}(q)$ is a non-negative function.

The long-time behavior of the flatness, as predicted by QNA, is as follows:

$$F_{Y,4}^{\mathrm{QNA}}(t) = \begin{cases} 3 + K_F^{*,QNA} t^{-1} + o(t^{-1}) & \text{for } \varepsilon < -2, \\ 3 + K_F^{\bullet,QNA} t^{\varepsilon/2} + o(t^{\varepsilon/2}) & \text{for } -2 < \varepsilon < 0, \\ K_F^{\sharp,QNA} + o(1) & \text{for } 0 < \varepsilon < 2, \end{cases}$$

where:

$$\begin{cases} K_F^{*,QNA} = \dfrac{K_4^{*,QNA}}{4(K_y^*)^2} < 0, \\ K_F^{\bullet,QNA} = \dfrac{K_4^{\bullet,QNA}}{4(K_y^*)^2} < 0, \\ K_F^{\sharp,QNA} = 3 + \dfrac{(2+\varepsilon)^2 K_4^{\sharp,QNA}}{16(K_2^\sharp)^2} = 6 \dfrac{(\Gamma((\varepsilon+4)/2))^2}{\Gamma(\varepsilon+3)}. \end{cases}$$

A plot of $K_F^{\sharp,QNA}$ as a function of ε is shown in Figure 8. Asymptotic calculations show that

$$\begin{cases} K_F^{\sharp,QNA} = 3 - \frac{3}{2}\varepsilon + O(\varepsilon^2) & \text{as } \varepsilon \to 0, \\ K_F^{\sharp,QNA} = 1 + o(1) & \text{as } \varepsilon \to 2. \end{cases}$$

The limit as $\varepsilon \to 2$ gives the flatness associated to the QNA approximation for a tracer just moving steadily (but with a random velocity) with a constant random velocity (27), because the long range correlations are so strong that the molecular diffusion induces negligible decorrelation of the velocity of the tracer along the shearing direction.

We see that the QNA predictions differ from the exact results in the following ways:

1. There are three rather than two phases of long-time behavior of $\mu_{0,4}(t)$, and the phase transition values are incorrect.
2. The long-time scaling exponent for $\mu_{0,4}(t)$ is incorrect for all $\varepsilon < 0$.
3. The scaling coefficients of $\mu_{0,4}^{\mathrm{QNA}}(t)$ are negative, whereas $\mu_{0,4}(t)$ should be positive for all time according to the exact formula.

5.2.4 DIA Predictions for Long-Time Asymptotics

$$\mu_{0,4}^{\mathrm{DIA}}(t) \sim \begin{cases} K_4^{*,DIA} t^{3/2} & \text{for } \varepsilon < -1, \\ o(t^{2+\varepsilon/2}) & \text{for } -1 < \varepsilon < 0, \\ K_4^{\sharp,DIA} t^{2+\varepsilon} & \text{for } 0 < \varepsilon < 2 \end{cases}$$

where the scaling coefficients are given by:

$$\begin{cases} K_4^{*,DIA} = 64\sqrt{\pi}\kappa^{-5/2} \displaystyle\int_0^\infty (\bar{E}(q))^2 q^{-4} dq, \\ K_4^{\sharp,DIA} = \dfrac{24 A_E^2 \kappa^{\varepsilon-2}}{\Gamma(\varepsilon+3)} \left(C_\varepsilon + \displaystyle\int_{\mathbf{R}^2} \frac{|qq'|^{1-\varepsilon}}{(1+q^2)^2(1+(q+q')^2)} dq' dq \right). \end{cases}$$

where

$$C_\varepsilon = \Gamma(-(2+\varepsilon)/2)^2 \left(\Gamma((4+\varepsilon)/2)^2 - \frac{1}{2}\Gamma(\varepsilon+3) \right).$$

At $\varepsilon = -1$ and $\varepsilon = 0$, logarithms enter. The precise asymptotics predicted by DIA are not reported for $-1 < \varepsilon < 0$ because they cannot be expressed simply in terms of an integral expression or the leading order asymptotics of $\bar{E}(k)$ at low wavenumber.

The long-time asymptotics of the flatness factor are given by:

$$F_4(t) = \begin{cases} 3 + K_F^{*,DIA} t^{-\frac{1}{2}} + o(t^{-\frac{1}{2}}) & \text{for } \varepsilon < -1, \\ 3 + o(t^{\varepsilon/2}) & \text{for } -\frac{1}{2} < \varepsilon < 0, \\ F_4^{\sharp,DIA} + o(1) & \text{for } 0 < \varepsilon < 2, \end{cases}$$

where:

$$\begin{cases} K_F^{*,DIA} = \dfrac{K_4^{*,DIA}}{4(K_y^*)^2} > 0, \\ F_4^{\sharp,DIA} = 3 + \dfrac{(2+\varepsilon)^2 K_4^{\sharp,DIA}}{16(K_2^{\sharp})^2}. \end{cases}$$

A plot of $F_4^{\sharp,DIA}$ as a function of ε is shown in Figure 8. Direct asymptotic calculations indicate that:

$$\begin{cases} F_4^{\sharp,DIA} = 3 + G_4^{\sharp,DIA}\varepsilon^2 + O(\varepsilon^3) & \text{as as } \varepsilon \to 0, \\ F_4^{\sharp,DIA} = 2 + o(1) & \text{as } \varepsilon \to 2, \end{cases}$$

where

$$G_4^{\sharp,DIA} \approx 1.1.$$

The limit as $\varepsilon \to 2$ gives the flatness associated to the DIA approximation for a tracer just moving steadily (but with a random velocity) along a single streamline of the shear flow [21].

We see therefore that the DIA does improve upon the QNA predictions in several ways for the present model:

1. The scaling exponent for $\mu_{0,4}(t)$ is correctly predicted by DIA for all ε except $-1 < \varepsilon < 0$.

2. The PDF for $Y(t)$ is correctly predicted to be slightly broader-than-Gaussian for $\varepsilon < -1$ at large but finite times, asymptotically approaching a Gaussian distribution.

3. For small positive values of ε, the DIA correctly predicts the tracer displacement PDF to be slightly broader-than-Gaussian. The flatness is, however, quantitatively underpredicted because $G_4^{\sharp,DIA}$ is about a factor of $1/4$ too small (see Eq. (137)).

4. For larger values of ε, the DIA, like the QNA, wrongly predicts a thinner-than-Gaussian PDF for $Y(t)$, but the underprediction is somewhat less pronounced.

5.2.5 MDIA Predictions for Long-Time Asymptotics

An interesting general fact, resulting from a close similarity between the exact and MDIA finite time formulas for $\mu_{0,4}(t)$ (Appendix D.2.2) is that *for all times*:

$$\frac{1}{2}\mu_{0,4}(t) \leq \mu_{0,4}^{\text{MDIA}}(t) \leq \mu_{0,4}(t).$$

The long time asymptotics for $\mu_{0,4}(t)$ are consequently correct except for the scaling constants:

$$\mu_{0,4}^{\mathrm{MDIA}}(t) \sim \begin{cases} K_4^{*,MDIA} t^{3/2} & \text{for } \varepsilon < -\frac{1}{2}, \\ K_4^{\sharp,MDIA} t^{2+\varepsilon} & \text{for } -\frac{1}{2} < \varepsilon < 2, \end{cases}$$

where:

$$\begin{cases} K_4^{*,MDIA} = \dfrac{64}{\kappa^{5/2}} \displaystyle\int_0^\infty (\bar{E}(q))^2 q^{-4} dq = \frac{1}{2} K_4^*, \\ K_4^{\sharp,MDIA} = \dfrac{384 A_E^2}{\kappa^{2-\varepsilon}\Gamma(3+\varepsilon)} \displaystyle\int_0^\infty \int_0^\infty I^{\mathrm{MDIA}}(q,q') dq' dq. \end{cases}$$

Here

$$I^{\mathrm{MDIA}}(q,q') = \frac{(qq')^{3-\varepsilon}}{(1+q^2)(1+(q-q')^2)(1+(q+q')^2)(1+q^2+q'^2)} \frac{1}{1+q^2}. \tag{138}$$

The flatness of the shear-parallel tracer displacement at long times also obeys the exact laws up to differences in scaling constants:

$$F_4(t) = \begin{cases} 3 + K_F^{*,MDIA} t^{-1/2} + o(t^{-1/2}) & \text{for } \varepsilon < -\frac{1}{2}, \\ 3 + K_F^{\bullet,MDIA} t^{\varepsilon} + o(t^{\varepsilon}) & \text{for } -\frac{1}{2} < \varepsilon < 0, \\ F_4^{\sharp,MDIA} + o(1) & \text{for } 0 < \varepsilon < 2, \end{cases}$$

where:

$$\begin{cases} K_F^{*,MDIA} = \dfrac{K_4^{*,MDIA}}{4(K_y^*)^2} = \dfrac{1}{2} K_F^*, \\ K_F^{\bullet,MDIA} = \dfrac{K_4^{\sharp,MDIA}}{4(K_y^*)^2}, \\ F_4^{\sharp,MDIA} = 3 + \dfrac{(2+\varepsilon)^2 K_4^{\sharp,MDIA}}{16 (K_2^\sharp)^2}. \end{cases}$$

Asymptotic calculations show that

$$\begin{cases} F_4^{\sharp,MDIA} = 3 + G_4^{\sharp,MDIA} \varepsilon^2 + O(\varepsilon^3) & \text{as } \varepsilon \to 0, \\ F_4^{\sharp,MDIA} = 3 + o(1) & \text{as } \varepsilon \to 2, \end{cases}$$

where

$$G_4^{\sharp,MDIA} = 3(\pi^2+4)/16 \approx 2.6$$

The MDIA alone, of all closure approximations considered in this work, correctly predicts the phase transition values, scaling exponents, and (positive) sign of the long time asymptotics of $\mu_{0,4}(t)$. A quantitative comparison between the exact and MDIA formulas for the asymptotic flatness of the tracer displacement PDF in the superdiffusive regime is plotted in Figure 8.

6 Conclusion

We have assessed the value of several standard closure approximations by testing their predictions on an exactly solvable model flow. The shear flow with cross sweep model which we considered is particularly well suited to this task. While it has some special features (Gaussian statistics and shear flow geometry), these are relatively natural and allow us to make a precise study of flows with widely varying and qualitatively different spatio-temporal statistical properties, such as rapid decorrelation in space and/or time, strong positive long-range correlations, and strong negative long-range correlations (which are associated with flows with an oscillatory character). We can infer from our model what kind of statistical features may cause difficulties for the various closure approximations.

When applied to these simple shear flows, we have found the MDIA to be the most successful closure approximation considered. The MDIA always predicts the correct second order moments for the tracer displacement in the model considered in this paper, and correctly describes the phase diagram for the large-scale, long-time statistics of the mean passive scalar density. It is the only approximation which makes qualitatively correct predictions for the higher-order statistics of the tracer displacement along the shear over all regimes of parameters in the IS-SFCS model, and it produces the exact equation for a wider range of situations than any of the other closure approximations considered.

The other closure approximations suffer serious qualitative deficiencies in at least certain subcases of the model considered. The QLA and QNA completely miss the nonlinear coupling of a fluctuating cross sweep velocity and the shear velocity. And in some simple cases where only one of these velocity components is present, the QLA cannot predict non-Gaussian features of the tracer displacement, even at long times, while the QNA predicts spurious persistent departures from Gaussianity in some simple cases.

The DIA does account for the nonlinear coupling between the sweeping velocity and the shear velocity, and can therefore predict the correct shape of the phase diagram demarcating qualitatively different long-time behaviors in the IS-SFCS model. Whenever we have been able to compute explicitly the second order moments of the tracer displacement in the the SFCS model, they have agreed with the exact results. However, even in the relatively simple setting of the SFCS model with a nonzero randomly fluctuating random sweep w, the DIA equation for the second order moment of the tracer displacement is a nonlinear integral equation which is difficult to solve. The exact formulas for these second order moments are much easier to obtain than their DIA approximations! Moreover, the DIA predictions for the higher order moments of the tracer displacement in non-diffusive regimes suffer from serious qualitative defects. The most dramatic failure

of the DIA in this paper is for the random sweeping motion (Subsubsection 5.1.2), wherein the DIA predicts unrealizable values for the fourth order moment of the tracer displacement when the sweeping velocity has its energy spectrum vanishing sufficiently rapidly at low frequencies. The DIA also predicts a qualitatively incorrect thinner-than-Gaussian PDF for the tracer displacement along a steady shear flow when there is sufficiently strong concentration of energy at low wavenumbers (ε large). Therefore, the DIA does not seem to be even qualitatively reliable for predicting the long-term properties of the higher-order statistics of tracer motion in our model for any situation in which there are departures from Gaussianity.

The nonlinearity in the RLA is in some ways milder than that of the MDIA and DIA, and the resulting equations for the passive scalar statistics are easier to analyze. Like the MDIA, the RLA always predicts the correct second order moments for the tracer displacement in the model considered in this paper, and correctly describes the phase diagram for the large-scale, long-time statistics of the mean passive scalar density. However, like the QLA, the RLA always predicts a Gaussian PDF for the tracer displacement, and therefore does not properly represent the higher order statistics when they deviate from Gaussianity. The RLA, therefore, can be viewed as a closure approximation which is not as accurate as the MDIA but is, on the other hand, considerably simpler to work with. For this reason the RLA might constitute the best alternative for more complex situations where the QLA fails but the MDIA is too complicated to analyze.

A Formal derivation of closure approximations

In this appendix we present a unified format for deriving the closure approximations used in main text. These approximations were originally derived using different approaches [10, 13, 29, 30, 61] and the formal approach presented here does not reveal much of the intuition which guided their development. The purpose of this appendix is simply to provide a systematic and self-contained (though non-rigorous) way of obtaining the closure approximations, and to show that each may be viewed as some sort of fairly natural attempt to partially resum a badly behaved perturbation series.

Each of the closure approximations we consider can be viewed as a particular simplification of the formal master equation obtained within the Zwanzig-Mori formalism [52, 73, 74]. To stress these aspects apart from particular details of the physical system under study, we will formulate them in this appendix for general random linear evolution (Liouville) equations:

$$\frac{\partial}{\partial t} f(t) = [L(t) + \lambda\, l(t)]\, f(t), \qquad f|_{t=0} = f_0. \tag{139}$$

The evolution operator has been expressed as a sum of a mean component $L(t)$ and a randomly fluctuating component $\lambda l(t)$ of zero mean with respect to a projection operator $\langle\cdot\rangle$. The scalar λ is introduced as an ordering parameter for constructing perturbation approximations, and will be set to unity at the end. For the advection-diffusion equation for the SFCS model considered in the main text, the operators take the form,

$$L(t) = \kappa\Delta, \qquad \lambda l(t) = -w(t)\frac{\partial}{\partial x} - v(x,t)\frac{\partial}{\partial y}, \tag{140}$$

and the projection $\langle\cdot\rangle$ is the expectation with respect to the statistics of the velocity, though the method presented below apply to arbitrary $L(t)$, $l(t)$, and $\langle\cdot\rangle$. Instead of f, it is convenient to work with the evolution operator $h(t|t')$, which satisfies:

$$\frac{\partial}{\partial t} h(t|t') = [L(t) + \lambda\, l(t)]\, h(t|t'), \qquad h(t|t) = \mathcal{I}, \tag{141}$$

with $\mathcal{I}$ representing the identity operator. Closure amounts to deriving an equation for $H(t|t') = \langle h(t|t')\rangle$ from Eq. (141) because the averaged Green's function is related to this averaged evolution operator by

$$G(\boldsymbol{r} - \boldsymbol{r}', t - t') = H(t|t')\, \delta(\boldsymbol{r} - \boldsymbol{r}'), \tag{142}$$

where we assumed statistical homogeneity in space and time of $l(t)$.

The equation (141) can be written equivalently as the integral equation

$$h(t|t') = H_0(t|t') + \lambda \int_{t'}^{t} ds\ H_0(t|s) l(s) h(s|t'). \tag{143}$$

where $H_0(t|t')$ is the evolution operator under the mean operator $L(t)$ alone,

$$\frac{\partial}{\partial t} H_0(t|t') = L(t) H_0(t|t'), \qquad H_0(t|t) = \mathcal{I}, \tag{144}$$

and H_0 will be considered to be available in suitably explicit form, as is true for the example (140) considered in the paper. Upon iterating and averaging, Eq. (143) leads to the following infinite perturbation series expansion for $H(t|t')$:

$$H(t|t') = H_0(t|t') + \sum_{n=2}^{\infty} \lambda^n H_n(t|t'), \tag{145}$$

where

$$\begin{aligned} H_n(t|t') = & \int_{t'}^{t} ds_1 \int_{t'}^{s_1} ds_2 \cdots \int_{t'}^{s_{n-1}} ds_n \\ & \times H_0(t|s_1) \left\langle l(s_1) H_0(s_1|s_2) \cdots l(s_{n-1}) H_0(s_{n-1}|s_n) l(s_n) \right\rangle H_0(s_n|t'). \end{aligned} \tag{146}$$

Truncation of Eq. (145) at any order yields an approximation for $H(t|t')$ only valid on a short time interval.

Improvement is obtained by partial resummation (or renormalization) [35, 65, 66] of the series (145). This can be achieved starting from the formal equation for H obtained within the Zwanzig-Mori formalism which leads a closed, exact but formal equation for H which can be cast into either one of the following two equivalent forms:

$$\frac{\partial}{\partial t} H(t|t') = L(t) H(t|t') + \lambda^2 \int_{t'}^{t} Q(t,s) H(s|t') ds. \tag{147}$$

$$\frac{\partial}{\partial t} H(t|t') = L(t) H(t|t') + \lambda^2 P(t,t') H(t|t'). \tag{148}$$

Within Zwanzig-Mori formalism, the operators P and Q are usually given in terms of formal expressions which involve (time-ordered) exponentials of the projection operator $\langle \cdot \rangle$ and can be explicitly evaluated only in some simple cases. The only way to give a meaning to those expression is to expand them, so we only give the corresponding (formal) series expansions for P and Q. All the closure approximation given below are obtained by truncation (possibly after resummation) of these series. For Q we obtain

$$\lambda^2 Q(t|t') = \sum_{n=2}^{\infty} \lambda^n Q_n(t|t'), \tag{149}$$

with

$$\begin{cases} Q_2(t|t') = \langle l(t) H_0(t|t') l(t') \rangle \\ Q_{n+2}(t|t') = \displaystyle\int_{t'}^{t} ds_n \cdots \int_{s_2}^{t} ds_1 \\ \qquad \times \langle l(t) H_0(t|s_1) [l(s_1) H_0(s_1|s_2) \cdots [l(s_n) H_0(s_n|t') l(t')] \cdots] \rangle \end{cases} \tag{150}$$

For P we obtain

$$\lambda^2 P(t|t') = \sum_{n=2}^{\infty} \lambda^n P_n(t|t'), \tag{151}$$

with

$$\begin{cases} P_2(t|t') = \displaystyle\int_{t'}^{t} ds \ \langle l(t) H_0(t|s) l(s) \rangle H_0^{-1}(t|s) \\ P_3(t|t') = \displaystyle\int_{t'}^{t} ds_1 \int_{t'}^{s_1} ds_2 \ \langle l(t) H_0(t|s_1) l(s_1) H_0(s_1|s_2) l(s_2) \rangle H_0^{-1}(t|s_2) \\ P_{n+3}(t|t') = -\displaystyle\sum_{p=2}^{n+1} P_p(t|t') H_{n+3-p}(t|t') \\ \quad + \displaystyle\int_{t'}^{t} ds_1 \int_{t'}^{s_1} ds_2 \cdots \int_{t'}^{s_{n+1}} ds_{n+2} \\ \qquad \times \langle l(t) H_0(t|s_1) l(s_1) \cdots H_0(s_{n+1}|s_{n+2}) l(s_{n+2}) \rangle H_0^{-1}(t|s_{n+2}) \end{cases} \tag{152}$$

Here H_0^{-1} is the inverse of H_0 (i.e. $H_0 H_0^{-1} = H_0^{-1} H_0 = \mathcal{I}$). Expansion (151) is the so-called time-ordered cumulant expansion [65, 66].

The series (149) and (151) are derived next. After that we will use the equations (147) and (148) to guide a partial resummation of the series (145) through appropriate approximations for $Q(t,t')$ and $P(t,t')$. The QNA and the DIA are obtained from such approximations for Q, while the QLA, MDIA, and RLA are obtained from such approximations for P.

Derivation of Eqs. (147) and (148) We first obtain the series expansion for Q. Decompose h into its mean component H and fluctuating component $\lambda\tilde{h}$:

$$h(t|t') = H(t|t') + \lambda \tilde{h}(t|t'), \qquad \langle \tilde{h} \rangle = 0. \tag{153}$$

From (141) H and $\tilde{h}$ satisfy

$$\begin{cases} \dfrac{\partial}{\partial t} H = L(t) H + \lambda^2 \langle l(t) \tilde{h} \rangle, \\ \dfrac{\partial}{\partial t} \tilde{h} = L(t) \tilde{h} + l(t) H + \lambda [l(t) \tilde{h}], \end{cases} \tag{154}$$

where here and below $[\cdot]$ denotes the projector orthogonal to $\langle\cdot\rangle$, i.e. $[g] = g - \langle g\rangle$. Using $\tilde{h}(t'|t') = 0$, the second equation in (154) is equivalent to the integral equation

$$\tilde{h}(t|t') = \int_{t'}^{t} ds H_0(t|s) l(s) H(s|t') + \lambda \int_{t'}^{t} ds H_0(t|s)[l(s)\tilde{h}(s|t')]. \tag{155}$$

Iteration of this equation produces a series expansion for $\tilde{h}$ which can be used to evaluate the term $\lambda^2\langle l(t)\tilde{h}\rangle$ in the first equation in (154). The expression one obtains can be written as $\lambda^2 \int_{t'}^{t} Q(t,s)H(s|t')ds$ as in (147) with Q given by the series in (149) with Q_n's as in (150).

We now obtain the series expansion for P. We rewrite Eq. (148) as

$$\lambda^2 P(t|t')H(t|t') = \frac{\partial}{\partial t} H(t|t') - L(t)H(t|t'), \tag{156}$$

and, using the expansions (145) and (151) for H and P, we expand both sides of (156) to get

$$\begin{aligned} &\sum_{n=2}^{\infty} \lambda^n P_n(t|t')H_0(t|t') + \sum_{n=4}^{\infty} \lambda^n \sum_{p=2}^{n-2} P_p(t|t')H_{n-p}(t|t') \\ &\quad = \sum_{n=2}^{\infty} \lambda^n \int_{t'}^{t} ds_1 \int_{t'}^{s_1} ds_2 \cdots \int_{t'}^{s_{n-1}} ds_n \ \langle l(t)H_0(t|s_1)\cdots l(s_n)\rangle H_0(s_n|t') \end{aligned} \tag{157}$$

Equating powers of λ in both sides we obtain Eq. (152).

A.1 The quasinormal approximation (QNA)

Truncation of Eq. (149) at order λ^2 and use of the result as an approximation for $Q(t,t')$ in (147) results in the QNA equation (setting $\lambda = 1$)

$$\frac{\partial H_{\mathrm{QNA}}}{\partial t} = L(t)H_{\mathrm{QNA}} + \int_{t'}^{t} \langle l(t)H_0(t|s)l(s)\rangle \, H_{\mathrm{QNA}}(s|t')ds. \tag{158}$$

Upon applying Eq. (158) to $\delta(\boldsymbol{r} - \boldsymbol{r}')$ an explicit equation for G_{QNA} is obtained; for our turbulent diffusion model it is Eq. (23). We note that the QNA equation (158) may be obtained alternatively under the assumption that the process $\{l(t), h(t|t')\}$ is Gaussian, or "normal," whence its name.

A.2 The quasilinear approximation (QLA)

Truncation of Eq. (151) at order λ^2 and use of the result as an approximation for $P(t,t')$ in (148) results in the QLA equation (setting $\lambda = 1$)

$$\frac{\partial H_{\mathrm{QLA}}}{\partial t} = L(t)H_{\mathrm{QLA}} + P_2(t,t')H_{\mathrm{QLA}}. \tag{159}$$

where P_2 is given in (152). The equation for $G_{\rm QLA}$ is obtained by applying Eq. (159) to $\delta(\boldsymbol{r}-\boldsymbol{r}')$. For the general case, this operation requires computing the operator $H_0^{-1}(t|s)H(t|t')$ which may be a nontrivial endeavor. For our turbulent diffusion model, it results in (30). For the general case it should also be stressed that, since $t' \leq s \leq t$, $\delta(\boldsymbol{r}-\boldsymbol{r}')$ is expected to belong to the domain of definition of $H_0^{-1}(t|s)H(t|t')$. Put differently, the QLA can be well-posed even though the operator $H_0^{-1}(t|s)$ may on its own not be defined on the solution space of interest. To the best of our knowledge, the QLA is not equivalent to any statistical assumption about the statistics of $\{l(t), h(t|t')\}$ analogous to that of the QNA.

We also note that when $L(t)$ is a first-order differential operator (such as the case of $\kappa = 0$ in (140)), the expression for P_2 in (152) is equivalent to

$$P_2(t,t') = \int_{t'}^{t} ds \;\; \langle l(t)[H_0(t|s)l(s)]\rangle \,, \tag{160}$$

where the last $H_0(t|s)$ only acts on the $l(s)$ at its direct right. Interestingly, it is straightforward to show that the operation which consist in cancelling the inverse operators $H_0^{-1}(t|s)$ can be done at any order in the series for $P(t,s)$ (i.e. for any $P_n(t,s)$). We shall use Eq. (160) subsequently for deriving the RLA: here, however, we will keep working with the expression for P_2 in (152) since this expression remains valid for general $L(t)$, unlike Eq. (160).

A.3 The direct interaction approximation (DIA)

Generally, the QNA and the QLA are only valid for all times if $H(t|t')$ evolves on a time-scale which is much longer than the correlation time of $l(t)$; i.e. if the Kubo number is small [65, 66]. One may hope to improve these approximations in more general situations by reworking the series for $Q(t,t')$ or $P(t,t')$ in terms of $H(t|t')$ rather than $H_0(t|t')$, since this operation achieves a further resummation of the original series (145). In the case of $Q(t,t')$, this gives

$$\lambda^2 Q(t,t') = \lambda^2 \bar{Q}_2(t,t') + \lambda^3 \bar{Q}_3(t,t') + \cdots, \tag{161}$$

where up to order λ^2

$$\bar{Q}_2(t,t') = \langle l(t)H(t|s)l(s)\rangle \,. \tag{162}$$

Truncation of Eq. (161) at order λ^2 is the DIA, i.e. this approximation leads to the following equation for $H(t|t')$ (for $\lambda = 1$):

$$\frac{\partial H_{\rm DIA}}{\partial t} = L(t)H_{\rm DIA} + \int_{t'}^{t} \langle l(t)H_{\rm DIA}(t|s)l(s)\rangle \, H_{\rm DIA}(s|t')ds. \tag{163}$$

For our turbulent diffusion model, the explicit equation for $G_{\rm DIA}$ which is obtained by applying Eq. (163) to $\delta(\boldsymbol{r}-\boldsymbol{r}')$ is given in (38). The DIA may alternatively be derived as the exact equation associated to a modified version of the original equation (141) –the so-called random coupling model [31] – which is obtained by further randomizing Eq. (141) via the introduction of appropriate random phase coefficients in front of the $l(t)h(t|t')$ term. This guarantees that the DIA is *realizable* in a weak sense, meaning that it produces a prediction $G_{\rm DIA}$ that is indeed the exact average solution to some underlying random evolution model, and therefore has certain statistical consistency properties. However, we shall see by an explicit example in Section 5 that when applied to turbulent diffusion models, where the solution should always be non-negative because G is a PDF, the DIA equation can produce solutions $G_{\rm DIA}$ which do become negative over certain space-time regions. Therefore, the DIA is not realizable in the strong sense [55] that its prediction $G_{\rm DIA}$ for a turbulent diffusion model corresponds to the exact Green's function for some other underlying turbulent diffusion model, and therefore inconsistent statistical properties of the tracer motion can be predicted.

A.4 The modified direct interaction approximation (MDIA)

The MDIA is derived by reworking the series for $P(t,t')$ in terms of $H(t|t')$ rather than $H_0(t|t')$, in a manner parallel to the DIA derivation given above. We obtain

$$\lambda^2 P(t,t') = \lambda^2 \bar{P}_2(t,t') + \lambda^3 \bar{P}_3(t,t') + \cdots, \tag{164}$$

where up to order λ^2

$$\bar{P}_2(t,t') = \int_{t'}^{t} \langle l(t) H(t|s) l(s) \rangle \, H^{-1}(t|s) ds. \tag{165}$$

In (165), the operator H^{-1} is the inverse of H. Truncation of Eq. (164) at order λ^2 produces the MDIA equation for H (for $\lambda = 1$):

$$\frac{\partial H_{\rm MDIA}}{\partial t} = L(t) H_{\rm MDIA} + P_2^{\rm MDIA}(t,t') H_{\rm MDIA}, \tag{166}$$

where

$$P_2^{\rm MDIA}(t,t') = \int_{t'}^{t} \langle l(t) H_{\rm MDIA}(t|s) l(s) \rangle \, H_{\rm MDIA}^{-1}(t|s) ds. \tag{167}$$

Thea application of Eq. (166) to $\delta(\boldsymbol{r}-\boldsymbol{r}')$ gives Eq. (51) for our turbulent diffusion model. For the general case the explicit realization of the MDIA equation may be even more complicated than for the QLA since it now

requires computing the operator $H^{-1}_{\rm MDIA}(t|s)H_{\rm MDIA}(t|t')$. However, as with the QLA, the MDIA is expected to be a well-posed approximation since, with $t' \le s \le t$, $\delta(\boldsymbol{r}-\boldsymbol{r}')$ should belong to the domain of definition of $H^{-1}_{\rm MDIA}(t|s)H_{\rm MDIA}(t|t')$. We did not find any statistical assumption on $\{l(t), h(t|t')\}$ which leads to the MDIA, nor did we obtain any modified version of Eq. (141) for which the MDIA would be exact. The MDIA, however, does have some features which are superior to the DIA, as shown in [68] and by its performance on the turbulent diffusion models discussed in the text.

A.5 The Renormalized Lagrangian Approximation (RLA)

Here we rework the series for $P(t,t')$ as a series in $H(t|t')$ rather than $H_0(t|t')$, as for the MDIA, but use expression (160) instead of the one in Eq. (151) for $P_2(t,t')$ (and similarly if higher order terms were to be concerned). As stated there, this is only legitimate for evolution operators with first-order spatial derivatives. This procedure leads to

$$\lambda^2 P(t,t') = \lambda^2 \breve{P}_2(t,t') + \lambda^3 \breve{P}_3(t,t') + \cdots, \tag{168}$$

where up to order λ^2

$$\breve{P}_2(t,t') = \int_{t'}^{t} \langle l(t)[H(t|s)l(s)]\rangle \, ds, \tag{169}$$

where $H(t|t')$ only acts on the $l(t)$ at its direct right. Truncation of Eq. (168) at order λ^2 gives the RLA (for $\lambda = 1$):

$$\frac{\partial H_{\rm RLA}}{\partial t} = L(t)H_{\rm RLA} + P_2^{\rm RLA}(t,t')H_{\rm RLA}, \tag{170}$$

where

$$P_2^{\rm RLA}(t,t') = \int_{t'}^{t} \langle l(t)[H_{\rm RLA}(t|s)l(s)]\rangle \, ds. \tag{171}$$

The application of Eq. (170) to $\delta(\boldsymbol{r}-\boldsymbol{r}')$ gives Eq. (65) for the turbulent diffusion model with $\kappa = 0$. Notice that the RLA equation has a rather simple nonlinearity and will usually be much simpler to write down than the MDIA (or even the QLA) equations since no inverse operator like $H^{-1}_{\rm MDIA}(t|s)$ or $H_0^{-1}(t|s)$ is involved. The RLA can be easily extended to turbulent diffusion situations with molecular diffusion by representing the latter as an additional white-noise random sweep, thereby transforming the parabolic advection-diffusion equation into a first-order pure advection PDE. We did not find any statistical assumption on $\{l(t), h(t|t')\}$ which leads to the RLA, nor did we obtain any modified version of Eq. (141) for which the RLA would be exact.

B Proof of Proposition 1

We provide here the proof of Proposition 1 in Subsection 2.3. The statement concerning $\mu_{a,b}(t)$ for a or b odd follows by noting that $\hat{G}(k,p,t)$ is even in k and p.

To compute $\mu_{2m,2}(t)$ (both for $m = 0$ and $m \geq 1$), we expand the argument in the functional average representation (15) for $\hat{G}(k,p,t)$ as a Taylor series in p:

$$\begin{aligned}
&\hat{G}(k,p,t) \\
&= \left\langle e^{-ikX(t)} \left(1 - \kappa p^2 t - \frac{1}{2}p^2 M(t) + O(p^4)\right)\right\rangle_{w,W_x} \\
&= \langle e^{-ikX(t)}\rangle_{w,W_x} \left(1 - \kappa p^2 t - \frac{1}{2}p^2 \bar{M}(t) + O(p^4)\right).
\end{aligned}$$

where

$$\begin{cases}
M(t) = \displaystyle\int_0^t \int_0^t \int_{\mathbf{R}} E(q, s-s') e^{iq(X(s)-X(s'))} dq ds' ds \\
\bar{M}(t) = \displaystyle\int_0^t \int_0^t \int_{\mathbf{R}} E(q, s-s') \frac{\langle e^{iq(X(s)-X(s'))-ikX(t)}\rangle_{w,W_x}}{\langle e^{-ikX(t)}\rangle_{w,W_x}} dq ds' ds.
\end{cases}$$

The generating function, $\rho = \ln \hat{G}$, for the cumulants can therefore be Taylor expanded about $p = 0$ as follows:

$$\rho(k,p,t) = \ln\langle e^{-ikX(t)}\rangle_{w,W_x} - \kappa p^2 t - \frac{1}{2}p^2 \bar{M}(t) + O(p^4) \tag{172}$$

On the other, using the fact that $X(t)$ is a Gaussian process, we have

$$\bar{M}(t) = \int_0^t \int_0^t \int_{\mathbf{R}} E(q, s-s') e^{-\frac{1}{2}q^2 \mu_{0,2}(s-s') + kq M_x(t,0;s,s')} dq ds' ds,$$

where we defined

$$M_x(t_1,t_2;t_3,t_4) = \langle (X(t_1) - X(t_2))(X(t_3) - X(t_4))\rangle.$$

This auxiliary function may be computed easily to give formula (20) stated in the proposition. Now evaluating the requisite derivatives of Eq. (172), we deduce the formulas $\mu_{2m,2}(t)$ with $m \geq 0$ stated in the proposition.

Finally, we compute $\mu_{0,4}(t)$, the fourth order cumulant of the shear-parallel tracer displacement, by using the following general formula valid when $\mu_{0,1}(t) = \mu_{0,3}(t) = 0$ as in the present case:

$$\mu_{0,4}(t) = \langle Y^4(t)\rangle - 3\langle Y^2(t)\rangle^2 = \langle Y^4(t)\rangle - 3\mu_{0,2}^2(t)$$

From Eq. (15), it follows that

$$\langle Y^4(t)\rangle = 3\int_0^t ds_1 \int_0^t ds_2 \int_0^t ds_3 \int_0^t ds_4 \int dq dq' \\ \times E(q, s_1 - s_2)E(q', s_3 - s_4) \left\langle \mathrm{e}^{iq[X(s_1)-X(s_2)]+iq'[X(s_3)-X(s_4)]} \right\rangle_{w,W_x}.$$

Using the Gaussianity of $X(t)$ to perform the remaining average, we are left with

$$\begin{aligned}\langle Y^4(t)\rangle = 3\int_0^t ds_1 \int_0^t ds_2 \int_0^t ds_3 \int_0^t ds_4 \int_{\mathbf{R}^2} dq\, dq' \\ \times\ E(q, s_1 - s_2)E(q', s_3 - s_4) \\ \times\ \mathrm{e}^{-\frac{1}{2}q^2\mu_{2,0}(s_1-s_2)-\frac{1}{2}q'^2\mu_{2,0}(s_3-s_4)-qq'M_x(s_1,s_2;s_3,s_4)}\end{aligned}$$

Substituting this result into the above equation for $\mu_{0,4}(t)$, we obtain the expression in (19).

C Renormalization of Closure Approximations

We collect here those derivations of the renormalized equations for the closure approximations which were too lengthy too include in Section 4. In Subsection C.1, we provide some details for the derivation of the renormalized equations for the shear-transverse Green's function under QNA and DIA. Then in Subsection C.2, we indicate how to derive the full renormalized Green's functions for all closure approximations.

C.1 Renormalization of Shear-Transverse Green's Function

C.1.1 Renormalization of QNA Equation for Shear-Transverse Green's Function

The Laplace transform of the shear-transverse Green's function under QNA is given by Eq. (24):

$$\tilde{G}_{x,\mathrm{QNA}}(k,\zeta) = \left[\zeta + k^2(\kappa + \tilde{R}_w(\zeta + \kappa k^2))\right]^{-1}.$$

The large-scale, long-time rescaling (70) induces the following rescaling under Laplace transformation:

$$\begin{aligned}\tilde{G}^{(\rho)}_{x,\mathrm{QNA}}(k,\zeta) &= \rho^2 \tilde{G}_{x,\mathrm{QNA}}(\alpha k, \rho^2\zeta) \\ &= \left[\zeta + \alpha^2\rho^{-2}k^2(\kappa + \tilde{R}_w(\rho^2\zeta + \alpha^2\kappa k^2))\right]^{-1}.\end{aligned}$$

The renormalization requires the ascertainment of the low ζ asymptotics of $\tilde{R}_w(\zeta)$. This can be computed either by relating it to $E_w(\omega)$ through the definition (71) or actually more simply by noting from Eq. (19) that $\tilde{\mu}_{2,0}(\zeta) = 2\tilde{R}_w(\zeta)\zeta^{-2}$ and using the low ζ asymptotics of $\tilde{\mu}_{2,0}(\zeta)$ as inferred from the large t asymptotics of $\mu_{2,0}(t)$ from Eqs. (87) and (88). There results:

$$\tilde{R}_w(\zeta) \sim \begin{cases} \frac{1}{2}K_x^{\circ}\zeta & \text{for } \beta < -1, \\ \Gamma(1+\beta)K_x^{\sharp}\zeta^{-\beta} & \text{for } -1 < \beta < 1, \end{cases} \tag{173}$$

as $\zeta \to 0$. Working from this in the same as we did for the exact shear-transverse Green's function, we find that the relationship between the rescaling factors α and ρ^2 is the same as for the exact case, and that the renormalized Laplace transform of the QNA Green's function is:

$$\tilde{\bar{G}}_{x,\mathrm{QNA}}(k,\zeta) = \left[\zeta + k^2\zeta\tilde{\bar{D}}_x(\zeta))\right]^{-1}, \tag{174}$$

provided that $\beta > -1$ or $\kappa > 0$. The function $\tilde{\bar{D}}_x(\zeta)$ is just the Laplace transform of the exact renormalized diffusivity $\bar{D}_x(t)$ Eq. (96) across the

shear. Expressed in real time variables, the renormalized equation for the QNA shear-transverse Green's function takes the form of the convolutive diffusion equation (103). The alternative forms for the equation (99) and (97) for the case of subdiffusive and superdiffusive cross sweeps can be deduced by analogy to the derivation of the corresponding renormalized DIA equations, which will be presented in the next subsubsection.

For the trapping regime ($\kappa = 0$ and $\beta < -1$), the renormalized diffusivity vanishes and the renormalized Laplace transform of the QNA Green's function is

$$\tilde{\tilde{G}}_{x,\mathrm{QNA}}(k,\zeta) = \left[\zeta(1 + \frac{1}{2}K_x^\circ k^2)\right]^{-1}.$$

C.1.2 Renormalization of DIA Equation for Shear-Transverse Green's Function

The DIA equation for the shear-transverse Green's function is not explicitly solvable for general $w(t)$, so we renormalize the implicit relationship for its Laplace transform (Eqs. (39) and (40)). Under the rescaling (70), we obtain:

$$\tilde{G}^{(\rho)}_{x,\mathrm{DIA}}(k,\zeta) = \left[\zeta + \alpha^2\rho^{-2}k^2(\kappa + \tilde{A}_{\mathrm{DIA}}(\alpha k, 0, \rho^2\zeta))\right]^{-1}, \tag{175}$$

where

$$\begin{aligned}\tilde{A}_{\mathrm{DIA}}(\alpha k, 0, \rho^2\zeta) &= \frac{1}{2\pi i}\int_{\mathcal{C}} \tilde{R}_w(\zeta')\tilde{G}_{x,\mathrm{DIA}}(\alpha k, \rho^2\zeta - \zeta')d\zeta' \\ &= \int_0^\infty e^{-\zeta\rho^2 t}R_w(t)\hat{G}_{x,\mathrm{DIA}}(\alpha k, t)dt\end{aligned} \tag{176}$$

To renormalize the shear-transverse DIA Green's function, we need to examine the asymptotic limit of Eq. (176) as $\alpha \to 0$ and $\rho \to 0$. The appearance of the unknown function $\tilde{G}_{\mathrm{DIA}}$ in this formula creates an extra complication which was not present in the QNA renormalization. A practical way to proceed is to posit certain natural limiting behavior for $\tilde{A}_{\mathrm{DIA}}(\alpha k, 0, \rho^2\zeta)$, and then check under what conditions those limits give rise to self-consistent, nontrivial expressions for $\tilde{\tilde{G}}_{x,\mathrm{DIA}}(k,\zeta)$. We show below that three different limiting behaviors exhaust all possibilities, other than a phase transition value $\beta = -\frac{1}{2}$ with which we do not concern ourselves.

The lack of an explicit solution for $\hat{G}_{x,\mathrm{DIA}}(k,t)$ also raises the question of how to specify the initial data for $\hat{\tilde{G}}_{x,\mathrm{DIA}}(k,t)$, since we saw that the renormalized exact solution can exhibit a discontinuity at $t = 0$. We can expect, however, that whenever there is persistent evolution of the passive scalar field to large scales over long times (that is, $\alpha \to 0$ as $\rho \to 0$), then

$\lim_{t\to 0} G_x(x,t) = \delta(x)$ and $\lim_{t\to 0} \hat{G}(k,t) = 1$ so that there is no discontinuity. Indeed, if the solution spreads in time, then under a large-scale, long-time-rescaling, the solution should appear to shrink to a delta function as the time approaches its initial value. The only time, therefore, we will be wary of a discontinuity at $t = 0$ for the renormalized Green's function is when there is no evolution of the Green's function to large scales, i.e. when the motion is trapped and $\alpha = 1$. As it turns out, the DIA falsely predicts there is no trapping regime so the issue of discontinuity of $\hat{G}_{x,\mathrm{DIA}}(k,t)$ at $t = 0$ does not arise; we assume it always connects continuously to the initial value $\hat{G}_{x,\mathrm{DIA}}(k, t = 0) = 1$.

Diffusive Cross-Shear Transport One obvious possible limit for Eq. (176) results by just assuming that α and ρ^2 are set equal to zero in the integrand on the right hand side:

$$\tilde{A}_{\mathrm{DIA}}(\alpha k, 0, \rho^2\zeta) \to \int_0^\infty R_w(t)\hat{G}_{\mathrm{DIA}}(0,0,t)dt = \int_0^\infty R_w(t)dt \qquad (177)$$

since $\hat{G}_{\mathrm{DIA}}(0,0,t) = 1$. Setting $\alpha = \rho$, this gives rise self-consistently to an ordinary diffusion equation (93) with correct constant renormalized diffusivity when either $\beta = 0$, or $\kappa > 0$ and $\beta \leq 0$.

Super-Diffusive Cross-Shear Transport For $0 < \beta < 1$, the formal limit (177) would be infinity. The self-consistent limit for this case is:

$$\begin{aligned}
&\alpha^2\rho^{-2}\tilde{A}_{\mathrm{DIA}}(\alpha k, 0, \rho^2\zeta) \\
&\quad = \alpha^2 \int_{\mathcal{C}} \frac{d\zeta'}{2\pi i} \tilde{R}_w(\rho^2\zeta')\tilde{G}_{x,\mathrm{DIA}}(\alpha k, \rho^2\zeta - \rho^2\zeta') \\
&\quad \sim \alpha^2\rho^{-2-2\beta}\Gamma(1+\beta)K_x^\sharp \int_{\mathcal{C}} \frac{d\zeta'}{2\pi i} \zeta'^{-\beta}\tilde{\tilde{G}}_{x,\mathrm{DIA}}(k, \zeta - \zeta') \\
&\quad = \alpha^2\rho^{-2-2\beta} \int_{\mathcal{C}} \frac{d\zeta'}{2\pi i} \tilde{\bar{D}}'_x(\zeta')\tilde{\tilde{G}}_{x,\mathrm{DIA}}(k, \zeta - \zeta'),
\end{aligned} \qquad (178)$$

where $\tilde{\bar{D}}'_x(\zeta)$ is the Laplace transform of $\bar{D}'_x(t)$, the derivative of the function given in (96). (We take the contour $\mathcal{C}$ to lie just to the right of the imaginary axis, so that it is invariant under the rescaling of integration variables in the first step). Choosing $\rho = \alpha^{1/(1+\beta)}$, we then obtain Eq. (98) after an inverse Laplace transform.

Sub-Diffusive Cross-Shear Transport with $-\frac{1}{2} < \beta < 0$ When $\kappa = 0$ and $\beta < 0$, the right hand side of Eq. (177) vanishes. To obtain a

nontrivial rescaled limit for $\tilde{A}_{\mathrm{DIA}}(\alpha k, 0, \rho^2\zeta)$ when $-\frac{1}{2} < \beta < 0$, we must rescale integration variables as in (178), but the limit stated in (178) is not appropriate when $\beta < 0$ because the integrand is not integrable at infinity. This divergence is treated by a renormalization technique typical in the theory of generalized functions [22]. It is most straightforward in this regard to work with the second expression for $\tilde{A}_{\mathrm{DIA}}(\alpha k, 0, \rho^2\zeta)$ in (176). Using the fact that

$$\int_0^\infty R_w(t)\,dt = \frac{1}{2}\int_{\mathbf{R}} R_w(t)\,dt = \frac{1}{2}E_w(\omega = 0) = 0 \text{ for } \beta < 0,$$

we can write

$$\tilde{A}_{\mathrm{DIA}}(\alpha k, 0, \rho^2\zeta) = \int_0^\infty \left(e^{-\zeta\rho^2 t}\hat{G}_{x,\mathrm{DIA}}(\alpha k, t) - 1\right) R_w(t)dt.$$

Now we can rescale variables and pass to the large-scale, long-time limit:

$$\begin{aligned}
&\alpha^2\rho^{-2}\tilde{A}_{\mathrm{DIA}}(\alpha k, 0, \rho^2\zeta) \\
&\quad = \alpha^2\rho^{-4}\int_0^\infty \left(e^{-\zeta t}\hat{G}_{x,\mathrm{DIA}}(\alpha k, t/\rho^2) - 1\right) R_w(t/\rho^2)dt \\
&\quad \sim \alpha^2\rho^{-4}\int_0^\infty \left(e^{-\zeta t}\hat{\tilde{G}}_{x,\mathrm{DIA}}(k, t) - 1\right) \beta K_x^\sharp (t/\rho^2)^{\beta-1}dt \\
&\quad = \alpha^2\rho^{-2-2\beta}\int_0^\infty \left(e^{-\zeta t}\hat{\tilde{G}}_{x,\mathrm{DIA}}(k, t) - 1\right) \bar{D}'_x(t)dt,
\end{aligned} \tag{179}$$

where we have inserted the long-time asymptotics of $R_w(t)$ [17]:

$$\begin{aligned}
R_w(t) &= \int_{\mathbf{R}} \cos(\omega t) A_{E,w}|\omega|^{-\beta}\psi_w(\omega)d\omega \\
&\sim 2^{1-\beta}\sqrt{\pi}\frac{\Gamma((1-\beta)/2)}{\Gamma(\beta/2)}A_{E,w}t^{\beta-1} = \beta K_x^\sharp t^{\beta-1},
\end{aligned} \tag{180}$$

for $\beta \neq 0, -2, -4, \ldots$. Choosing $\rho = \alpha^{1/(1+\beta)}$, we formally obtain the following equation for the renormalized Green's function:

$$\zeta\tilde{\hat{G}}_{x,\mathrm{DIA}} + k^2\left[\int_0^\infty \left(e^{-\zeta t}\hat{\tilde{G}}_{x,\mathrm{DIA}}(k, t) - 1\right)\bar{D}'_x(t)\,dt\right]\tilde{\hat{G}}_{x,\mathrm{DIA}} = 1. \tag{181}$$

We have to check, however, that this renormalized equation is self-consistently sensible. In particular, it is no longer clear whether the integral converges because the large-scale, long-time renormalized Green's function $\hat{\tilde{G}}_{x,\mathrm{DIA}}$ need not be smooth at $t = 0$. Clearly, we must have $\hat{\tilde{G}}_{x,\mathrm{DIA}}|_{t=0} = 1$, otherwise the integral will diverge at $t = 0$. But the next term in the small

time expansion for $\hat{\tilde{G}}_{x,\mathrm{DIA}}$ must be evaluated to ascertain self-consistent convergence of the integral, and we obtain this term through calculation of the large ζ behavior predicted for $\tilde{\tilde{G}}_{x,\mathrm{DIA}}$ by Eq. (181) . We begin by noting that as $\zeta \to \infty$

$$\begin{aligned}
&\int_0^\infty \left(e^{-\zeta t}\hat{\tilde{G}}_{x,\mathrm{DIA}}(k,t) - 1\right) \bar{D}'_x(t)dt \\
&\quad \sim \int_0^\infty \left(e^{-\zeta t} - 1\right) \beta K_x^\sharp t^{\beta-1} dt \\
&\quad = \beta\Gamma(\beta) K_x^\sharp \zeta^{-\beta} = \Gamma(\beta+1) K_x^\sharp \zeta^{-\beta},
\end{aligned}$$

where we have used the regularized expression [22, p. 53] for the analytical continuation of the Gamma function to the left half complex plane. Substituting this result into Eq. (181), we obtain as $\zeta \to \infty$

$$\begin{aligned}
\tilde{\tilde{G}}_{x,\mathrm{DIA}}(k,\zeta) &\sim \frac{1}{\zeta + \Gamma(\beta+1)K_x^\sharp k^2 \zeta^{-\beta}} \\
&\sim \zeta^{-1} - \Gamma(\beta+1)K_x^\sharp k^2 \zeta^{-\beta-2} + O(\zeta^{-2\beta-3}),
\end{aligned}$$

which implies [69] that

$$\tilde{\tilde{G}}_{x,\mathrm{DIA}}(k,t) \sim 1 - \frac{K_x^\sharp}{\beta+1} k^2 t^{\beta+1},$$

as $t \to 0$. So the integral in (181) will be self-consistently convergent when the expression

$$(e^{-\zeta t} t^\beta - 1) t^{\beta-1}$$

is integrable near $t = 0$, which is true for $-\frac{1}{2} < \beta < 0$. Note that the equation (181) is not self-consistent for $\beta < -\frac{1}{2}$ due to divergence of the integral at $t = 0$ and is not self-consistent for $\beta > 0$ due to divergence of the integral at $t = \infty$.

Having established the formal self-consistency of Eq. (181) for the parameter range $-\frac{1}{2} < \beta < 0$ under consideration, we now show this equation is equivalent to Eq. (98) by verifying the following Laplace transform rela-

tionship:

$$\begin{aligned}
&\int_0^\infty e^{-\zeta t}\left[\int_0^\infty \bar{D}'_x(s)\left(\hat{\tilde{G}}_{x,\mathrm{DIA}}(k,s)\hat{\tilde{G}}_{x,\mathrm{DIA}}(k,t-s)-\hat{\tilde{G}}_{x,\mathrm{DIA}}(k,t)\right)ds\right]dt\\
&\quad=\int_0^\infty\int_0^\infty\Big[(\mathrm{e}^{-\zeta s}\hat{\tilde{G}}_{x,\mathrm{DIA}}(k,s)-1)\bar{D}'_x(s)\mathrm{e}^{-\zeta(t-s)}\hat{\tilde{G}}_{x,\mathrm{DIA}}(k,t-s)\\
&\qquad\qquad+\bar{D}'_x(s)\left(e^{-\zeta(t-s)}\hat{\tilde{G}}_{x,\mathrm{DIA}}(k,t-s)-e^{-\zeta t}\hat{\tilde{G}}_{x,\mathrm{DIA}}(k,t)\right)\Big]\,ds\,dt\\
&\quad=\int_0^\infty\int_0^\infty(\mathrm{e}^{-\zeta s}\hat{\tilde{G}}_{x,\mathrm{DIA}}(k,s)-1)\bar{D}'_x(s)e^{-\zeta u}\hat{\tilde{G}}_{x,\mathrm{DIA}}(k,u)\,du\,ds\\
&\qquad\qquad+\int_0^\infty\bar{D}'_x(s)\int_0^\infty e^{-\zeta(t-s)}\hat{\tilde{G}}_{x,\mathrm{DIA}}(k,t-s)\,dt\,ds\\
&\qquad\qquad-\int_0^\infty\bar{D}'_x(s)\int_0^\infty e^{-\zeta t}\hat{\tilde{G}}_{x,\mathrm{DIA}}(k,t)\,dt\,ds\\
&\quad=\left[\int_0^\infty\left(\mathrm{e}^{-\zeta s}\hat{\tilde{G}}_{x,\mathrm{DIA}}(k,s)-1\right)\bar{D}'_x(s)\,ds\right]\tilde{\tilde{G}}_{x,\mathrm{DIA}}(k,\zeta),
\end{aligned}$$

We have made the change of variables $u = t - s$ in some summands and used the fact $\hat{\tilde{G}}_{\mathrm{DIA}}(k,p,t) = 0$ for $t < 0$.

Sub-Diffusive and Trapping Cross-Shear Transport with $\beta < -\frac{1}{2}$ When $\kappa = 0$ and $\beta < -\frac{1}{2}$, the renormalization strategy adopted above did not produce a self-consistent result, and there is no apparent way of taming the divergence through further subtraction of terms. Instead a quite different renormalization strategy will produce a self-consistent solution.

Consider a Taylor expansion of $\tilde{A}_{\mathrm{DIA}}(\alpha k, 0, \rho^2\zeta)$ for small α:

$$\begin{aligned}
&\tilde{A}_{\mathrm{DIA}}(\alpha k,0,\rho^2\zeta)\\
&\quad=\int_0^\infty e^{-\zeta\rho^2 t}\left(\hat{G}^{(0)}_{x,\mathrm{DIA}}(t)+\alpha k\hat{G}^{(1)}_{x,\mathrm{DIA}}(t)+\frac{1}{2}\alpha^2k^2\hat{G}^{(2)}_{x,\mathrm{DIA}}(t)\right)R_w(t)\,dt\\
&\quad+o(\alpha^2).
\end{aligned}\tag{182}$$

where $\hat{G}^{(1)}_{x,\mathrm{DIA}}(t) = \partial^n\tilde{G}_{x,\mathrm{DIA}}(k,t)/\partial k^n|_{k=0}$ are the the Taylor coefficients of the expasion of $\tilde{G}_{x,\mathrm{DIA}}(k,t)$. Using Eq. (39) with $p = 0$, they may be represented in terms of Laplace transforms as follows:

$$\begin{cases}
\tilde{G}^{(0)}_{x,\mathrm{DIA}}(\zeta) = \zeta^{-1},\\
\tilde{G}^{(1)}_{x,\mathrm{DIA}}(\zeta) = 0,\\
\tilde{G}^{(2)}_{x,\mathrm{DIA}}(\zeta) = -2\zeta^{-2}\tilde{A}_{\mathrm{DIA}}(0,0,\zeta) = -2\zeta^{-2}R_w(\zeta).
\end{cases}$$

Substituting the inverse Laplace transforms of these expressions into the expansion in (182), we obtain the leading order asymptotics

$$\tilde{A}_{\rm DIA}(\alpha k,0,\rho^2\zeta) \sim \tilde{R}_w(\rho^2\zeta) - \alpha^2 k^2 \int_0^\infty e^{-\zeta\rho^2 t} R_w(t) \int_0^t (t-s) R_w(s) ds dt,$$

for small α and arbitrary ρ (including the possibility that ρ is much smaller than α). Considering now the small ρ limit as well, we have

$$\begin{aligned} &\tilde{A}_{\rm DIA}(\alpha k,0,\rho^2\zeta) \\ &\quad \sim O(\rho^{\min(2,-2\beta)}) - \alpha^2 k^2 \int_0^\infty R_w(t) \int_0^t (t-s) R_w(s) ds dt \\ &\quad = O(\rho^{\min(2,-2\beta)}) + \alpha^2 k^2 \int_0^\infty D_x^2(t) dt, \end{aligned} \tag{183}$$

where we have used the low ζ asymptotics (173) of $\tilde{R}_w(\zeta)$ and integrated by parts in the second term using Eq. (78) and Eq. (180). The first term could be explicitly presented, but we argue now that it must be subdominant in a self-consistent renormalized limit. For, if it were dominant, we would, from Eq. (175), have to choose $\alpha = \rho^{\min(0,1+\beta)}$, but then this would imply, for $\beta < -\frac{1}{2}$, that in fact the explicitly presented α^2 term in Eq. (183) makes the dominant contribution to $\tilde{A}_{\rm DIA}(\alpha k,0,\rho^2\zeta)$ in the renormalized limit. Therefore, the only self-consistent possibility is

$$\tilde{A}_{\rm DIA}(\alpha k,0,\rho^2\zeta) \sim \alpha^2 k^2 \int_0^\infty dt\, D_x^2(t),$$

so that upon substitution into Eq. (175), we choose $\alpha = \rho^{1/2}$ and obtain the following nontrivial renormalized limit

$$\tilde{\tilde{G}}_{x,\rm DIA}(k,\zeta) = \left[\zeta + K^\circ_{4,\rm DIA} k^4\right]^{-1},$$

with

$$K^\circ_{4,\rm DIA} = \int_0^\infty D_x^2(t) dt.$$

Upon inverse Laplace transformation, we obtain the renormalized equation (101) and solution (102), which are formally self-consistent for all $\beta < -\frac{1}{2}$.

We should also consider the possibility of another self-consistent renormalized solution with $\alpha = 1$, which would indeed be appropriate for the renormalization of the exact Green's function when $\beta < -1$. From inspection of (175), we see that the self-consistency of this choice of rescaling would require as a necessary condition that

$$0 = \lim_{\rho\to 0} \tilde{A}_{\rm DIA}(k,0,\rho^2\zeta) = \tilde{A}_{\rm DIA}(k,0,0) = \int_0^\infty R_w(t) \hat{G}_{x,\rm DIA}(k,t)\, dt.$$

While $R_w(t)$ has zero integral, one should not expect in general that its product with $\hat{G}_{x,\mathrm{DIA}}(k,t)$ should continue to have zero integral; there would have to be a rather special coherent relationship between the two functions for this to be the case. There is no evident way of checking whether this special condition holds, so we are naturally led to presume that the self-consistent renormalized solution with $\alpha = \rho^{1/2}$ is the only appropriate one.

As noted in Subsubsection 4.2.2, the renormalized solution $\hat{\tilde{G}}_{x,\mathrm{DIA}}(k,t)$ is unrealizable in the sense that it is not the Fourier transform of a probability density function. This unrealizability is, however, a separate issue from self-consistency of $\hat{\tilde{G}}_{x,\mathrm{DIA}}(k,t)$ as a renormalized solution of the DIA equations. Our above analysis indicates that the renormalized solution (101) presented for $\hat{\tilde{G}}_{x,\mathrm{DIA}}(k,t)$ is at least formally self-consistent; its unrealizability is an intrinisic defect in the DIA equations. This is verified by the rigorous computations in Subsubsection 5.1.2, which show that the fourth order cumulant of $X(t)$ is negative at large times, and is consistent with the results of the formal renormalization procedure conducted here.

C.2 Renormalization of Full Green's Function

C.2.1 Full Renormalization under QNA

We start with the explicit formula for the Laplace transform of the QNA Green's function (24), and apply the rescaling (70) in Laplace transform space:

$$\begin{aligned}\tilde{G}^{(\rho)}_{\mathrm{QNA}}(k,p,\zeta) &= \rho^2 \tilde{G}_{\mathrm{QNA}}(\alpha k, \lambda p, \rho^2 \zeta) \\ &= \Big[\zeta + \alpha^2\rho^{-2}k^2 \tilde{A}_{\mathrm{QNA}}(\alpha k, \lambda p, \rho^2\zeta) + \lambda^2\rho^{-2}p^2 \tilde{B}_{\mathrm{QNA}}(\alpha k, \lambda p, \rho^2\zeta)\Big]^{-1},\end{aligned} \tag{184}$$

where

$$\begin{cases} \tilde{A}_{\mathrm{QNA}}(\alpha k, \lambda p, \rho^2\zeta) = \kappa + \tilde{R}_w(\rho^2\zeta + \alpha^2\kappa k^2 + \lambda^2 \kappa p^2), \\ \tilde{B}_{\mathrm{QNA}}(\alpha k, \lambda p, \rho^2\zeta) = \kappa + \displaystyle\int_{\mathbf{R}} dq \int_{\mathcal{C}} \frac{d\zeta'}{2\pi i} \tilde{E}(q,\zeta') \tilde{G}_0(\alpha k - q, \lambda p, \rho^2\zeta - \zeta') \end{cases} \tag{185}$$

and

$$\tilde{G}_0(k,p,\zeta) = \big(\zeta + \kappa(k^2+p^2)\big)^{-1}$$

is the Laplace transform of the Green's function in the absence of random velocity fluctuations (see Appendix A). We rewrote the expression for $\tilde{B}_{\mathrm{QNA}}$ in the convolution form because it will facilitate the renormalization process and makes the QNA renormalization formally generalizable to the DIA renormalization. The required asymptotics for $\tilde{A}_{\mathrm{QNA}}$ have been

already developed in Subsubsection C.1.1; one need only modify those results to take into account the presence of the p^2 term. On the other hand, the function $\tilde{B}_{\mathrm{QNA}}$ has three different kinds of limits, depending on the regime. We consider each regime separately. Note that the QNA equation completely ignores any effect of the fluctuating cross sweep $w(t)$ on the shear-parallel motion. Consequently, it is bound to give incorrect equations whenever $w(t)$ is nonzero and relevant at large-scales and long times (namely, in the D regime with $w(t) \neq 0$ and in the SD-w regime.) We therefore restrict attention to the case $w(t) \equiv 0$, in which case QNA at least predicts the correct phase diagram. These renormalization calculations also apply to the case $w(t) \neq 0$ in those regimes where the fluctuating cross sweep is asymptotically irrelevant.

D In the D regime, the renormalized limit may be taken directly inside the integrand of $\tilde{B}_{\mathrm{QNA}}$ in (185):

$$\begin{aligned}
&\tilde{B}_{\mathrm{QNA}}(\alpha k, \lambda p, \rho^2 \zeta) \\
&\quad \sim \kappa + \int_{\mathbf{R}} dq \int_{\mathcal{C}} \frac{d\zeta'}{2\pi i} \tilde{E}(q, \zeta') \tilde{G}_0(-q, 0, -\zeta')) \\
&\quad = \kappa + \int_{\mathbf{R}} dq \int_0^\infty dt\, E(q,t) \hat{G}_0(-q, 0, t) \\
&\quad = \kappa + \int_0^\infty dt \int_{\mathbf{R}} dq\; E(q,t) e^{-\kappa q^2 t}
\end{aligned} \tag{186}$$

The fact that this limit is constant implies that the renormalized limit $\hat{\tilde{G}}_{\mathrm{QNA}}(k, p, t)$ of Eq. (184) obeys an equation which has ordinary diffusive behavior in the shear-parallel direction, with $\lambda = \rho$ and diffusivity given by Eq. (186).

A careful asymptotic analysis, using for example the dominated convergence theorem, shows that equation (186) converges only within the D regime. Outside the D regime, low q contributions to the integral which converge to zero nonuniformly give rise to a total contribution which diverges in time [46, Sec. 3.2.5.2].

Consequently, outside the D regime, the shear-parallel tracer motion must be superdiffusive ($\rho \gg \lambda$) for self-consistent renormalization. We next separately consider the case in which the rescaling functions α and ρ satisfy $\alpha \gg \rho^{2/z}$ and $\alpha \ll \rho^{2/z}$, which correspond to the SD-t regime and the SD-s regime, respectively.

SD-t The appropriate limit for Eq. (185) in the SD-t Regime is obtained by first rescaling the integration variables $q \to \rho^{2/z} \tilde{q}$, $\zeta' \to \rho^2 \tilde{\zeta}'$ to zoom in

on the low q, low ζ zone from which the dominant contribution arises.

$$\tilde{B}_{\mathrm{QNA}}(\alpha k, \lambda p, \rho^2\zeta)$$
$$= \kappa + \rho^{2+2/z}\int_{\mathbf{R}} d\tilde{q}\int_{\mathcal{C}}\frac{d\tilde{\zeta}'}{2\pi i}\tilde{E}(\rho^{2/z}\tilde{q},\rho^2\tilde{\zeta}')\tilde{G}_0(\alpha k-\rho^{2/z}\tilde{q},\lambda p,\rho^2(\zeta-\tilde{\zeta}')). \tag{187}$$

The choice of the rescaling of the wavenumber q is that which corresponds to assuming the time scale of the shear-parallel motion due to a shear mode of wavenumber q is set by the Eulerian correlation time $\tau(q)\sim A_\tau|q|^{-z}$ at small q, and can be justified self-consistently within the SD-t Regime where Eulerian temporal decorrelation is dominant.

In this regime, we have that $\rho^2 \gg \lambda^2$ and $\alpha \gg \rho^{2/z}$ so that the leading-order large-scale, long-time asymptotics of Eq. (187) may be written:

$$\begin{aligned}
&\tilde{B}_{\mathrm{QNA}}(\alpha k, \lambda p, \rho^2\zeta)\\
&\quad= \kappa + \rho^{2+2/z}\int_{\mathbf{R}} d\tilde{q}\int_{\mathcal{C}}\frac{d\tilde{\zeta}'}{2\pi i}\bar{E}(\rho^{2/z}\tilde{q})\tau(\rho^{2/z}\tilde{q})\\
&\qquad\qquad\times\tilde{\phi}(\rho^2\tilde{\zeta}'\tau(\rho^{2/z}\tilde{q}))\tilde{G}_0(\alpha k-\rho^{2/z}\tilde{q},\lambda p,\rho^2(\zeta-\tilde{\zeta}'))\\
&\quad\sim \kappa + \rho^{2/z}\int_{\mathbf{R}} d\tilde{q}\int_{\mathcal{C}}\frac{d\tilde{\zeta}'}{2\pi i}A_E|\rho^{2/z}\tilde{q}|^{1-\varepsilon}A_\tau|\rho^{2/z}\tilde{q}|^{-z}\\
&\qquad\qquad\times\tilde{\phi}(A_\tau\tilde{\zeta}'|\tilde{q}|^{-z})\tilde{\bar{G}}_0(k,0,(\zeta-\tilde{\zeta}'))\\
&\quad\sim \rho^{2(2-\varepsilon-z)/z}\tilde{\bar{B}}_{\mathrm{QNA}}(k,p,\zeta),
\end{aligned}$$

where

$$\begin{aligned}
&\tilde{\bar{B}}_{\mathrm{QNA}}(k,p,\zeta)\\
&\quad= A_E A_\tau\int_{\mathbf{R}} d\tilde{q}\,|\tilde{q}|^{1-\varepsilon-z}\int_{\mathcal{C}}\frac{d\tilde{\zeta}'}{2\pi i}\tilde{\phi}(A_\tau\tilde{\zeta}'|\tilde{q}|^{-z})\tilde{\bar{G}}_0(k,0,\zeta-\tilde{\zeta}')
\end{aligned} \tag{188}$$

Here we have introduced the function $\tilde{\bar{G}}_0(k,p,\zeta)$ representing the large-scale, long-time limiting behavior of the *zeroth order* Green's function, which was defined precisely in Eq. (121). As $\varepsilon+z>2$ in the SD-t regime, we noted that the κ term in $\tilde{B}_{\mathrm{QNA}}$ is asymptotically irrelevant. By changing the integration variable $\tilde{q}$ to $s=A_\tau\tilde{\zeta}'|\tilde{q}|^{-z}$, and expressing $\tilde{\phi}$ directly as the Laplace transform of ϕ, we can rewrite

$$\tilde{\bar{B}}_{\mathrm{QNA}}(k,p,\zeta)=\int_{\mathcal{C}}\frac{d\tilde{\zeta}'}{2\pi i}\tilde{\zeta}'\tilde{\bar{D}}_y(\tilde{\zeta}')\tilde{\bar{G}}_0(k,0,\zeta-\tilde{\zeta}'),$$

where $\bar{D}_y(t)$ is defined in Eq. (119).

Completing now the renormalization, we find the proper rescaling is $\lambda = \rho^{z/(2z+\varepsilon-2)}$, and the renormalized QNA Green's function has Laplace transform:

$$\tilde{\bar{G}}_{\mathrm{QNA}}(k,p,\zeta) = \left[\zeta + \kappa k^2 + p^2 \tilde{\bar{B}}_{\mathrm{QNA}}(k,p,\zeta)\right]^{-1}$$

Multiplying through by the inverse of the right hand side and undoing the Laplace transform, we obtain the convolution-in-time equation (120) for the renormalized QNA Green's function in the SD-t Regime.

SD-s For the QNA, we consider only the SD-κ regime, and assume that the fluctuating cross sweep $w(t)$ vanishes or is at least asymptotically irrelevant in the large-scale, long-time limit. In these regimes, the shear-parallel tracer motion is dominated by spatial decorrelation due to cross-shear transport, and the appropriate rescalings satisfy $\alpha \ll \rho^{2/z}$. We therefore rescale the integration variables in (185) by $\zeta' \to \rho^2\tilde{\zeta}'$ and $q \to \alpha\tilde{q}$ to zoom in on large-scales and long-times, with the space-time rescalings chosen to preserve the structure of the factor of $\tilde{G}_0$, which represents the effects of spatial decorrelation:

$$\begin{aligned}
&\tilde{B}_{\mathrm{QNA}}(\alpha k, \lambda p, \rho^2\zeta) \\
&\quad = \kappa + \alpha\rho^2 \int_{\mathbf{R}} d\tilde{q} \int_{\mathcal{C}} \frac{d\tilde{\zeta}'}{2\pi i} \tilde{E}(\alpha\tilde{q}, \rho^2\tilde{\zeta}')\tilde{G}_0(\alpha(k-\tilde{q}), \lambda p, \rho^2(\zeta - \tilde{\zeta}')) \\
&\quad = \kappa + \alpha\rho^2 \int_{\mathbf{R}} d\tilde{q} \int_{\mathcal{C}} \frac{d\tilde{\zeta}'}{2\pi i} \bar{E}(\alpha\tilde{q})\tau(\alpha\tilde{q})\tilde{\phi}(\rho^2\tilde{\zeta}'\tau(\alpha\tilde{q})) \\
&\qquad\qquad \times \tilde{G}_0(\alpha(k-\tilde{q}), \lambda p, \rho^2(\zeta - \tilde{\zeta}')).
\end{aligned} \tag{189}$$

Since $\alpha \ll \rho^{2/z}$ and $\tau(k) \sim A_\tau |k|^{-z}$ for small k , the argument of $\tilde{\phi}$ goes to infinity under the rescaling. Because $\phi(t)$ is a smooth function with $\phi(0) = 1$, we have $\tilde{\phi}(\zeta) \sim \zeta^{-1}$ for large ζ and so

$$\tau(\alpha\tilde{q})\tilde{\phi}(\rho^2\tilde{\zeta}'\tau(\alpha\tilde{q})) \sim \rho^{-2}\tilde{\zeta}'^{-1} \quad \text{as } \rho \to 0,$$

This removes the dependence of the Green's function on the temporal decorrelation rate $\tau(k)$, as we would expect in the SD-κ regime. We can now explicitly compute the contour integral over the Laplace variable $\tilde{\zeta}'$, and use the definition (121) to write the limit of Eq. (189) as follows:

$$\tilde{B}_{\mathrm{QNA}}(\alpha k, \lambda p, \rho^2\zeta) \sim \alpha^{2-\varepsilon}\rho^{-2}\tilde{\bar{B}}^{(s)}_{\mathrm{QNA}}(k,\zeta), \tag{190}$$

as $\rho \to 0$, with

$$\tilde{\bar{B}}^{(s)}_{\mathrm{QNA}}(k,\zeta) = A_E \int_{\mathbf{R}} |\tilde{q}|^{1-\varepsilon}\tilde{\bar{G}}_0(k-\tilde{q}, 0, \zeta)d\tilde{q}.$$

The additive κ term does not contribute to his limit because $\alpha^{2-\varepsilon}\rho^{-2}$ diverges in the SD-κ regime, reflecting the fact that the shear-parallel motion is superdiffusive.

Substituting the limit (190) into Eq. (184) we find that λ should rescale with α and $\rho = \alpha$ as $\lambda = \rho^2\alpha^{(\varepsilon-2)/2}$, which correctly implies $\rho = \lambda^{2/(2+\varepsilon)}$. The renormalized QNA Green's function in the SD-κ regime is therefore:

$$\tilde{\bar{G}}_{\mathrm{QNA}}(k,p,\zeta) = \left[\zeta + \kappa k^2 + p^2 \tilde{\bar{B}}^{(s)}_{\mathrm{QNA}}(k,\zeta)\right]^{-1}.$$

Inverting the Laplace transform, we obtain the following convolution-in-time equation for the renormalized Green's function in the SD-κ regime:

$$\frac{\partial \hat{\bar{G}}_{\mathrm{QNA}}}{\partial t} = -\kappa k^2 \hat{\bar{G}}_{\mathrm{QNA}} - p^2 \int_0^t \bar{B}^{(s)}_{\mathrm{QNA}}(k,s)\hat{\bar{G}}_{\mathrm{QNA}}(k,p,t-s)ds,$$

where

$$\bar{B}^{(s)}_{\mathrm{QNA}}(k,t) = A_E \int_{\mathbf{R}} |\tilde{q}|^{1-\varepsilon} \hat{\bar{G}}_0(k-\tilde{q},0,t)d\tilde{q}.$$

From this equation we may deduce equation (122) in the main text for the case of the SD-κ regime.

C.2.2 Full Renormalization under QLA and RLA

The exact solutions (36) and (67) can be renormalized directly in a similar manner to that of the QNA, except the calculations are easier to perform due to the absence of temporal convolutions.

C.2.3 Full Renormalization under DIA

The renormalization of the DIA equation can be carried out formally in the same way as we did for the QNA equation in Subsubsection C.2.1. The main difference is that $\tilde{B}_{\mathrm{DIA}}(k,p,\zeta)$ involves convolution against $\tilde{G}_{\mathrm{DIA}}$ instead of $\tilde{G}_0$ (compare Eq. (185) and Eq. (47)). This just requires some extra attention to the self-consistency of the renormalization procedure since $\tilde{G}_{\mathrm{DIA}}$ is not an explicitly known function.

C.2.4 Full Renormalization under MDIA

Rescaling the exact MDIA equation (63) according to Eq. (70), we obtain

$$\begin{aligned}\frac{\partial \hat{G}^{(\rho)}_{\mathrm{MDIA}}}{\partial t} =& -\alpha^2\rho^{-2}D_x(t)k^2\hat{G}^{(\rho)}_{\mathrm{MDIA}} \\ &- \lambda^2\rho^{-2}D_{y,\mathrm{MDIA}}(\alpha k,\lambda p,t/\rho^2)p^2\hat{G}^{(\rho)}_{\mathrm{MDIA}},\end{aligned}$$

where

$$D_{y,\mathrm{MDIA}}(\alpha k, \lambda p, t/\rho^2) = \int_0^{t/\rho^2} \int_{\mathbb{R}} E(q,s) \frac{\hat{G}_{\mathrm{MDIA}}(\alpha k - q, \lambda p, s)}{\hat{G}_{\mathrm{MDIA}}(\alpha k, \lambda p, s)} dq ds. \tag{191}$$

The different regimes of shear-parallel transport arise from different kinds of self-consistent renormalized limits of $D_{y,\mathrm{MDIA}}(\alpha k, \lambda p, t/\rho^2)$. We consider the renormalization in the phase regimes separately.

D Within the D regime, the renormalized limit of Eq. (191) may be taken directly:

$$D_{y,\mathrm{MDIA}}(\alpha k, \lambda p, t/\rho^2) \to \int_0^{\infty} \int_{\mathbb{R}} E(q,s) \hat{G}(-q, 0, s) dq ds. \tag{192}$$

where we used $\hat{G}_{\mathrm{MDIA}}(0,0,s) = 1$. We noted that the MDIA Green's function is exact for the shear-transverse dynamics. The result is a constant which is finite in the D regime, and one may choose a self-consistent diffusive scaling in the shear-parallel direction: $\rho = \lambda$. The renormalized Green's function is found to be exact since Eq. (192) is equal to the exact shear-parallel diffusivity K_y^* (116).

One must be careful to check that in fact there is actual convergence to the limit in (192). Of course this cannot be done rigorously because the formula for $\hat{G}_{\mathrm{MDIA}}$ is not generally known at finite times, but one can check for self-consistent convergence by substituting $\hat{\tilde{G}}_{\mathrm{MDIA}}$ for $\hat{G}_{\mathrm{MDIA}}$ in (191).

In proceeding with this caution, one will find that Eq. (192) is not self-consistent outside the D regime due to a divergence at low wavenumbers. A superdiffusive shear-parallel transport ($\rho \gg \lambda$) is thereby indicated. As with the other approximations, we find two different kinds of superdiffusive limits depending on whether $\alpha \gg \rho^{2/z}$ or $\alpha \ll \rho^{2/z}$, corresponding respectively to the SD-t and SD-s regimes, respectively.

SD-t In the superdiffusive phase regime where low wavenumber contributions dominate at large times, and the temporal decorrelation properties of the flow field set the asymptotic tracer transport rate, it is natural to rescale the integration variables in (191) by $s = \tilde{s}/\rho^2$ and $q = \rho^{2/z}\tilde{q}$, which preserves the structure of the spatio-temporal energy spectrum $E(q,s)$ in

the renormalized limit as $\rho \to 0$:

$$\begin{aligned}
&D_{y,\mathrm{MDIA}}(\alpha k, \lambda p, t/\rho^2) \\
&\quad = \rho^{2(1-z)/z} \int_0^t d\tilde{s} \int_{\mathbf{R}} d\tilde{q}\, \bar{E}(\tilde{q}\rho^{2/z}) \phi\left(\tilde{s}/(\rho^2 \tau(\tilde{q}\rho^{2/z}))\right) \\
&\qquad\qquad \times \frac{\hat{G}^{(\rho)}_{\mathrm{MDIA}}(k - \alpha^{-1}\rho^{2/z}\tilde{q}, p, \tilde{s})}{\hat{G}^{(\rho)}_{\mathrm{MDIA}}(k, p, \tilde{s})} \qquad (193) \\
&\quad \sim \rho^{2(1-z)/z} \int_0^t d\tilde{s} \int_{\mathbf{R}} d\tilde{q}\, A_E |\tilde{q}\rho^{2/z}|^{1-\varepsilon} \phi(A_\tau^{-1}\tilde{s}\tilde{q}^z) \\
&\quad = \rho^{2(2-\varepsilon-z)/z} D^{(t)}_{y,\mathrm{MDIA}}(k, p, t)
\end{aligned}$$

where

$$D^{(t)}_{y,\mathrm{MDIA}}(k, p, t) \equiv \int_0^t \int_{\mathbf{R}} A_E |\tilde{q}|^{1-\varepsilon} \phi(\tilde{s}/(A_\tau \tilde{q}^{-z})) d\tilde{q} d\tilde{s},$$

and this expression is in fact equal to the exact shear-parallel time-dependent diffusivity $\bar{D}_y(t)$ given in (119). Consequently, the appropriate rescaling is $\rho = \lambda^{z/(2z+\varepsilon-2)}$, and the MDIA renormalized equation is the exact time-dependent diffusion equation (118). In taking the limit in (193), we used the assumption that $\alpha \gg \rho^{2/z}$. The convergence asserted in (193) can be checked to be self-consistent precisely within the SD-t regime.

SD-s The natural choice of rescaling the integration variables in (191) which zooms in on the low wavenumbers dominating the long-time transport and preserves the structure of the Green's functions modelling the effect of sweeping across the streamlines is: $s = \tilde{s}/\rho^2$, $q = \alpha\tilde{q}$. Then when $\alpha \ll \rho^{2/z}$, we obtain the formal limit as $\rho \to 0$:

$$\begin{aligned}
&D_{y,\mathrm{MDIA}}(\alpha k, \lambda p, t/\rho^2) \\
&\quad = \alpha/\rho^2 \int_0^t \int_{\mathbf{R}} \bar{E}(\alpha\tilde{q}) \phi(s/(\rho^2 \tau(\alpha\tilde{q}))) \frac{\hat{G}^{(\rho)}_{\mathrm{MDIA}}(k - q, p, s)}{\hat{G}^{(\rho)}_{\mathrm{MDIA}}(k, p, s)}\, d\tilde{q}\, d\tilde{s} \\
&\quad \sim \alpha/\rho^2 \int_0^t d\tilde{s} \int_{\mathbf{R}} d\tilde{q}\, A_E |\alpha\tilde{q}|^{1-\varepsilon} \frac{\hat{\bar{G}}_{\mathrm{MDIA}}(k - q, p, s)}{\hat{\bar{G}}_{\mathrm{MDIA}}(k, p, s)} \\
&\quad = \alpha^{2-\varepsilon}\rho^{-2} D^{(s)}_{y,\mathrm{MDIA}}(k, p, t)
\end{aligned}$$

where

$$D^{(s)}_{y,\mathrm{MDIA}}(k, p, t) \equiv A_E \int_0^t \int_{\mathbf{R}} |\tilde{q}|^{1-\varepsilon} \frac{\hat{\bar{G}}_{\mathrm{MDIA}}(k - q, p, s)}{\hat{\bar{G}}_{\mathrm{MDIA}}(k, p, s)} d\tilde{q} d\tilde{s}.$$

The rescaling corresponding to this limit is $\lambda = \rho^2 \alpha^{(\varepsilon-2)/2} = \rho^{(4+\nu(\varepsilon-2))/2}$, and the indicated convergence is self-consistent in the SD-s regime. The renormalized MDIA equation in this regime may now seen to be that reported in (130).

D Derivation of Long Time Asymptotics for Fourth Order Cumulants

D.1 Sweeping Motion

We show here how to rigorously compute the long-time asymptotic behavior of the QNA and DIA predictions for the the fourth order cumulant of $X(t)$, which is subject only to a mean zero, Gaussian random sweeping field $w(t)$, with correlation function

$$\langle w(t+t')w(t')\rangle \equiv R_w(t) = \int_{\mathbf{R}} E_w(\omega)e^{i\omega t}d\omega,$$

with

$$E_w(\omega) = A_{E,w}|\omega|^{-\beta}\psi_w(|\omega|)$$

The exact results and other closure approximation predictions are all Gaussian at all times, and require no further discussion.

D.1.1 Derivation of QNA Prediction

Referring to Eq. (25), we write the QNA prediction for the fourth order cumulant of $X(t)$ as

$$\mu_{4,0}^{\mathrm{QNA}}(t) = \langle X^4(t)\rangle_{\mathrm{QNA}} - 3\langle X^2(t)\rangle,$$

where

$$\begin{cases} \langle X^4(t)\rangle_{\mathrm{QNA}} = 24\displaystyle\int_0^t\int_0^s D_x^{(0)}(s-s')D_x^{(0)}(s')ds'ds, \\ \langle X^2(t)\rangle = \mu_{2,0}(t) = 2\displaystyle\int_0^t D_x^{(0)}(s)ds. \end{cases}$$

The Laplace transform of the first term is given by

$$\widetilde{\langle X^4\rangle}_{\mathrm{QNA}} = \frac{24}{\zeta}(\tilde{D}_x^{(0)}(\zeta))^2 = \frac{24}{\zeta^3}(\tilde{R}_w(\zeta))^2,$$

and its low ζ asymptotics can be deduced from Eq. (173):

$$\widetilde{\langle X^4\rangle}_{\mathrm{QNA}} \sim \begin{cases} 6(K_x^\circ)^2\zeta & \text{for } \beta < -1, \\ 24(\Gamma(1+\beta))^2(K_x^\sharp)^2\zeta^{-2\beta-3} & \text{for } -1 < \beta < 1. \end{cases}$$

The long time asymptotics of $\langle X^4(t)\rangle$ can now be obtained by a Tauberian theorem [69]:

$$\langle X^4(t)\rangle_{\mathrm{QNA}} \sim \begin{cases} 6(K_x^\circ)^2 & \text{for } \beta < -1, \\ \dfrac{24}{(1+\beta)^2}\dfrac{(\Gamma(2+\beta))^2}{\Gamma(2\beta+3)}(K_x^\sharp)^2 t^{2\beta+2} & \text{for } -1 < \beta < 1. \end{cases} \tag{194}$$

Along with the long-time asymptotics for $\mu_{2,0}(t)$ in Subsection 4.2.1, we arrive at the results presented in Subsubsection 5.1.1.

D.1.2 Derivation of DIA Prediction

We first write the formula for the DIA approximation of $\langle X^4(t)\rangle$:

$$\langle X^4(t)\rangle_{\text{DIA}} = \langle X^4(t)\rangle_{\text{DIA,I}} + \langle X^4(t)\rangle_{\text{DIA,II}},$$

where

$$\begin{cases} \langle X^4(t)\rangle_{\text{DIA,I}} = 24\displaystyle\int_0^t \int_0^s D_x^{(0)}(s-s')D_x^{(0)}(s')ds'ds, \\ \langle X^4(t)\rangle_{\text{DIA,II}} = -24\displaystyle\int_0^t (t-s)(D_x^{(0)}(s))^2\,ds. \end{cases}$$

The first term is identical to $\langle X^4(t)\rangle_{\text{QNA}}$, with asymptotics given by Eq. (194).

Using Eq. (173), we find that $D_x^{(0)}(s)$ decays rapidly enough for $\beta < -\frac{1}{2}$ so that $(D_x^{(0)}(s))^2$ is integrable and

$$\langle X^4(t)\rangle_{\text{DIA,II}} \sim -24t\int_0^t (D_x^{(0)}(s))^2\,ds \quad \text{for } \beta < -\frac{1}{2}.$$

as $t \to \infty$. On the other hand for $\beta > -\frac{1}{2}$, the integral for $\langle X^4(t)\rangle_{\text{DIA,II}}$ is dominated by the large s contribution, which may be computed using the large t asymptotics of $D_x^{(0)}(t)$ inferred from Eq. (173):

$$D_x^{(0)}(t) \sim K_x^\sharp t^\beta \quad \text{for } -1 < \beta < 1.$$

We thereby find

$$\begin{aligned} \langle X^4(t)\rangle_{\text{DIA,II}} &\sim -24t^2\int_0^1 (1-u)(D_x^{(0)}(tu))^2\,du \\ &\sim -24t^{2+2\beta}(K_x^\sharp)^2\int_0^t (1-u)u^{2\beta}du \\ &= -24\frac{(K_x^\sharp)^2}{(2\beta+1)(2\beta+2)}t^{2+2\beta}. \end{aligned}$$

Putting together the asymptotics for $\langle X^4(t)\rangle_{\text{DIA,I}}$ and $\langle X^4(t)\rangle_{\text{DIA,II}}$, we obtain the results stated in Subsubsection 5.1.2.

D.2 Steady Random Shear Flow with Molecular Diffusion

We present here the main steps in the derivation of the long time asymptotics reported in Subsection 5.2 for the fourth order cumulant $\mu_{0,4}(t)$ of the tracer displacement along a steady shear:

$$\boldsymbol{v}(x,y,t) = \begin{pmatrix} 0 \\ v(x) \end{pmatrix}$$

when molecular diffusion is present ($\kappa > 0$).

It will be convenient for us first to exhibit the asymptotic derivations in the following sequence: the exact result (Subsection D.2.1), the MDIA (Subsection D.2.2), the QNA (Subsection D.2.3), and the DIA (Subsection D.2.4). The reason for this ordering is that the MDIA prediction for $\mu_{0,4}(t)$ in this special model is equal to one of the summands in the exact formula, and the DIA formula for $\mu_{0,4}(t)$ is equal to the QNA formula plus an additional term (which creates some cancellation in the leading order asymptotics).

D.2.1 Exact formula for long time asymptotics

Alternative Finite Time Formula Our asymptotic calculation is facilitated by rewriting the exact formula in (19) for $\mu_{0,4}(t)$ in the following equivalent form for the special submodel under consideration:

$$\begin{aligned} \mu_{0,4}(t) = 24 \int_0^t ds_1 \int_0^{s_1} ds_2 \int_0^{s_2} ds_3 \int_0^{s_3} ds_4 \int_{\mathbf{R}^2} dq\, dq' \\ \times \bar{E}(|q|)\bar{E}(|q'|)e^{-\kappa q^2 s_{12}} \\ \times (e^{-\kappa(q-q')^2 s_{23}} - e^{-\kappa(q^2+q'^2)s_{23}})(e^{-\kappa q^2 s_{34}} + e^{-\kappa q'^2 s_{34}}). \end{aligned} \tag{195}$$

We use here a shorthand (which will also appear in the finite-time formulas for the approximate closure formulas):

$$s_{ij} \equiv s_i - s_j.$$

The formula (195) can be obtained from Eq. (19) by reordering the integration variables so that $t \geq s_1 \geq s_2 \geq s_3 \geq s_4 \geq 0$, or directly using an argument from [72]. A Laplace transform simplifies the formula by replacing the time integrations with rational functions of ζ, thanks to the convolutive structure of the integrand which is in turn a consequence of

the Markovian nature of the cross-shear transport:

$$\begin{aligned}
&\tilde{\mu}_{0,4}(\zeta) \\
&\quad = 24\zeta^{-2}\int_{\mathbf{R}^2} dq\, dq'\, \bar{E}(|q|)\bar{E}(|q'|)\frac{1}{\zeta+\kappa q^2} \\
&\qquad \times\left(\frac{1}{\zeta+\kappa(q-q')^2}-\frac{1}{\zeta+\kappa(q^2+q'^2)}\right)\left(\frac{1}{\zeta+\kappa q^2}+\frac{1}{\zeta+\kappa q'^2}\right) \\
&\quad = 48\kappa\zeta^{-2}\int_{\mathbf{R}^2} dq\, dq'\, \bar{E}(|q|)\bar{E}(|q'|) \\
&\qquad \times\frac{1}{\zeta+\kappa q^2}\frac{qq'}{(\zeta+\kappa(q-q')^2)(\zeta+\kappa(q^2+q'^2))}\left(\frac{1}{\zeta+\kappa q^2}+\frac{1}{\zeta+\kappa q'^2}\right).
\end{aligned}$$

The long time limit of $\mu_{0,4}(t)$ will be inferred, through the Tauberian theorem [69], in terms of the low ζ asymptotics.

It will be useful to change integration variables to obtain the scaling factors of κ more easily:

$$\begin{aligned}
\tilde{\mu}_{0,4}(\zeta) = 48\kappa^{-1}\zeta^{-2}\int_{\mathbf{R}^2} d\tilde{q}\, d\tilde{q}'\, \bar{E}(\kappa^{-1/2}|\tilde{q}|)\bar{E}(\kappa^{-1/2}|\tilde{q}'|) \\
\times\frac{1}{\zeta+\tilde{q}^2}\frac{\tilde{q}\tilde{q}'}{(\zeta+(\tilde{q}-\tilde{q}')^2)(\zeta+(\tilde{q}^2+\tilde{q}'^2))}\left(\frac{1}{\zeta+\tilde{q}^2}+\frac{1}{\zeta+\tilde{q}'^2}\right).
\end{aligned} \tag{196}$$

We will separately analyze the cases $\varepsilon < -\frac{1}{2}$ and $\varepsilon > -\frac{1}{2}$.

Case: $\varepsilon < -\frac{1}{2}$ The dominant contribution to $\tilde{\mu}_{0,4}(\zeta)$ comes from the diagonal in wavenumber space $\tilde{q} = \tilde{q}'$, as we will rigorously demonstrate later. A heuristic way to see this is to note that taking a formal $\zeta \to 0$ limit under the integral in (196) will lead to a divergent integral due to the factor $(\tilde{q}-\tilde{q}')^{-2}$. So let us consider first the auxiliary function $\tilde{\mu}^*_{0,4}(\zeta)$ obtained by replacing the appearance of $\tilde{q}'$ everywhere in (196) by $\tilde{q}$, except where it appears in the denominator through the difference $\tilde{q}-\tilde{q}'$:

$$\begin{aligned}
\tilde{\mu}^*_{0,4}(\zeta) = 48\kappa^{-1}\zeta^{-2}\int_{\mathbf{R}^2} \bar{E}(\kappa^{-1/2}|\tilde{q}|)\bar{E}(\kappa^{-1/2}|\tilde{q}|) \\
\times\frac{2\tilde{q}\tilde{q}'}{(\zeta+(\tilde{q}-\tilde{q}')^2)(\zeta+2\tilde{q}^2)(\zeta+\tilde{q}^2)^2}\, d\tilde{q}\, d\tilde{q}'.
\end{aligned}$$

Now we change integration variable to $\tilde{q}' = \tilde{q}+\xi\sqrt{\zeta}$:

$$\tilde{\mu}^*_{0,4}(\zeta) = 48\kappa^{-1}\zeta^{-5/2}\int_{\mathbf{R}^2} d\tilde{q}\, d\xi\, (\bar{E}(\kappa^{-1/2}|\tilde{q}|))^2\frac{2\tilde{q}(\tilde{q}+\xi\sqrt{\zeta})}{(1+\xi^2)(\zeta+2\tilde{q}^2)(\zeta+\tilde{q}^2)^2}. \tag{197}$$

We find by the dominated convergence theorem that the $\zeta \to 0$ limit may be taken directly within the integrand of Eq. (197) when $\varepsilon < -\frac{1}{2}$, so that

$$\begin{aligned}\tilde{\mu}^*_{0,4}(\zeta) &\sim 96\kappa^{-1}\zeta^{-5/2}\int_{\mathbf{R}} d\tilde{q}\,(\bar{E}(\kappa^{-1/2}|\tilde{q}|))^2\tilde{q}^{-4}\int_{\mathbf{R}} d\xi\,(1+\xi^2)^{-1} \\ &= \frac{96\pi}{\kappa^{5/2}\zeta^{5/2}}\int_0^\infty (\bar{E}(q))^2 q^{-4}\,dq.\end{aligned}$$

as $\zeta \to 0$. By the Tauberian theorem [69], as $t \to \infty$,

$$\begin{aligned}&\mu^*_{0,4}(t) \sim K^*_4 t^{3/2}, \\ &K^*_4 = \frac{1}{\Gamma(5/2)}\frac{96\pi}{\kappa^{5/2}}\int_0^\infty (\bar{E}(q))^2 q^{-4}\,dq = \frac{128\sqrt{\pi}}{\kappa^{5/2}}\int_0^\infty (\bar{E}(q))^2 q^{-4}\,dq.\end{aligned} \tag{198}$$

All that is left is for us to show that $\mu_{0,4}(t) = \mu^*_{0,4}(t) + o(t^{3/2})$, so that the long time asymptotics of $\mu_{0,4}(t)$ are given by Eq. (198). This will follow from the fact

$$|\tilde{\mu}_{0,4}(\zeta) - \tilde{\mu}^*_{0,4}(\zeta)| = o(\zeta^{-5/2}), \tag{199}$$

which we now prove.

We begin, as usual, by estimating the difference between the integrals represented by $\mu_{0,4}(\zeta)$ and $\mu^*_{0,4}(\zeta)$ in terms of the absolute difference of their integrands:

$$\begin{aligned}|\tilde{\mu}_{0,4}(\zeta) - \tilde{\mu}^*_{0,4}(\zeta)| \le 48\kappa^{-1}\zeta^{-2}&\int_{\mathbf{R}^2} d\tilde{q}\,d\tilde{q}'\,\frac{\tilde{q}\bar{E}(\kappa^{-1/2}|\tilde{q}|)}{(\zeta+\tilde{q}^2)(\zeta+(\tilde{q}-\tilde{q}')^2)} \\ \times\Bigg|\bar{E}(\kappa^{-1/2}|\tilde{q}'|)&\frac{\tilde{q}'}{\zeta+(\tilde{q}^2+\tilde{q}'^2)}\left(\frac{1}{\zeta+\tilde{q}^2}+\frac{1}{\zeta+\tilde{q}'^2}\right) \\ &-\bar{E}(\kappa^{-1/2}|\tilde{q}|)\frac{\tilde{q}}{\zeta+2\tilde{q}^2}\left(\frac{2}{\zeta+\tilde{q}^2}\right)\Bigg|.\end{aligned} \tag{200}$$

Now, we break up the absolute value into a sum of two parts: one involving differences in the numerator and one involving differences in the denominator. There are two natural ways to do this, and it helps us to choose carefully between the alternatives depending on the relative magnitude of

$\tilde{q}$ and $\tilde{q}'$:

$$\left|\frac{\tilde{q}'\bar{E}(\kappa^{-1/2}|\tilde{q}'|)}{\zeta+(\tilde{q}^2+\tilde{q}'^2)}\left(\frac{1}{\zeta+\tilde{q}^2}+\frac{1}{\zeta+\tilde{q}'^2}\right)-\frac{\tilde{q}\bar{E}(\kappa^{-1/2}|\tilde{q}|)}{\zeta+2\tilde{q}^2}\left(\frac{2}{\zeta+\tilde{q}^2}\right)\right| \leq$$

$$\frac{2|\tilde{q}'\bar{E}(\kappa^{-1/2}|\tilde{q}'|)-\tilde{q}\bar{E}(\kappa^{-1/2}|\tilde{q}|)|}{(\zeta+2\tilde{q}^2)(\zeta+\tilde{q}^2)}$$

$$+\bar{E}(\kappa^{-1/2}|\tilde{q}'|)\left|\frac{\tilde{q}'}{\zeta+\tilde{q}^2+\tilde{q}'^2}\left(\frac{1}{\zeta+\tilde{q}^2}+\frac{1}{\zeta+\tilde{q}'^2}\right)-\frac{1}{\zeta+2\tilde{q}^2}\frac{2}{\zeta+\tilde{q}^2}\right|$$

$$\text{for } |\tilde{q}| \geq |\tilde{q}'|,$$

$$\frac{2|\tilde{q}'\bar{E}(\kappa^{-1/2}|\tilde{q}'|)-\tilde{q}\bar{E}(\kappa^{-1/2}|\tilde{q}|)|}{\zeta+\tilde{q}^2+\tilde{q}'^2}\left(\frac{1}{\zeta+\tilde{q}^2}+\frac{1}{\zeta+\tilde{q}'^2}\right)$$

$$+\bar{E}(\kappa^{-1/2}|\tilde{q}|)\left|\frac{\tilde{q}}{\zeta+\tilde{q}^2+\tilde{q}'^2}\left(\frac{1}{\zeta+\tilde{q}^2}+\frac{1}{\zeta+\tilde{q}'^2}\right)-\frac{1}{\zeta+2\tilde{q}^2}\frac{2}{\zeta+\tilde{q}^2}\right|$$

$$\text{for } |\tilde{q}| \leq |\tilde{q}'|.$$

Simplifying these expressions through the use of some elementary inequalities, we achieve:

$$\left|\frac{\tilde{q}'\bar{E}(\kappa^{-1/2}|\tilde{q}'|)}{\zeta+(\tilde{q}^2+\tilde{q}'^2)}\left(\frac{1}{\zeta+\tilde{q}^2}+\frac{1}{\zeta+\tilde{q}'^2}\right)-\frac{\tilde{q}\bar{E}(\kappa^{-1/2}|\tilde{q}|)}{\zeta+2\tilde{q}^2}\left(\frac{2}{\zeta+\tilde{q}^2}\right)\right|$$

$$\leq \begin{cases} \frac{2|\bar{E}(\kappa^{-1/2}|\tilde{q}'|)\tilde{q}'-\bar{E}(\kappa^{-1/2}|\tilde{q}|)\tilde{q}|}{(\zeta+2\tilde{q}^2)(\zeta+\tilde{q}^2)}+\frac{3\bar{E}(\kappa^{-1/2}|\tilde{q}'|)|\tilde{q}\tilde{q}'||\tilde{q}-\tilde{q}'|}{(\zeta+\tilde{q}^2)(\zeta+2\tilde{q}^2)(\zeta+\tilde{q}'^2)} & \text{for } |\tilde{q}| \geq |\tilde{q}'|, \\ \frac{2|\bar{E}(\kappa^{-1/2}|\tilde{q}'|)\tilde{q}'-\bar{E}(\kappa^{-1/2}|\tilde{q}|)\tilde{q}|}{(\zeta+\tilde{q}'^2)(\zeta+\tilde{q}^2)}+\frac{3\bar{E}(\kappa^{-1/2}|\tilde{q}|)|\tilde{q}\tilde{q}'||\tilde{q}-\tilde{q}'|}{(\zeta+\tilde{q}^2)(\zeta+2\tilde{q}^2)(\zeta+\tilde{q}'^2)} & \text{for } |\tilde{q}| \leq |\tilde{q}'|. \end{cases} \tag{201}$$

We next note the following inequality, valid for all infrared scaling exponent $\varepsilon < 1$,

$$|q\bar{E}(|q|)-q'\bar{E}(|q'|)| \leq \begin{cases} C_\varepsilon q'^{1-\varepsilon}|q-q'| & \text{for } q \leq q' \leq 2, \\ C_\varepsilon q^{1-\varepsilon}|q-q'| & \text{for } q' \leq q \leq 2, \\ F_\varepsilon(q)\frac{|q-q'|}{|q'|} & \text{for } 1 \leq q \leq q', \\ F_\varepsilon(q')\frac{|q-q'|}{|q|} & \text{for } 1 \leq q' \leq q, \\ C_\varepsilon q^{1-\varepsilon}+F_\varepsilon(q') & \text{for } q \leq 1, 2 \leq q', \\ C_\varepsilon q'^{1-\varepsilon}+F_\varepsilon(q) & \text{for } q' \leq 1, 2 \leq q. \end{cases} \tag{202}$$

Here C_ε is some finite constant and F_ε is a smooth integrable function. Both C_ε and F_ε may depend on ε but on no other parameter. Substituting now Eq. (202) into Eq. (201), and the latter inequality into Eq. (196), we obtain an estimate for $\tilde{\mu}_{0,4}(\zeta) - \tilde{\mu}^*_{0,4}(\zeta)$ as a sum of several integrals

over certain intervals of $\tilde{q}$ and $\tilde{q}'$, each of which may be straightforwardly estimated. There results:

$$|\tilde{\mu}_{0,4}(\zeta) - \tilde{\mu}^*_{0,4}(\zeta)| \leq \tilde{C}_\varepsilon \left[(1+\ln\zeta^{-1})\zeta^{-3-\varepsilon} + \zeta^{-2}\right] \text{ for } \varepsilon < 1.$$

The error is therefore $o(\zeta^{-5/2})$ for $\varepsilon < -\frac{1}{2}$, as claimed in (199).

Case: $\varepsilon > -\frac{1}{2}$ There is sufficient energy at low wavenumbers so that the dominant contribution to the integral in (196) shifts to the origin. This contribution can be isolated by rescaling integration variables $\tilde{q} = \zeta^{1/2}\xi$, $\tilde{q}' = \zeta^{1/2}\xi'$:

$$\begin{aligned}\tilde{\mu}_{0,4}(\zeta) = 48\kappa^{-1}\zeta^{-4} \int_{\mathbf{R}^2} d\xi\, d\xi'\, \bar{E}(\sqrt{\zeta/\kappa}|\xi|)\bar{E}(\sqrt{\zeta/\kappa}|\xi'|) \\ \times \frac{1}{1+\xi^2}\frac{\xi\xi'}{(1+(\xi-\xi')^2)(1+(\xi^2+\xi'^2))}\left(\frac{1}{1+\xi^2}+\frac{1}{1+\xi'^2}\right).\end{aligned}$$

Then, using the low wavenumber asymptotics for the energy spectrum, we have formally for $\zeta \to 0$:

$$\begin{aligned}\tilde{\mu}_{0,4}(\zeta) &\sim 48\kappa^{-1}\zeta^{-4} \int_{\mathbf{R}^2} d\xi\, d\xi'\, A_E(\sqrt{\zeta/\kappa}|\xi|)^{1-\varepsilon} A_E(\sqrt{\zeta/\kappa}|\xi'|)^{1-\varepsilon} \\ &\quad \times \frac{1}{1+\xi^2}\frac{\xi\xi'}{(1+(\xi-\xi')^2)(1+(\xi^2+\xi'^2))}\left(\frac{1}{1+\xi^2}+\frac{1}{1+\xi'^2}\right) \\ &= 48A_E^2\kappa^{\varepsilon-2}\zeta^{-3-\varepsilon} \int_{\mathbf{R}^2} d\xi\, d\xi' \left(\frac{1}{1+\xi^2}+\frac{1}{1+\xi'^2}\right) \\ &\quad \times \frac{1}{1+\xi^2}\frac{\xi|\xi|^{1-\varepsilon}\xi'|\xi'|^{1-\varepsilon}}{(1+(\xi-\xi')^2)(1+(\xi^2+\xi'^2))}..\end{aligned} \tag{203}$$

We shall justify this step rigorously at the end of the calculation. At the moment, we collapse the integration domain onto the first quadrant:

$$\begin{aligned}\tilde{\mu}_{0,4}(\zeta) \sim 384A_E^2\kappa^{\varepsilon-2}\zeta^{-3-\varepsilon} \int_0^\infty d\xi \int_0^\infty d\xi' \frac{1}{1+\xi^2}\left(\frac{1}{1+\xi^2}+\frac{1}{1+\xi'^2}\right) \\ \times \frac{\xi^{3-\varepsilon}\xi'^{3-\varepsilon}}{(1+(\xi-\xi')^2)(1+(\xi+\xi')^2)(1+(\xi^2+\xi'^2))}.\end{aligned}$$

Applying now the Tauberian theorem for the Laplace transform, we obtain the result stated in Subsubsection 5.2.1.

We are just left to justify the formal asymptotic statement (203). To do this, we note that $\bar{E}(k)$ can be bounded on the whole positive real axis by a constant multiple of $k^{\varepsilon-1}$ since $\bar{E}(k)$ is, by assumption, bounded by some

multiple of $k^{1-\varepsilon}$ at small k and by a monotonically decreasing integrable function at large k. Therefore, the dominated convergence theorem can be applied in this case to show that Eq. (203) is the rigorously correct asymptotics whenever the integrand in the limiting expression is absolutely integrable. This condition can be verified to hold for $-\frac{1}{2} < \varepsilon < 2$ by chopping up the integration domain into regions on which simple bounds are possible for each factor of the integrand.

D.2.2 Long Time Asymptotics For MDIA

Fortunately, the MDIA prediction for $\mu_{0,4}(t)$ can be related in a simple way to the exact formula. To see this, we recast the formula (64) for the MDIA prediction, specialized to the present submodel, into a form comparable with the exact formula (195) used above.

$$\begin{aligned}
\mu_{0,4}^{\mathrm{MDIA}}(t) &= 24 \int_0^t ds\,(t-s) \int_0^s ds'\,(s-s') \int_{\mathbf{R}^2} dq\,dq'\ \bar{E}(|q|)\bar{E}(|q'|) \\
&\qquad \times \mathrm{e}^{-\kappa(q^2 s + q'^2 s')} \left(\mathrm{e}^{-2\kappa q q' s'} - 1\right) \\
&= 24 \int_0^t ds_1 \int_0^{s_1} ds_2 \int_0^{s_2} ds_3 \int_0^{s_3} ds_4 \int_{\mathbf{R}^2} dq\,dq' \bar{E}(|q|)\bar{E}(|q'|) \\
&\qquad \times \mathrm{e}^{-\kappa(q^2 s_{14} + q'^2 s_{23})} \left(\mathrm{e}^{-2\kappa q q' s_{23}} - 1\right) \\
&= 24 \int_0^t ds_1 \int_0^{s_1} ds_2 \int_0^{s_2} ds_3 \int_0^{s_3} ds_4 \int_{\mathbf{R}^2} dq\,dq' \bar{E}(|q|)\bar{E}(|q'|) \\
&\qquad \times \mathrm{e}^{-\kappa q^2 s_{12}} \left(\mathrm{e}^{-\kappa(q-q')^2 s_{23}} - \mathrm{e}^{-\kappa(q^2+q'^2)} s_{23}\right) \mathrm{e}^{-\kappa q^2 s_{34}}.
\end{aligned}$$

The substantial step in this transformation is indicated by the second equality, in which the integration variables s and s' were replaced by s_{14} and s_{23} respectively, where $s_{ij} \equiv s_i - s_j$. The factor $(t-s)(s-s')$ corresponds to the two-dimensional area of phase space available to the points $0 \le s_1 \le s_2 \le s_3 \le s_4 \le t$ subject to the constraints $s = s_{14}$ and $s' = s_{23}$. In the last equality, we changed variables $q' \to -q'$.

We observe now that the MDIA formula coincides with the exact formula (195) for $\mu_{0,4}(t)$ except that the factor

$$\left[e^{-\kappa q^2 s_{34}} + e^{-\kappa q'^2 s_{34}}\right]$$

in the exact formula has been replaced by

$$e^{-\kappa q^2 s_{34}}$$

in the MDIA approximation. Therefore, the long time asymptotics of $\mu_{0,4}^{\rm MDIA}(t)$ may be computed in the same way as the exact results were; some terms are just omitted.

We demonstrate finally the remarkable bound on the relative magnitude of the ratio of the MDIA approximation to the exact value of $\mu_{0,4}(t)$ at all times:

$$\frac{1}{2} \leq \frac{\mu_{0,4}^{\rm MDIA}(t)}{\mu_{0,4}(t)} \leq 1.$$

To compare the MDIA and exact formulas most clearly, let us re-express them by collapsing the integration over q and q' to the first quadrant, and then symmetrize the integrand with respect to the integration variables:

$$\begin{cases} \mu_{0,4}(t) & = 48 \int_0^t ds_1 \int_0^{s_1} ds_2 \int_0^{s_2} ds_3 \int_0^{s_3} ds_4 \int_{\mathbf{R}^2} dq\, dq'\, \bar{E}(|q|)\bar{E}(|q'|) \\ & \quad \times e^{-\kappa(q^2+q'^2)s_{23}}(\cosh(2\kappa q q' s_{23}) - 1) \\ & \quad \times \left(e^{-\kappa q^2 s_{12}} + e^{-\kappa q'^2 s_{12}}\right)\left(e^{-\kappa q^2 s_{34}} + e^{-\kappa q'^2 s_{34}}\right) \\ \mu_{0,4}^{\rm MDIA}(t) & = 48 \int_0^t ds_1 \int_0^{s_1} ds_2 \int_0^{s_2} ds_3 \int_0^{s_3} ds_4 \int_{\mathbf{R}^2} dq\, dq'\, \bar{E}(|q|)\bar{E}(|q'|) \\ & \quad \times e^{-\kappa(q^2+q'^2)s_{23}}(\cosh(2\kappa q q' s_{23}) - 1) \\ & \quad \times \left(e^{-\kappa q^2 (s_{12}+s_{34})} + e^{-\kappa q'^2 (s_{12}+s_{34})}\right). \end{cases}$$

Now we need only observe that both integrands are manifestly nonnegative,

$$\begin{aligned} &\left(e^{-\kappa q^2 (s_{12}+s_{34})} + e^{-\kappa q'^2 (s_{12}+s_{34})}\right) \\ &\qquad \leq \left(e^{-\kappa q^2 s_{12}} + e^{-\kappa q'^2 s_{12}}\right)\left(e^{-\kappa q^2 s_{34}} + e^{-\kappa q'^2 s_{34}}\right), \end{aligned}$$

and

$$\begin{aligned} &\left(e^{-\kappa q^2 (s_{12}+s_{34})} + e^{-\kappa q'^2 (s_{12}+s_{34})}\right) \\ &\qquad - \frac{1}{2}\left(e^{-\kappa q^2 s_{12}} + e^{-\kappa q'^2 s_{12}}\right)\left(e^{-\kappa q^2 s_{34}} + e^{-\kappa q'^2 s_{34}}\right) \\ &= \frac{1}{2}\left(e^{-\kappa q^2 s_{12}} - e^{-\kappa q'^2 s_{12}}\right)\left(e^{-\kappa q^2 s_{34}} - e^{-\kappa q'^2 s_{34}}\right) \geq 0 \end{aligned}$$

D.2.3 Long Time Asymptotics For QNA

From Eq. (29), the fourth order cumulant for the shear-parallel tracer motion is predicted by QNA to be :

$$\mu_{0,4}^{\rm QNA}(t) = \langle Y^4(t)\rangle_{\rm QNA}^I - 3(\langle Y^2(t)\rangle_{\rm QNA}^I)^2, \tag{204}$$

where

$$\begin{cases} \langle Y^4(t)\rangle^I_{\rm QNA} &= 24\int_0^t ds\int_0^s ds'\; D_y^{(\kappa)}(s-s')D_y^{(\kappa)}(s'), \\ \langle Y^2(t)\rangle^I_{\rm QNA} &\equiv \mu^I_{0,2}(t) = 2\int_0^t ds\, D_y^{(\kappa)}(s). \end{cases}$$

Note that $\langle Y^4(t)\rangle^I_{\rm QNA}$ and $\mu^I_{0,2}(t)$ are, respectively, the QNA predictions for the fourth order moment and second order cumulant $\mu_{0,2}(t)$ of the shear-parallel tracer displacement without the terms proportional to powers of κ.

Working in Laplace transform space, we have

$$\begin{cases} \tilde\mu^I_{0,2}(\zeta) &= 4\zeta^{-2}\int_0^\infty dq\,\bar E(q)/(\zeta+\kappa q^2), \\ \langle Y^4(t)\rangle^I_{\rm QNA} &= 6\zeta(\tilde\mu^I_{0,2}(\zeta))^2, \end{cases} \tag{205}$$

so the long time asymptotics of $\langle Y^4(t)\rangle^I_{\rm QNA}$ can be computed readily from the asymptotics of $\mu^I_{0,2}(t)$. The leading order asymptotics of $\mu^I_{0,2}(t)$ can be readily obtained from Eq. (134). However, the leading order asymptotics for each of the terms in Eq. (204) cancel each other for $\varepsilon < 0$, so we will need to work the asymptotics of each term out to second order for $\varepsilon < 0$. As we show below,

$$\tilde\mu^I_{0,2}(\zeta) \sim \begin{cases} \frac{2\Gamma(-(2+\varepsilon)/2)\Gamma((4+\varepsilon)/2)A_E}{\kappa^{(2-\varepsilon)/2}}\zeta^{-2-\varepsilon/2} & \text{for } 0<\varepsilon<2, \\ 2K^I_y\zeta^{-2} - \frac{2\Gamma(-\varepsilon/2)\Gamma((2+\varepsilon)/2)A_E}{\kappa^{(2-\varepsilon)/2}}\zeta^{-2-\varepsilon/2} & \text{for } -2<\varepsilon<0, \\ 2K^I_y\zeta^{-2} - K^{Ib}_y\zeta^{-1} & \text{for } \varepsilon<-2, \end{cases} \tag{206}$$

as $\zeta \to 0$, where the scaling coefficients involving integrals are

$$K^I_y = 2\int_0^\infty \frac{\bar E(q)}{\kappa q^2}\,dq, \qquad K^{Ib}_y = 4\int_0^\infty \frac{\bar E(q)}{\kappa^2 q^4}\,dq.$$

The results stated in Subsubsection 5.2.3 are now derived by simple combination of the above equations and the use of the Tauberian theorem.

Asymptotic Computation of $\tilde\mu^I_{0,2}(\zeta)$ for $\varepsilon < 0$ We begin by separating out the leading order contribution:

$$\tilde\mu^I_{0,2}(\zeta) = 2K^I_y\zeta^{-2} + \tilde\mu^{Ib}_{0,2}(\zeta)$$

where $K^I_y \equiv 2\int_0^\infty \frac{\bar E(q)}{\kappa q^2}\,dq$ and the correction to the leading order asymptotics is

$$\tilde\mu^{Ib}_{0,2}(\zeta) \equiv \frac{4}{\zeta^2}\int_0^\infty dq\,\left[\frac{\bar E(q)}{\zeta+\kappa q^2} - \frac{\bar E(q)}{\kappa q^2}\right] = -\frac{4}{\kappa\zeta}\int_0^\infty dq\,\frac{\bar E(q)}{(\zeta+\kappa q^2)q^2}.$$

To obtain the results stated in Eq. (206), we now just need to compute the leading order asymptotics for this correction term $\tilde{\mu}_{0,2}^{Ib}(\zeta)$ for $\varepsilon < 0$. But this can be mapped onto the problem of finding the leading order asymptotics for $\tilde{\mu}_{0,2}^{I}(\zeta)$ by replacing $\bar{E}(q)$ with $-\bar{E}(q)\zeta/(\kappa q^2)$. In this way, we deduce the results in (206) after recognizing $\Gamma(-(4+\varepsilon)/2)\Gamma((6+\varepsilon)/2) = \Gamma(-\varepsilon/2)\Gamma((2+\varepsilon)/2)$ by a Gamma function identity [40, Sec. 1.2.2].

D.2.4 Long Time Asymptotics for DIA

The DIA prediction for the fourth order cumulant may be written as the sum of the QNA prediction and an extra term:

$$\begin{cases} \mu_{0,4}^{\mathrm{DIA}}(t) & = \mu_{0,4}^{\mathrm{QNA}}(t) + \mu_{0,4}^{\mathrm{DIA,III}}(t), \\ \mu_{0,4}^{\mathrm{DIA,III}}(t) & = 24 \int_0^t ds\,(t-s) \int_0^s ds'\,(s-s') \\ & \qquad \times \int_{\mathbf{R}^2} dq\,dq'\,\bar{E}(|q|)\bar{E}(|q'|) e^{-\kappa q^2 s - \kappa(q'^2 + 2qq')s'}. \end{cases} \tag{207}$$

The long-time asymptotics of $\mu_{0,4}^{\mathrm{QNA}}(t)$ were developed in (D.2.3), and here we focus on the additional term.

Taking a Laplace transform, we obtain

$$\tilde{\mu}_{0,4}^{\mathrm{DIA,III}}(\zeta) = \frac{24}{\zeta^2} \int_{\mathbf{R}^2} dq\,dq'\,\frac{\bar{E}(|q|)\bar{E}(|q'|)}{(\zeta+\kappa q^2)^2(\zeta+\kappa(q+q')^2)}.$$

We analyze this term much as we did the summands in the exact formula for $\tilde{\mu}_{0,4}(\zeta)$ in (D.2.1). Since the techniques are very similar (and much easier in the present context), we simply sketch the asymptotic calculation. The asymptotics presented in Subsubsection 5.2.4 can be deduced by combining the following results with those for $\mu_{0,4}^{\mathrm{QNA}}(t)$ from Subsubsection 5.2.3. We note that in the regime $-1 < \varepsilon < 0$, the leading order contribution from $\mu_{0,4}^{\mathrm{DIA,III}}(t)$ exactly cancels that of $\mu_{0,4}^{\mathrm{QNA}}(t)$. We did not pursue an accurate description of the asymptotics for $\mu_{0,4}^{\mathrm{DIA}}(t)$ in this regime because they cannot be general be expressed in terms comparable to those of the other asymptotics presented in Section 5.

Case: $\varepsilon < -1$ In this domain, the dominant contribution comes from the domain near the diagonal $q+q'=0$. We therefore zoom onto this diagonal by the change of variables

$$q' = -q + \xi\sqrt{\zeta/\kappa},$$

which yields

$$\tilde{\mu}_{0,4}^{\mathrm{DIA,III}}(\zeta) = \frac{24}{\zeta^{5/2}\kappa^{1/2}} \int_{\mathbf{R}^2} \frac{\bar{E}(|q|)\bar{E}(|q-\xi\sqrt{\zeta/\kappa}|)}{(\zeta+\kappa q^2)^2(1+\xi^2)}\,dq\,d\xi..$$

Using the same sort of approximation error estimates as in Subsubsection D.2.1, it can be rigorously shown that for $\varepsilon < -1$,

$$\begin{aligned}\tilde{\mu}_{0,4}^{\mathrm{DIA,III}}(\zeta) &\sim \frac{24}{\zeta^{5/2}\kappa^{1/2}} \int_{\mathbf{R}^2} \frac{(\bar{E}(|q|))^2}{(\kappa q^2)^2(1+\xi^2)}\, dq\, d\xi \\ &= \frac{24\pi}{\zeta^{5/2}\kappa^{5/2}} \int_{\mathbf{R}} dq\, (\bar{E}(|q|))^2 q^{-4}.\end{aligned}$$

as $\zeta \to 0$. Note carefully that the integral is actually finite for all $\varepsilon < -\frac{1}{2}$, but only provides the correct asymptotics for $\varepsilon < -1$.

The long time asymptotics of $\mu_{0,4}^{\mathrm{DIA,III}}(t)$ are obtained from those of $\tilde{\mu}_{0,4}^{\mathrm{DIA,III}}(\zeta)$ via the Tauberian theorem:

$$\mu_{0,4}^{\mathrm{DIA,III}}(t) \sim 32\pi^{1/2}\kappa^{-5/2}t^{3/2} \int_{\mathbf{R}} dq\, (\bar{E}(|q|))^2 q^{-4} \text{ for } \varepsilon < -1.$$

Case: $-1 < \varepsilon < 0$ In this regime, the integral expression for $\tilde{\mu}_{0,4}^{\mathrm{DIA,III}}(\zeta)$ is dominated by a contribution from all along the vicinity of the $q = 0$ axis. Accordingly rescaling the integration variable $q = \sqrt{\zeta/\kappa}\xi$, we compute the following formal $\zeta \to 0$ asymptotics:

$$\begin{aligned}\tilde{\mu}_{0,4}^{\mathrm{DIA,III}}(\zeta) &\sim 24\kappa^{-1/2}\zeta^{-3/2} \int_{\mathbf{R}^2} d\xi\, dq'\, \frac{\bar{E}(\sqrt{\zeta/\kappa}|\xi|)\bar{E}(|q'|)}{\zeta^2(1+\xi^2)^2(\zeta+\kappa(\sqrt{\zeta/\kappa}q+q')^2)} \\ &\sim 24\kappa^{-3/2}\zeta^{-7/2} \int_{\mathbf{R}^2} d\xi\, dq'\, \frac{A_E(\zeta/\kappa)^{(1-\varepsilon)/2}|\xi|^{1-\varepsilon}\bar{E}(|q'|)}{(1+\xi^2)^2 q'^2} \\ &= 48\kappa^{(\varepsilon-4)/2}\zeta^{-3-\varepsilon/2}A_E B\left(1-\frac{\varepsilon}{2}, 1+\frac{\varepsilon}{2}\right) \int_0^\infty dq'\, \bar{E}(q')q'^{-2},\end{aligned} \tag{208}$$

where $B(x,y) = (\Gamma(x)\Gamma(y))/\Gamma(x+y)$ is the beta function.

We note that the limit stated in (208) is finite for $-2 < \varepsilon < 0$, but is actually the correct limit only over the range $-1 < \varepsilon < 0$. To prepare for a legitimate dominated convergence argument, we define the function

$$\tilde{\mu}_{0,4}^{*\mathrm{DIA,III}}(\zeta) \equiv \frac{24}{\zeta^2} \int_{\mathbf{R}^2} dq\, dq'\, \frac{\bar{E}(|q|)\bar{E}(|q'|)}{(\zeta+\kappa q^2)^2(\zeta+\kappa q'^2)}$$

and establish the estimate

$$|\tilde{\mu}_{0,4}^{\mathrm{DIA,III}}(\zeta) - \tilde{\mu}_{0,4}^{*\mathrm{DIA,III}}(\zeta)| = O(\zeta^{-5/2} + \zeta^{-(5+\varepsilon)/2} + \zeta^{-(3+\varepsilon)}), \tag{209}$$

which is negligible compared to the claimed $\zeta^{-(3+\varepsilon/2)}$ limiting behavior (208) of $\tilde{\mu}_{0,4}^{\mathrm{DIA,III}}(\zeta)$ at small ζ when $-1 < \varepsilon < 0$. The estimate (209) is

obtained by dividing the integration domain into portions on which simple estimates of the differences of the integrands of $\tilde{\mu}_{0,4}^{\mathrm{DIA,III}}(\zeta)$ and $\tilde{\mu}_{0,4}^{*\mathrm{DIA,III}}(\zeta)$ can be made.

A dominated convergence theorem argument can now be applied to prove that $\tilde{\mu}_{0,4}^{*\mathrm{DIA,III}}(\zeta)$ converges to the limit on the final right hand side of Eq. (208) whenever that limit is absolutely integrable because a finite multiple of the integrand appearing in the limit serves as a dominating function for the integrand of $\tilde{\mu}_{0,4}^{*\mathrm{DIA,III}}(\zeta)$. Therefore, $\tilde{\mu}_{0,4}^{*\mathrm{DIA,III}}(\zeta)$ converges to the limit in (208) for $-2 < \varepsilon < 0$, but the actual function of interest $\tilde{\mu}_{0,4}^{\mathrm{DIA,III}}(\zeta)$ converges to this limit only over the parameter domain $-1 < \varepsilon < 0$ where $\tilde{\mu}_{0,4}^{*\mathrm{DIA,III}}(\zeta)$ is a good approximation of $\tilde{\mu}_{0,4}^{\mathrm{DIA,III}}(\zeta)$.

Finally returning to the physical time domain via a Tauberian theorem, we have

$$\begin{aligned}\mu_{0,4}^{\mathrm{DIA,III}}(t) &\sim 48\kappa^{(\varepsilon-4)/2}t^{2+\varepsilon/2}A_E\frac{B\left(1-\frac{\varepsilon}{2},1+\frac{\varepsilon}{2}\right)}{\Gamma\left(3+\frac{\varepsilon}{2}\right)}\int_0^\infty dq'\,\bar{E}(q')q'^{-2}\\ &= -24\varepsilon\kappa^{(\varepsilon-4)/2}A_E t^{2+\varepsilon/2}\Gamma\left(-\frac{4+\varepsilon}{2}\right)\int_0^\infty dq'\,\bar{E}(q')q'^{-2}.\end{aligned}$$

as $t \to \infty$. This term exactly cancels that of $\mu_{0,4}^{\mathrm{QNA}}(t)$ for $-1 < \varepsilon < 0$, so

$$\mu_{0,4}^{\mathrm{DIA}}(t) = \mu_{0,4}^{\mathrm{QNA}}(t) + \mu_{0,4}^{\mathrm{DIA,III}}(t) = o(t^{2+\varepsilon/2}) \text{ for } -1 < \varepsilon < 0.$$

Case: $0 < \varepsilon < 2$ In this regime, the integral over wavenumbers has dominant contribution from small wavenumbers so we now rescale

$$q = \xi\sqrt{\zeta/\kappa}, \qquad q' = \xi'\sqrt{\zeta/\kappa}.$$

Then a formal computation gives for $\zeta \to 0$:

$$\begin{aligned}\tilde{\mu}_{0,4}^{\mathrm{DIA,III}}(\zeta) &\sim \frac{24}{\zeta^4\kappa}\int_{\mathbf{R}^2} d\xi\,d\xi'\,\frac{\bar{E}(|\xi\sqrt{\zeta/\kappa}|)\bar{E}(|\xi'\sqrt{\zeta/\kappa}|)}{(1+\xi^2)^2(1+(\xi+\xi')^2)}\\ &\sim \frac{24}{\zeta^4\kappa}\int_{\mathbf{R}^2} d\xi\,d\xi'\,\frac{A_E|\xi\sqrt{\zeta/\kappa}|^{1-\varepsilon}A_E|\xi'\sqrt{\zeta/\kappa}|^{1-\varepsilon}}{(1+\xi^2)^2(1+(\xi+\xi')^2)}\\ &= 24A_E^2\kappa^{\varepsilon-2}\zeta^{-3-\varepsilon}\int_{\mathbf{R}^2} d\xi\,d\xi'\,\frac{|\xi\xi'|^{1-\varepsilon}}{(1+\xi^2)^2(1+(\xi+\xi')^2)}.\end{aligned}$$

This asymptotic statement can be rigorously verified for $0 < \varepsilon < 2$ by a dominated convergence theorem, as in Subsubsection D.2.1.

A Tauberian theorem yields the long-time asymptotics for $\mu_{0,4}^{\mathrm{DIA,III}}(t)$:

$$\mu_{0,4}^{\mathrm{DIA,III}}(t) \sim \frac{24A_E^2}{\Gamma(3+\varepsilon)}\kappa^{\varepsilon-2}t^{2+\varepsilon}\int_{\mathbf{R}^2} d\xi\,d\xi'\,\frac{|\xi\xi'|^{1-\varepsilon}}{(1+\xi^2)^2(1+(\xi+\xi')^2)}.$$

D.2.5 Numerical evaluation of integrals for flatness factors

Some of the scaling coefficients for the asymptotic behavior of the exact fourth order cumulants, as well as their DIA and MDIA approximations, involve integrals for which we do not know a simple closed form expression in terms of special functions. We therefore integrate them numerically, using MATLAB, and plot their values in Figure 8. Some care must be taken in these numerical quadratures because, for certain values of ε, the integrands are slowly decaying. Moreover, the integrands for the exact (136) and MDIA formulas (138) exhibit a pronounced ridge near $q = q' \gg 1$, and the DIA formula exhibits a similar relative spike near $q = -q'$ for $|q| \gg 1$. We therefore preprocess these integrands, through changes of variables and subtraction of the ridge contribution as suggested in [1], so that the only integrals which must be evaluated numerically involve bounded functions over bounded square domains. These numerical quadratures are checked against separate analytical evaluations of the integral formulas which are possible at $\varepsilon = 0$ and $\varepsilon = 1$.

Acknowledgements E. V.-E. is partially supported by NSF Grant DMS-9510356. A. M. is partially supported by ARO-DAAD19-01-10810, NSF-DMS9972865, ONR-N00014-96-1-0043.

References

[1] Forman S. Acton. *Real computing made real*, chapter 3. Princeton University Press, Princeton, NJ, 1996.

[2] Marco Avellaneda and Andrew J. Majda. Mathematical models with exact renormalization for turbulent transport. *Comm. Pure Appl. Math.*, 131:381–429, 1990.

[3] Marco Avellaneda and Andrew J. Majda. An integral representation and bounds on the effective diffusivity in passive advection by laminar and turbulent flows. *Comm. Math Phys.*, 138:339–391, 1991.

[4] Marco Avellaneda and Andrew J. Majda. Approximate and exact renormalization theories for a model for turbulent transport. *Phys. Fluids A*, 4(1):41–56, January 1992.

[5] Marco Avellaneda and Andrew J. Majda. Mathematical models with exact renormalization for turbulent transport, II: Fractal interfaces, non-Gaussian statistics and the sweeping effect. *Comm. Pure Appl. Math.*, 146:139–204, 1992.

[6] Marco Avellaneda and Andrew J. Majda. Superdiffusion in nearly stratified flows. *J. Statist. Phys.*, 69(3/4):689–729, 1992.

[7] Marco Avellaneda and Andrew J. Majda. Simple examples with features of renormalization for turbulent transport. *Phil. Trans. R. Soc. Lond. A*, 346:205–233, 1994.

[8] Denis Bernard, Krzysztof Gawędzki, and Antti Kupiainen. Slow modes in passive advection. *J. Statist. Phys.*, 90(3-4):519–569, 1998.

[9] A. Bourlioux and A. J. Majda. Elementary models with PDF intermittency for passive scalars with a mean gradient. To appear in *Physics of Fluids*, submitted June 1, 2001 and accepted September 15, 2001.

[10] R. C. Bourret. Stochastically perturbed fields, with applications to wave propagation in random media. *Nuovo Cimento (10)*, 26:1–31, 1962.

[11] A. Brissaud and U. Frisch. Solving linear stochastic differential equations. *J. Mathematical Phys.*, 15:524–534, 1974.

[12] Michael Chertkov and G. Falkovich. Anomalous scaling exponents of a white-advected passive scalar. *Phys. Rev. Lett.*, 76(15):2706–2709, April 8 1996.

[13] S. Corrsin. Progress report on some turbulent diffusion research. In *Advances in Geophysics, Vol. 6 (Symposium on Atmospheric Diffusion and Air Pollution, Oxford, 1958)*, pages 161–164. Academic Press, New York, 1959.

[14] G. T. Csanady. *Turbulent diffusion in the environment*, volume 3 of *Geophysics and Astrophysics Monographs*. D. Reidel, Dordrecht, Boston, Lancaster, Tokyo, 1973.

[15] Gedeon Dagan. Theory of solute transport by groundwater. In *Annual review of fluid mechanics*, volume 19, pages 183–215. Annual Reviews, Palo Alto, CA, 1987.

[16] Frank W. Elliott, Jr, David J. Horntrop, and Andrew J. Majda. Monte Carlo methods for turbulent tracers with long range and fractal random velocity fields. *Chaos*, 7(1):39–48, 1997.

[17] A. Erdélyi. *Asymptotic expansions*, section 2.8. Dover Publications Inc., New York, 1956.

[18] Adrienne L. Fairhall, Omri Gat, Victor L'vov, and Itamar Procaccia. Anomalous scaling in a model of passive scalar advection: Exact results. *Phys. Rev. E*, 53(4A):3518–3535, 1996.

[19] Albert Fannjiang and George Papanicolaou. Diffusion in turbulence. *Prob. Th. Rel. Fields*, 105(3):279–334, 1996.

[20] William Feller. *An introduction to probability theory and its applications*, volume 2, chapter V.8, page 155. John Wiley & Sons, New York, London, Sydney, second edition, 1971.

[21] U. Frisch and R. Bourret. Parastochastics. *J. Mathematical Phys.*, 11:364–390, 1970.

[22] I. M. Gel'fand and G. E. Shilov. *Generalized functions. Properties and operations*, volume 1. Academic Press, New York, 1964.

[23] Hermann Haken. *Synergetics: an introduction*. Springer-Verlag, Berlin, third edition, 1983. Nonequilibrium phase transitions and self-organization in physics, chemistry, and biology.

[24] Jackson R. Herring and Robert M. Kerr. Comparison of direct numerical simulations with predictions of two-point closures for isotropic turbulence convecting a passive scalar. *J. Fluid Mech.*, 118:205–219, 1982.

[25] Jackson R. Herring and Robert H. Kraichnan. Comparison of some approximations for isotropic turbulence. In J. Ehlers, K. Hepp, and H. A. Weidenmüller, editors, *Statistical Models and Turbulence*, volume 12 of *Lecture Notes in Physics*, pages 148–194, Berlin, 1972. Springer-Verlag. Proceedings of a Symposium held at the University of California, San Diego (La Jolla).

[26] David J. Horntrop and Andrew J. Majda. Subtle statistical behavior in simple models for random advection-diffusion. *J. Math. Sci. Univ. Tokyo*, 1:1–48, 1994.

[27] A. P. Kazantsev. Enhancement of a magnetic field by a conducting fluid. *Sov. Phys. JETP*, 26:1031, 1968.

[28] V. I. Klyatskin, W. A. Woyczynski, and D. Gurarie. Short-time correlation approximations for diffusing tracers in random velocity fields: a functional approach. In *Stochastic modelling in physical oceanography*, volume 39 of *Progr. Probab.*, pages 221–269. Birkhäuser Boston, Boston, 1996.

[29] Robert H. Kraichnan. Irreversible statistical mechanics of incompressible hydromagnetic turbulence. *Phys. Rev. (2)*, 109:1407–1422, 1958.

[30] Robert H. Kraichnan. The structure of isotropic turbulence at very high Reynolds number. *J. Fluid Mech.*, 5:497–543, 1959.

[31] Robert H. Kraichnan. Dynamics of nonlinear stochastic systems. *J. Mathematical Phys.*, 2:124–148, 1961.

[32] Robert H. Kraichnan. Kolmogorov's hypotheses and Eulerian turbulence theory. *Phys. Fluids*, 7(11):1723–1734, November 1964.

[33] Robert H. Kraichnan. Lagrangian-history closure approximation for turbulence. *Phys. Fluids*, 8(4):575–598, April 1965.

[34] Robert H. Kraichnan. Small-scale structure of a scalar field convected by turbulence. *Phys. Fluids*, 11(5):945–953, May 1968.

[35] Robert H. Kraichnan. Turbulent diffusion: Evaluation of primitive and renormalized perturbation series by padé approximations and by expansion of stieltjes transforms into contributions from continuous

orthogonal functions. In John L. Gammel, editor, *The Padé approximant in theoretical physics*, pages xii+378 pp. ISBN 0–12–074850–9. Academic Press, New York, 1970. Mathematics in Science and Engineering, Vol. 71.

[36] Robert H. Kraichnan. Eulerian and Lagrangian renormalization in turbulence theory. *J. Fluid Mech.*, 83:349–374, 1977.

[37] Robert H. Kraichnan. Anomalous scaling of a randomly advected passive scalar. *Phys. Rev. Lett.*, 72(7):1016–1019, February 1994.

[38] J. A. Krommes. Statistical descriptions and plasma physics. In M. N. Rosenbluth and R. Z. Sagdeev, editors, *Handbook of Plasma Physics*, volume 2. North Holland-Elsevier Science Publishers, Amsterdam, New York, Oxford, 1984.

[39] Gregory F. Lawler. *Introduction to stochastic processes*, chapter 8. Chapman & Hall, New York, 1995.

[40] N. N. Lebedev. *Special functions & their applications*. Dover, New York, 1972.

[41] Marcel Lesieur. *Turbulence in fluids*, chapter 5.4, 5.5, pages 161–163. Number 1 in Fluid Mechanics and its Applications. Kluwer, Dordrecht, second revised edition, 1990.

[42] D. C. Leslie. *Developments in the theory of turbulence*. Oxford Science Publications. The Clarendon Press Oxford University Press, New York, 1983. Corrected reprint of the 1973 original.

[43] T. C. Lipscombe, A. L. Frenkel, and D. ter Haar. On the convection of a passive scalar by a turbulent Gaussian velocity field. *J. Statist. Phys.*, 63(1-2):305–313, 1991.

[44] T. S. Lundgren and Y. B. Pointin. Turbulent self-diffusion. *Phys. Fluids*, 19(3):355–358, mar 1976.

[45] Andrew J. Majda. Explicit inertial range renormalization theory in a model for turbulent diffusion. *J. Statist. Phys.*, 73:515–542, November 1993.

[46] Andrew J. Majda and Peter R. Kramer. Simplified models for turbulent diffusion: Theory, numerical modelling and physical phenomena. *Phys. Rep.*, 314(4–5):237–574, June 1999.

[47] Andrew J. Majda and Richard M. McLaughlin. The effect of mean flows on enhanced diffusivity in transport by incompressible periodic velocity fields. *Stud. Appl. Math.*, 89(3):245–279, 1993.

[48] W. D. McComb. *The physics of fluid turbulence*, volume 25 of *Oxford Engineering Science Series*. Clarendon Press, New York, 1991.

[49] Stanislav A. Molchanov. Ideas in the theory of random media. *Acta Applicandae Math.*, 22:139–282, 1991.

[50] A. S. Monin and A. M. Yaglom. *Statistical fluid mechanics: mechanics of turbulence*, volume 1. MIT Press, Cambridge, MA, 1975.

[51] A. S. Monin and A. M. Yaglom. *Statistical fluid mechanics: mechanics of turbulence*, volume 2. MIT Press, Cambridge, MA, 1975.

[52] Hazime Mori, Hirokazu Fujisaka, and Hideto Shigematsu. A new expansion of the master equation. *Progr. Theoret. Phys.*, 51(1):109–122, January 1974.

[53] Karl Oelschläger. Homogenization of a diffusion process in a divergence-free random field. *Ann. Probab.*, 16(3):1084–1126, 1988.

[54] Steven A. Orszag. Lectures on the statistical theory of turbulence. In *Fluid dynamics/Dynamique des fluides (École d'Été de Physique Théorique, Les Houches, 1973)*, pages 235–374. Gordon and Breach, London, 1977.

[55] Steven A. Orszag and Robert H. Kraichnan. Model equations for strong turbulence in a vlasov plasma. *Phys. Fluids*, 10(8):1720–1736, August 1967.

[56] George C. Papanicolaou and S. R. S Varadhan. Boundary value problems with rapidly oscillating random coefficients. In J. Fritz, J. L. Lebowitz, and D. Szasz, editors, *Random fields: rigorous results in statistical mechanics and quantum field theory*, volume 2 of *Colloquia Mathematica Societatis János Bolyai*, pages 835–873. North Holland-Elsevier Science Publishers, Amsterdam, New York, Oxford, 1979.

[57] I. Proudman and W. H. Reid. On the decay of a normally distributed and homogeneous turbulent velocity field. *Philos. Trans. Roy. Soc. London. Ser. A.*, 247:163–189, 1954.

[58] A. K. Rajagopal and E. C. G. Sudarshan. Some generalizations of the Marcinkiewicz theorem and its implications to certain approximation schemes in many-particle physics. *Phys. Rev. A (3)*, 10:1852–1857, 1974.

[59] H. Risken. *The Fokker-Planck equation*, section 2.2. Springer-Verlag, Berlin, second edition, 1989.

[60] P. H. Roberts. Analytical theory of turbulent diffusion. *J. Fluid Mech.*, 11:257–283, 1962.

[61] P. G. Saffman. An approximate calculation of the Lagrangian autocorrelation coefficient for stationary homogenous turbulence. *Appl. Sci. Res.*, 11:245–255, 1963.

[62] Tomomasa Tatsumi, Shigeo Kida, and Jiro Mizushima. The multiple-scale cumulant expansion for isotropic turbulence. *J. Fluid Mech.*, 85(1):97–142, 1978.

[63] H. Tennekes and J. L. Lumley. *A first course in turbulence*, chapter 8. MIT Press, Cambridge, MA, 1972.

[64] R. H. Terwiel. Projection operator method applied to stochastic linear differential equations. *Physica*, 74:248–265, 1974.

[65] N. G. van Kampen. A cumulant expansion for stochastic linear differential equations. I, II. *Physica*, 74:215–238; ibid. 74 (1974), 239–247, 1974.

[66] N. G. van Kampen. Stochastic differential equations. *Phys. Rep.*, 24(3):171–228, 1976.

[67] Eric Vanden Eijnden. *Contribution to the Statistical Theory of Turbulence: Application to Anomalous Transport in Plasmas*. PhD thesis, Université Libre de Bruxelles, July 1997. Faculté des Sciences, Physique Statistique.

[68] Eric Vanden Eijnden. Studying random differential equations as a tool for turbulent diffusion. *Phys. Rev. E*, 58:R5229–5232, 1998.

[69] David Vernon Widder. *The Laplace Transform*, chapter V.4.3. Princeton University Press, Princeton, N. J., 1941. Princeton Mathematical Series, v. 6.

[70] A. M. Yaglom. *Correlation theory of stationary and related random functions. Volume I: Basic results*. Springer-Verlag, Berlin, 1987.

[71] Craig L. Zirbel and Erhan Çinlar. Mass transport by Brownian flows. In S. A. Molchanov, editor, *Stochastic models in geosystems*, IMA Volumes in Mathematics and its Applications. Springer-Verlag, Berlin, 1996.

[72] G. Zumofen, J. Klafter, and A. Blumen. Enhanced diffusion in random velocity fields. *Phys. Rev. A*, 42(8):4601–4608, October 15 1990.

[73] Robert Zwanzig. Ensemble method in the theory of irreversibility. *J. Chem. Phys.*, 33:1338–1341, 1960.

[74] Robert Zwanzig. Memory effects in irreversible thermodynamics. *Phys. Rev.*, 124(4):983–992, November 15 1961.